50272-101

REPORT DOCUMENTATION PAGE	1. REPORT NO. NCEER-93-0001	2.	3. PB93-227510

4. Title and Subtitle
An Experimental Study on the Seismic Performance of Brick-Infilled Steel Frames With and Without Retrofit

5. Report Date
January 29, 1993

6.

7. Author(s)
J.B. Mander, B. Nair, K. Woktkowski and J. Ma

8. Performing Organization Rept. No.

9. Performing Organization Name and Address
State University of New York at Buffalo
Department of Civil Engineering
Buffalo, New York 14260

10. Project/Task/Work Unit No.

11. Contract(C) or Grant(G) No.
(C) BSC 90-25010
(G) NEC-91029

12. Sponsoring Organization Name and Address
National Center for Earthquake Engineering Research
State University of New York at Buffalo
Red Jacket Quadrangle
Buffalo, New York 14261

13. Type of Report & Period Covered
Technical Report

14.

15. Supplementary Notes
This research was conducted at the State University of New York at Buffalo and was partially supported by the National Science Foundation under Grant No. BCS 90-25010 and the New York State Science and Technology Foundation under Grant No. NEC-91029.

16. Abstract (Limit: 200 words)
Experimental results are presented for three infill frame sub-assemblages. The specimens were constructed from bolted steel frames, infilled with clay brick masonry, and tested in-plane under quasi-static cyclic loading. Each specimen was either retrofitted or, following initial testing, repaired with a thin ferrocement overlay. Results showed that all specimens performed well up to interstory drifts of approximately 1.5%. The inclusion of ferrocement gave a marginal improvement in energy dissipation. Conclusions are drawn on the efficacy of ordinary brick or rehabilitated infills as seismic resisting elements.

17. Document Analysis a. Descriptors

b. Identifiers/Open-Ended Terms
Brick masonry infill. Infilled frames. Bolted steel frames. Ferrocement jacketing. Retrofitting. Energy dissipation. Experimental tests. Cyclic loads. Earthquake Engineering.

c. COSATI Field/Group

18. Availability Statement	19. Security Class (This Report)	21. No. of Pages
Release Unlimited	Unclassified	148
	20. Security Class (This Page) Unclassified	22. Price

NATIONAL CENTER FOR EARTHQUAKE ENGINEERING RESEARCH

State University of New York at Buffalo

An Experimental Study on the Seismic Performance of Brick-Infilled Steel Frames With and Without Retrofit

by

J.B. Mander, B. Nair, K. Wojtkowski and J. Ma

State University of New York at Buffalo
Department of Civil Engineering
Buffalo, New York 14260

Technical Report NCEER-93-0001

January 29, 1993

This research was conducted at the State University of New York at Buffalo and was partially supported by the National Science Foundation under Grant No. BCS 90-25010 and the New York State Science and Technology Foundation under Grant No. NEC-91029.

NOTICE

This report was prepared by the State University of New York at Buffalo as a result of research sponsored by the National Center for Earthquake Engineering Research (NCEER) through grants from the National Science Foundation, the New York State Science and Technology Foundation, and other sponsors. Neither NCEER, associates of NCEER, its sponsors, the State University of New York at Buffalo, nor any person acting on their behalf:

a. makes any warranty, express or implied, with respect to the use of any information, apparatus, method, or process disclosed in this report or that such use may not infringe upon privately owned rights; or

b. assumes any liabilities of whatsoever kind with respect to the use of, or the damage resulting from the use of, any information, apparatus, method or process disclosed in this report.

Any opinions, findings, and conclusions or recommendations expressed in this publication are those of the author(s) and do not necessarily reflect the views of the National Science Foundation, the New York State Science and Technology Foundation, or other sponsors.

An Experimental Study on the Seismic Performance of Brick-Infilled Steel Frames With and Without Retrofit

by

J.B. Mander[1], B. Nair[2], K. Wojtkowski[2] and J. Ma[2]

January 29, 1993

Technical Report NCEER-93-0001

NCEER Project Number 91-3122A

NSF Master Contract Number BCS 90-25010
and
NYSSTF Grant Number NEC-91029

1 Assistant Professor, Department of Civil Engineering, State University of New York at Buffalo

2 Graduate Research Assistant, Department of Civil Engineering, State University of New York at Buffalo

NATIONAL CENTER FOR EARTHQUAKE FNGINEERING RESEARCH
State University of New York at Buffalo
Red Jacket Quadrangle, Buffalo, NY 14261

PREFACE

The National Center for Earthquake Engineering Research (NCEER) was established to expand and disseminate knowledge about earthquakes, improve earthquake-resistant design, and implement seismic hazard mitigation procedures to minimize loss of lives and property. The emphasis is on structures in the eastern and central United States and lifelines throughout the country that are found in zones of low, moderate, and high seismicity.

NCEER's research and implementation plan in years six through ten (1991-1996) comprises four interlocked elements, as shown in the figure below. Element I, Basic Research, is carried out to support projects in the Applied Research area. Element II, Applied Research, is the major focus of work for years six through ten. Element III, Demonstration Projects, have been planned to support Applied Research projects, and will be either case studies or regional studies. Element IV, Implementation, will result from activity in the four Applied Research projects, and from Demonstration Projects.

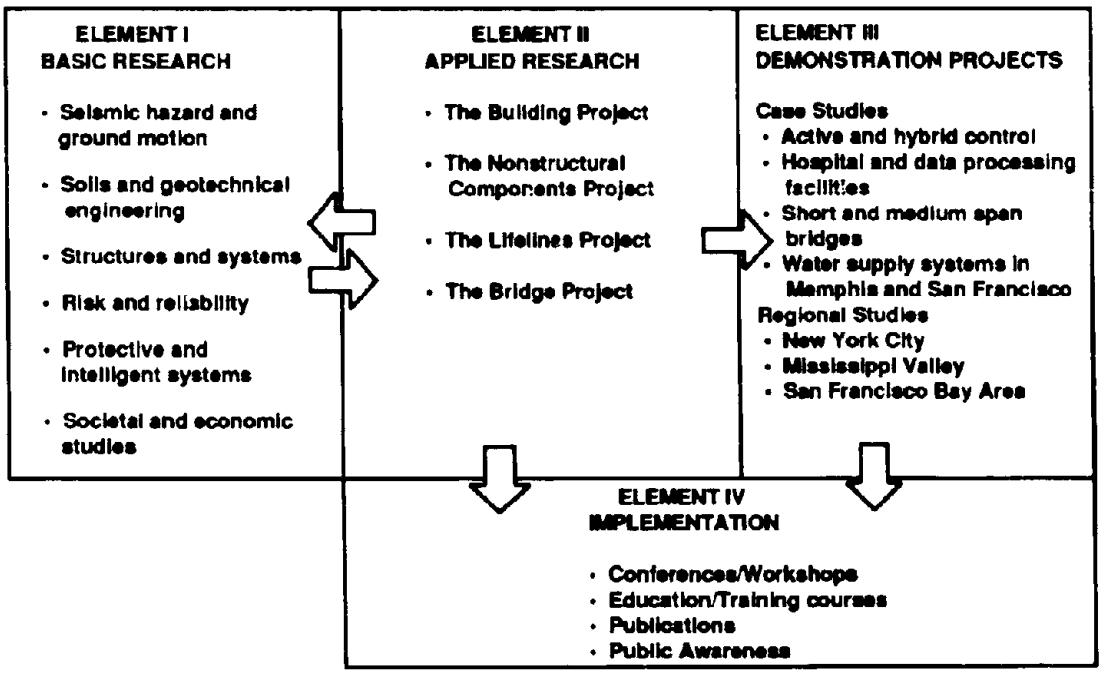

Research in the **Building Project** focuses on the evaluation and retrofit of buildings in regions of moderate seismicity. Emphasis is on lightly reinforced concrete buildings, steel semi-rigid frames, and masonry walls or infills. The research involves small- and medium-scale shake table tests and full-scale component tests at several institutions. In a parallel effort, analytical models and computer programs are being developed to aid in the prediction of the response of these buildings to various types of ground motion.

Two of the short-term products of the **Building Project** will be a monograph on the evaluation of lightly reinforced concrete buildings and a state-of-the-art report on unreinforced masonry.

The **structures and systems program** constitutes one of the important areas of research in the **Building Project**. Current tasks include the following:

1. Continued testing of lightly reinforced concrete external joints.
2. Continued development of analytical tools, such as system identification, idealization, and computer programs.
3. Perform parametric studies of building response.
4. Retrofit of lightly reinforced concrete frames, flat plates and unreinforced masonry.
5. Enhancement of the IDARC (inelastic damage analysis of reinforced concrete) computer program.
6. Research infilled frames, including the development of an experimental program, development of analytical models and response simulation.
7. Investigate the torsional response of symmetrical buildings.

The purpose of the experimental study described in this report was to examine how an unreinforced brick masonry infill panel interacts with a surrounding steel frame in resisting lateral forces, and how its strength and behavior may be enhanced by various strengthening schemes. The study contrasts seismic performance of conventional brick infill panels, and those that have been either retrofitted before experiencing lateral loads, or repaired after having been damaged by lateral loads. The report is limited only to infill panels that are subjected to lateral forces applied within their plane, but serves as a basis for subsequent research on out-of-plane strength of cracked walls.

The research reported herein fits within NCEER's ***Building Project*** *under the category of ureinforced masonry construction, specifically infill-frame structures. Since the focus of the overall project is on evaluation and retrofit of existing buildings, many of which may not have been designed to resist seismic loads, the research project on infill frames is quite appropriate. A large number of building structures across the nation are of this type, and a number of questions exist on how masonry infills should be considered for a seismic evaluation, and how they should be retrofitted to resist anticipated earthquakes, or repaired following a seismic event.*

ABSTRACT

Experimental results are presented for three infill frame sub-assemblages. The specimens were constructed from bolted steel frames, infilled with clay brick masonry, and tested in-plane under quasi-static cyclic loading. Each specimen was either retrofitted or, following initial testing, repaired with a thin ferrocement overlay. Results showed that all specimens performed well up to interstory drifts of ±1.5%. The inclusion of ferrocement gave a marginal improvement in energy dissipation. Conclusions are drawn on the efficacy of ordinary brick or rehabilitated infills as seismic resisting elements.

TABLE OF CONTENTS

TABLE OF CONTENTS (cont'd)

LIST OF FIGURES

LIST OF FIGURES (cont'd)

LIST OF FIGURES (cont'd)

LIST OF TABLES

SECTION 1

INTRODUCTION

1.1 Background on Infilled Frames

Masonry infills exist in many framed structures, but their role in strengthening and stiffening the structure as a whole is commonly ignored by the designer. As early as 1953, research had commenced on the behavior of infilled frames[5]. Since that time, infilled frames have been studied predominantly by performing static lateral load tests on models ranging from small scale to near full-size sub-assemblages. The frame materials were either steel or reinforced concrete and the infills typically included bricks, concrete blocks (both reinforced and unreinforced), and reinforced concrete. The major parameters found to be important affecting the behavior and mode of failure of infilled frames were: strength, stiffness, hysteretic energy absorption characteristics, boundary conditions, distribution of strains and stresses within the infill panel, induced forces on the frame, initial lack of fit, openings and types of construction. Only a few studies have been concerned with simulating seismic response through cyclic load testing in the inelastic range[1,5]. Considering such a large number of interacting parameters, it is not surprising that no consensus has emerged leading to a unified approach for the design of infilled frame systems, despite four decades of research.

For seismic design, there are two approaches for considering the inclusion of an infill in a frame: either the infill is isolated from the frame and its contribution to the structural behavior can be neglected, or the infill is so placed that the interaction with the frame, and thus the structure, must be taken into account[1]. If the infill is not connected to the frame, there is a possibility that during an earthquake, the infill could impact against the frame, inducing high moments and shears in the column and lead to a short column snap-through shear failure, particularly in lightly reinforced concrete frames. For infills integrally connected with frames, large lateral loads can cause either infill and/or frame failure depending on the relative panel to frame strength. The interstory drift capacity depends on the type of infill, the frame material, and whether ductile detailing has been included in the construction.

For gravity load design, infills are placed by the architect after the structural frame has been designed. The composite behavior is thus ignored in the design process. The additional stiffness and strength, resulting from placement of infills in frames, both significantly affect the behavior of the structure under dynamic lateral loading. Under seismic excitations, stiffness affects the natural period of vibration and attracts additional loads, while the strength capacity affects the ductility demand on the elements.

Pseudo-static seismic design loads taken from design code loading spectra imply that structures will not possess sufficient strength to respond elastically to lateral loads, thus requiring an inelastic and preferably ductile structural response. Most seismic provisions in building codes now days provide for this inelastic response of structures by reducing the site-dependent elastic response spectra either explicitly or implicitly to derive inelastic design spectra. The amount of the force (acceleration) reduction depends on the ductility of the materials used in the structural system. For example, low force reductions imply relatively brittle materials such as masonry walls, whereas high force reductions imply ductile materials such as steel or reinforced concrete frames with special detailing. It should be noted that force reduction (or performance) factors are not normally given by design codes for unreinforced masonry-infilled frames. However, design codes generally now permit non-linear time-history analysis to be carried out for design and/or checking purposes of complex or unusual structures. Strictly, this is not currently possible with infilled frames because methods for obtaining an appropriate hysteretic rule are not yet readily available.

One of the purposes of this study was to experimentally investigate the inelastic behavior of infilled frames so that improved modelling can be done in conjunction with inelastic design spectra. Such experimental results also provide a basis for developing hysteretic rules to be used in dynamic time-history analysis computer programs. In this report, experimental results are presented for three infill frame sub-assemblages constructed from bolted steel frames, infilled with clay brick masonry, and tested in-plane under quasi-static cyclic loading. Specimen 1 was tested, then repaired with ferrocement and retested. Specimen 2 was initially retrofitted with ferrocement and retested. Specimen 3 was tested similar to Specimen 1, except a thicker ferrocement overlay was used which included diagonal rebars. Results showed that all specimens

performed well with interstory drifts as large as ±1.5%. The inclusion of ferrocement gave a marginal improvement in energy dissipation. Conclusions are drawn on the efficacy of ordinary brick or rehabilitated infills as seismic resisting elements.

1.2 Previous Experimental Research

There has been a considerable amount of experimental investigations done on the behavior of infilled frames in the past. These tests examined a varied number of parameters although few of them actually have dealt with seismic design. Most tests have been concentrated on monotonic loading, and little hysteretic behavior has been considered. Three of the types of structures that have been tested recently are existing structures, structures that have been repaired and retrofitted structures.

Cyclic tests on infilled frames have been conducted by quite a few researchers in the past.
a) Zarnic and Tomazevic[5] conducted a series of cyclic raking tests on masonry infilled concrete frames. Four half scale models were tested by them and each had a distinct arrangement. The four types of arrangements were: no infill, unreinforced infill, infill with horizontal reinforcement and infill with horizontal reinforcement anchored to the frame. The specimens were fixed onto a constant vertical load acting on each column (22.48 kips) and a cyclic horizontal load acting on the beam. They determined hysteresis curves, envelopes, and showed crack patterns, ultimate loads, cracking loads and cracking displacements.

They also tested eight concrete block masonry infilled frames under cyclic loading. Four types of infills were used - unreinforced, infills with horizontal reinforcement, infills with horizontal reinforcement anchored to the columns and with additional beam anchorage. The mean compressive strengths of the frame, concrete, concrete blocks, mortar and infill masonry were 2.22, 1.75, 1.54 and 0.79 ksi. Elastic modulus of frame concrete and infill masonry were 1600 and 414 ksi respectively.

Based on their experimental results, Zarnic and Tomazevic stated that the degree of strength deterioration increases with increased deformations and the process at each amplitude of deformation tends to stabilize after the third cycle. It was observed that 70% of the deterioration was during the 2nd cycle of loading and 30% between the second and third cycle. The strength

deterioration was maximum just after the attainment of maximum lateral load and less severe as the lateral deflection increases.

b) Parducci and Mezzi[5] conducted cyclic loading tests on half-scale infilled reinforced concrete frames under constant lateral displacement. Two types of frames - one with a stiff beam and another with a soft beam were infilled by hollow and semi-solid blocks. They stated that strength deterioration can be improved by making a gap between the infill and one of the columns.

c) Lian *et al*[6] conducted cyclic loading tests on brick infilled concrete frames. He stated that repeated loading didn't cause any reduction of the strength reduction capacity.

d) Bertero and Brokken[5] conducted 18 cyclic loading tests and concluded that hysteretic behavior depends on type of infill, amount and arrangement of reinforcement, the way the panel is anchored to the frame and loading history. They established that the peak strength under cyclic loading was smaller than that under monotonic loading. They used an external wire mesh that was welded to the frame anchors and indicated that this reinforcement type performed excellent hysteretic behavior especially when used with solid infills.

e) Mainstone[5] conducted a few tests on model scale micro-concrete infilled frames at load levels of 50% and 75% of peak load. He concluded that this cyclic loading didn't impair either the stiffness or strength.

f) Liauw[5] carried out dynamic tests on small-scale model four story infilled frames. A harmonic load of a maximum frequency of 8.3 Hz was applied to the top of the frame. The amplitude and frequency of the load, aspect ratio shear connectors and openings were the parameters that were varied throughout the experiment.

g) Liauw[5] concluded that a small variation in structural response was obtained on varying the frequency from 2 to 8 Hz.

h) Liauw and Kwan[5] carried out model scale tests on 4 story steel frames infilled with micro-concrete. They tested six specimens and employed three types of shear connectors by welding them to the frame.

i) Dawe, Schriver and Sofocleous[1] compared experimentally determined dynamic responses of

ten scale models of masonry infilled steel frames with the results of three simple analytical methods. Effects investigated included stiffening and strengthening contribution of the masonry infill, degradation of the system, motion intensity, frame stiffness, and rotational joint rigidity at slab-to-column intersections. They arrived at the conclusion that a simple single degree of freedom model satisfactorily predicts the linear behavior of infilled frames with rotationally rigid joint conditions. Reasonably successful predictions of the linear and initial stages of the nonlinear response of flexible systems could be made with a braced frame model.

1.3 Scope of Present Study

In this report, experimental results are presented for infilled frame sub-assemblages constructed from bolted steel frames, infilled with clay brick masonry, and tested in-plane under quasi-static cyclic loading. The specimens were either repaired or retrofitted with ferrocement overlays. Section 2 describes the experimental system developed for investigating the in-plane seismic performance of infilled frames. Section 3 summarizes experimental results of steel frame behavior without the presence of the infill panel (details of the performance of the steel frame after removing the brick infill are reported in Appendix A). Section 4 presents the experimental results for each of the three infilled frame specimens. In Section 5, the experimental results are analyzed to determine net infill performance and the masonry contact stresses against the steel frame. Finally, conclusions of this study are presented in Section 6.

SECTION 2

THE SPECIMENS AND THE EXPERIMENTAL SYSTEM

2.1 Specimen Configuration and Testing Procedure

Fig. 2.1 shows a typical structural frame in which infill walls have been placed. It is generally the first and/or second story infill that is of concern under lateral earthquake loading as high story shears may cause distress in those elements. To model such critical regions under lateral story drifts (Fig. 2.1 (b)) a symmetrical substructure has been abstracted from the frame (Fig. 2.1 (c)). Under lateral load the substructure is doubly antisymmetric as shown in Fig 2.1 (d). This idealized form of behavior was the starting point in the physical modelling scheme adopted in this study. The outer half-bays which also contain infills, were replaced with diagonal braces whose stiffness was similar to the infill itself. Thus under lateral loading the boundary conditions within the test panel are similar to prototype construction, where plastic hinges form at beam end (or joint connections) and a diagonal compression strut forms in the infill.

Each test specimen consisted of a steel frame either with or without the central bay infilled with bricks as shown in Fig. 2.2. Beams were connected to the columns by bolted semi-rigid (top and bottom angle seat) connections. The additional bracing placed between the columns and the top and bottom beams to provide end half-bay stiffness similar to the infill panels consisted of double angles (3.5" x 3" x 5/16"). These were bolted to WT sections which in turn were bolted to the columns above and below the brick infill. The additional bracing was also necessary to ensure that the column legs, above and below the infill, did not yield during lateral load testing. The semi-rigid connections were designed so that their capacity was about 50% of the connecting members. Thus, under lateral loading frame yielding was concentrated in the angles preserving the principal members from being damaged. The diagonal pin-jointed braces in the lower and upper bays were designed such that the half-story stiffness was similar to the adjacent infill panel. Single wythe clay brick masonry infills were snug-fit in the central bay of each specimen. Structurally engineered ferrocement overlays were used to either repair or retrofit each specimen.

The specimens were tested by applying lateral load at the top beam with a 50-kip actuator which was connected to a stiff reaction frame. Each specimen was tested under cyclic load in drift

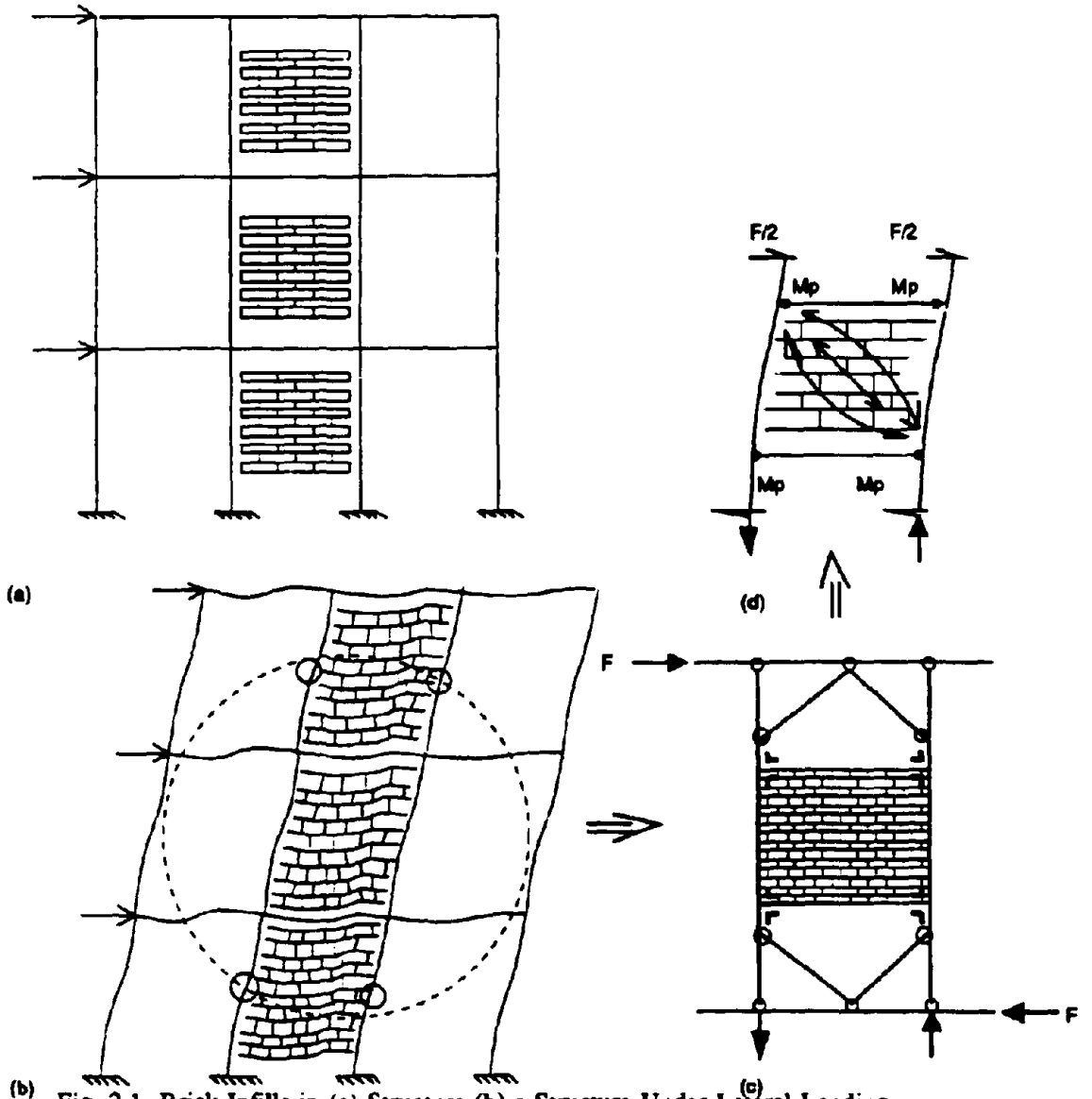

Fig. 2.1 Brick Infills in (a) Structure (b) a Structure Under Lateral Loading (c) Experimental Subassemblage (d) Boundary Conditions of Subassemblage

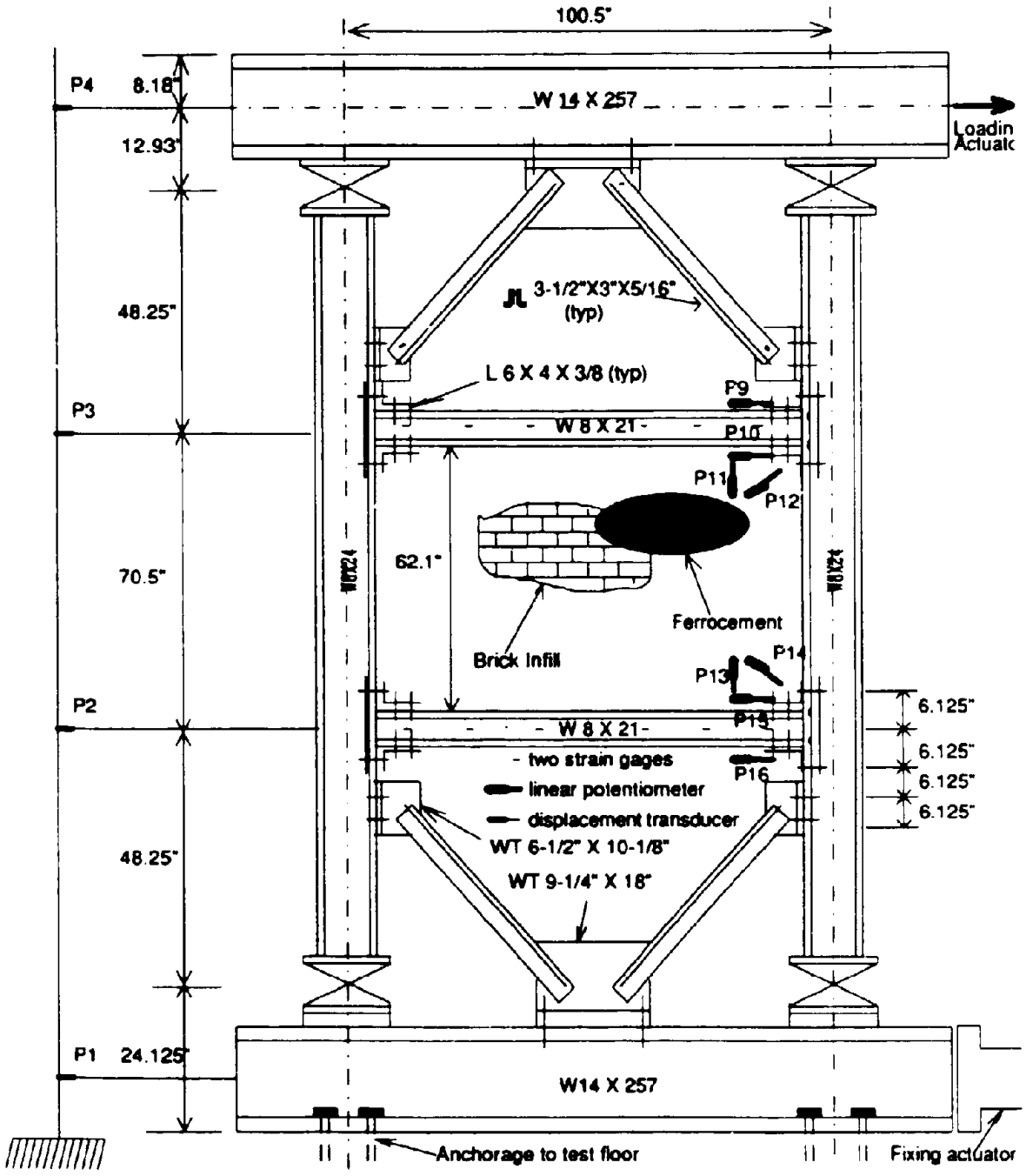

Fig. 2.2 Test specimen configuration showing instrumentation

control with a cyclic sine wave frequency of 0.01 Hz and a data recording frequency of 1 Hz.

2.2 Specimen Details

Specimen 1

Following the initial testing of the virgin brick infilled specimen, Specimen 1 was repaired using a 1/2 inch thick ferrocement coating as shown in Fig. 2.7 (a) to one of its sides. The mesh was fixed to the bricks by 1/4 inch concrete anchors and covered by an inch diameter washer with 3/8 inch diameter hole. This was to provide some relative movement between the ferrocement, anchor and wall. The mesh was laid in place using 1/4 inch anchors and then the mortar was plastered in. From each batch of mortar, several cylinders were made.

Specimen 2

Using a 1/2 inch coating of ferrocement, Specimen 2 was retrofitted with the same procedure adopted for repairing Specimen 1.

Specimen 3

For Specimen 3, an enhanced ferrocement coating was used. This consisted of removing the yielded rebars from the infill and replacing with new diagonal rebars. The ferrocement mesh was placed in a new orientation with additional layers providing better reinforcement. Two layers of mesh were provided: an inner diagonal and an outer horizontal layer The anchor bolt spacing was varied and a closer spacing was adopted. A thicker ferrocement coating of 1", as shown in Fig. 2.7 (b) was used in this enhanced overlay. The purpose of the two layers of mesh was two-fold: (i) to provide a better reinforcement to the thicker coating and (ii) to act along with the diagonal rebars in providing direct resistance to the principal tension strains and hence improve the distribution of tension cracks. The diagonal rebars on the other hand had three specific purposes: (i) to provide additional lateral load capacity by direct tension; (ii) to provide some confining action to the bricks as observed in Phase I; and (iii) to finely distribute the diagonal tension cracks across the diagonal. Figs. 2.8 (a) and (b) shows the arrangement of the diagonal rebars.

Load and Displacement

The lateral load applied to the top W14x257 beam was measured by a load cell attached directly to the 250 kip servo controlled hydraulic actuator.

Temposonic displacement transducers, namely P1, P2, P3 and P4 as shown in Fig. 2.3, were used to measure used to measure the displacements at the top of the W14x257 beam, at the upper and lower W8x21 beams and at the bottom W14x257 beam, at the upper and lower W8x21 beams and at the bottom W14x257 beam. The range of the displacement transducers was ±4 inches at the base, ±8 inches at the middle two beams and ±15 inches at the top.

All experiments were performed in drift control such that the control signal was based on the displacement difference between upper and lower beams surrounding the infill panel. Thus drift was defined as:

$$\theta_d = \frac{(\Delta_3 - \Delta_2)}{70.5}$$

in which Δ_3 and Δ_2 are the displacements in inches of the sonic transducers P3 and P2 respectively, and 70.5 is the story height in inches.

Joint Rotations

Relative joint rotations between the beams and columns were measured by a pair of displacement transducers. Linear potentiometers with a 1 in. stroke (type LCP12A-25) were used. Due to symmetry only two of the joints were instrumented - namely the lower and the upper right joints. Potentiometers are indicated by P9 through P16 on Fig. 2.2. The two positions utilized at the joints for the bare frame test for measuring joint rotations were kept the same for the infilled frame test.

Beam/Column Curvatures and Axial Forces

In order to measure the curvatures and axial forces in the beams and columns, 1/4 inch CEA-06-

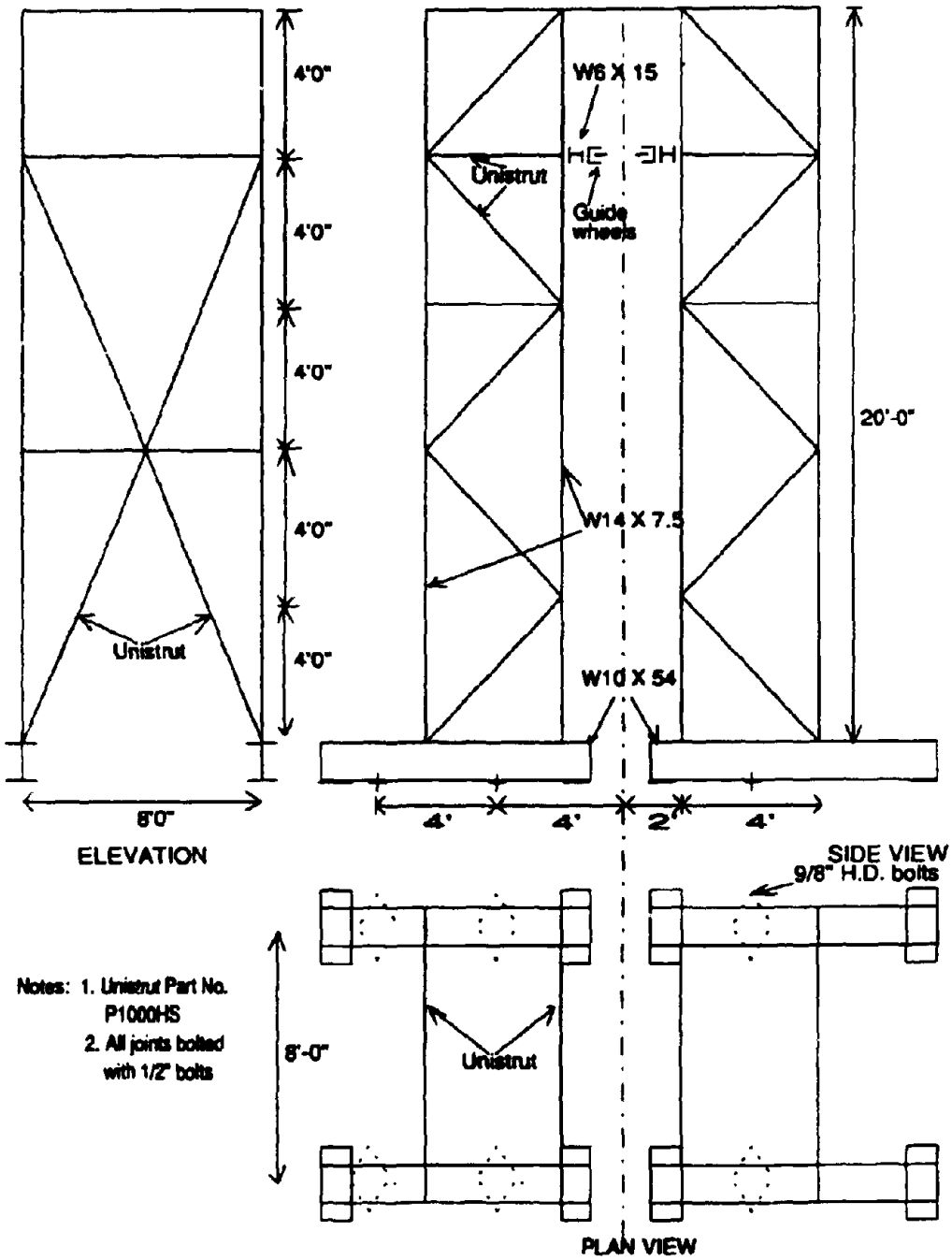

Fig. 2.3 Stabilizing frame for inplane test specimens

250UW-120 electrical resistance strain gages were used at specific locations along the bottom and top beams, and the right and left columns. The gage factor was 2.045 ±0.5% with a resistance of 120.0±0.3% Ohms. The transverse sensitivity factor was (+0.1±0.2)%. Bending moments were found by differencing readings in strain gage pairs, and axial forces by averaging strain readings, thus

$$\begin{pmatrix} M \\ P \end{pmatrix} = \begin{pmatrix} \frac{EI}{y} & \frac{-EI}{y} \\ \frac{EA}{2} & \frac{EA}{2} \end{pmatrix} \begin{pmatrix} e_1 \\ e_2 \end{pmatrix}$$

where y = distance between strain gages.

2.3 Material Properties

Steel Frame

All steel members were in accordance with American Society of Testing and Materials (ASTM) A36 requirements. The bolts used for the semi-rigid connections and the pinned bases were 7/8 inch diameter ASTM A325 (high strength).

Angles for Semi-rigid Connections

Three samples were cut lengthwise from the left over piece of the angle (two from the six inch leg and one from the four inch leg). The samples were machined into standard test specimen shapes and tested using a 60-kip capacity Riehle testing machine. A dial gage was clamped to the specimen across the central two-inch gage length. Both load and displacement readings were manually recorded during testing. A stress-strain curve for each of the three coupon specimens and an average theoretical stress-strain curve together with values adopted for the control parameters is shown in Fig. 2.4.

Brick Infill

As each brick infill was constructed, mortar cylinders were cast when the brick infill was about 50% complete. This was done in order to have a representative sample of the mortar strength at the middle of the infill when diagonal cracking was expected to commence. Four cylinders were cast for each of the three walls.

One mortar cylinder from each of the three walls was tested for its compressive strength twenty-eight days after casting. The top end of each of the cylinders was dipped in a mixture of melted basolite sulfur cement which later hardened and provided a level surface area for testing. The cylinders were tested in a 250-kip capacity Soiltest, Inc. testing machine.

For each of the three brick infills, three different brick prism specimens were built. Two of the prism types were vertical in orientation and the third one was horizontally oriented. Two 1/4 inch threaded rods were cast into the mortar beds for the purpose of attaching dial gages.

Some prism specimens were tested in compression (Fig. 2.5) and others were tested in shear (Fig. 2.6). Normally the results were taken as the average of three specimens. A thin coating of hydrostone gypsum cement was applied to each end of the prism specimen to ensure a level testing surface. Either a 60-capacity Riehle testing machine or a 120-kip capacity Tinius Olsen testing machine were used to test the prism specimens.

Following compression testing of specimens 1 and 3, the angle of internal friction in a Mohr-Coulomb failure criteria was established using the method suggested by Riddington[7], such that

$$\tau_u=\tau_0+\mu\sigma_c$$

where τ_0 is the shear strength (cohesion) at zero precompression and $\mu=\tan\Phi$ is the coefficient of internal friction. To determine the angle of friction Φ, these prism specimens were placed on a board which was gradually lifted at one end until the bricks started to slide on one another. The friction angles recorded were 44.4 and 41.0 degrees for the masonry in walls 1 and 3, respectively. These parameters (τ_0 and Φ) are useful in predicting sliding shear failure[6], and are applied in Section 5 of this report.

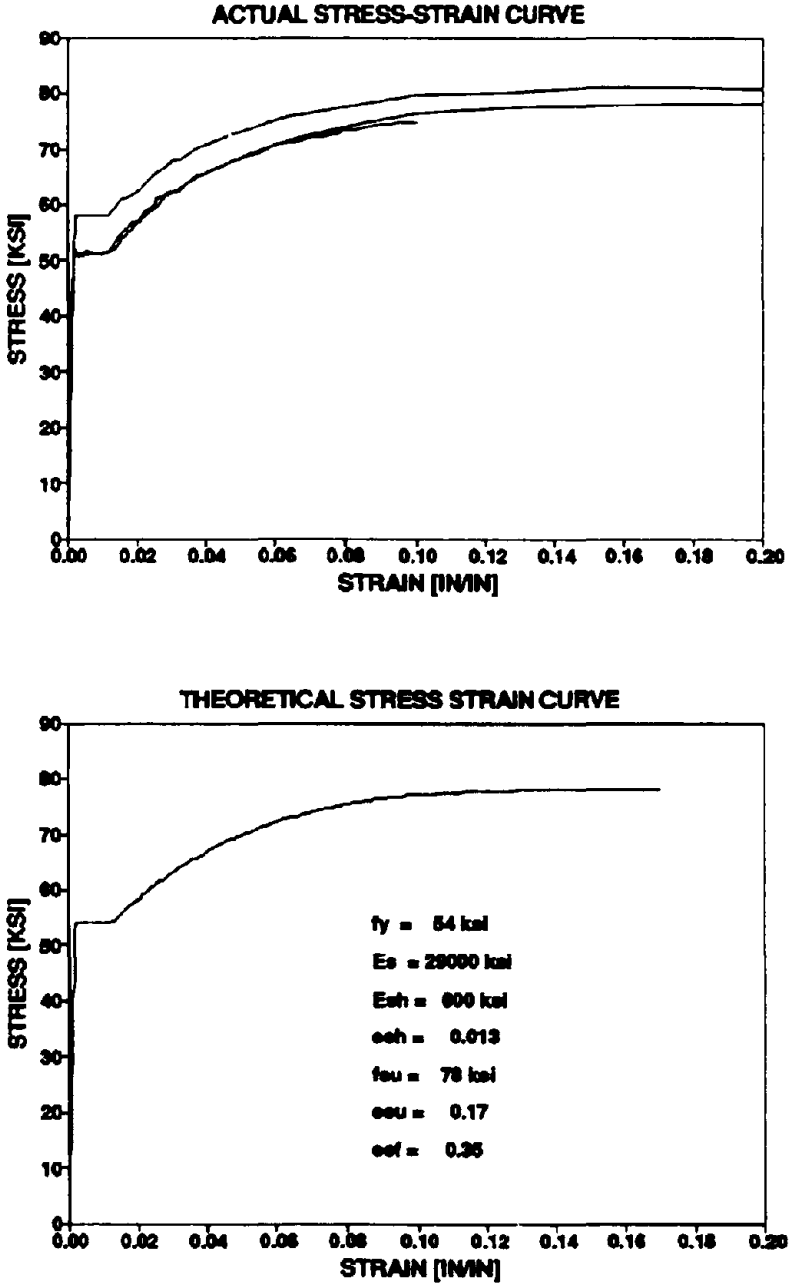

Fig. 2.4 Stress-strain results of angles for semi-rigid connections

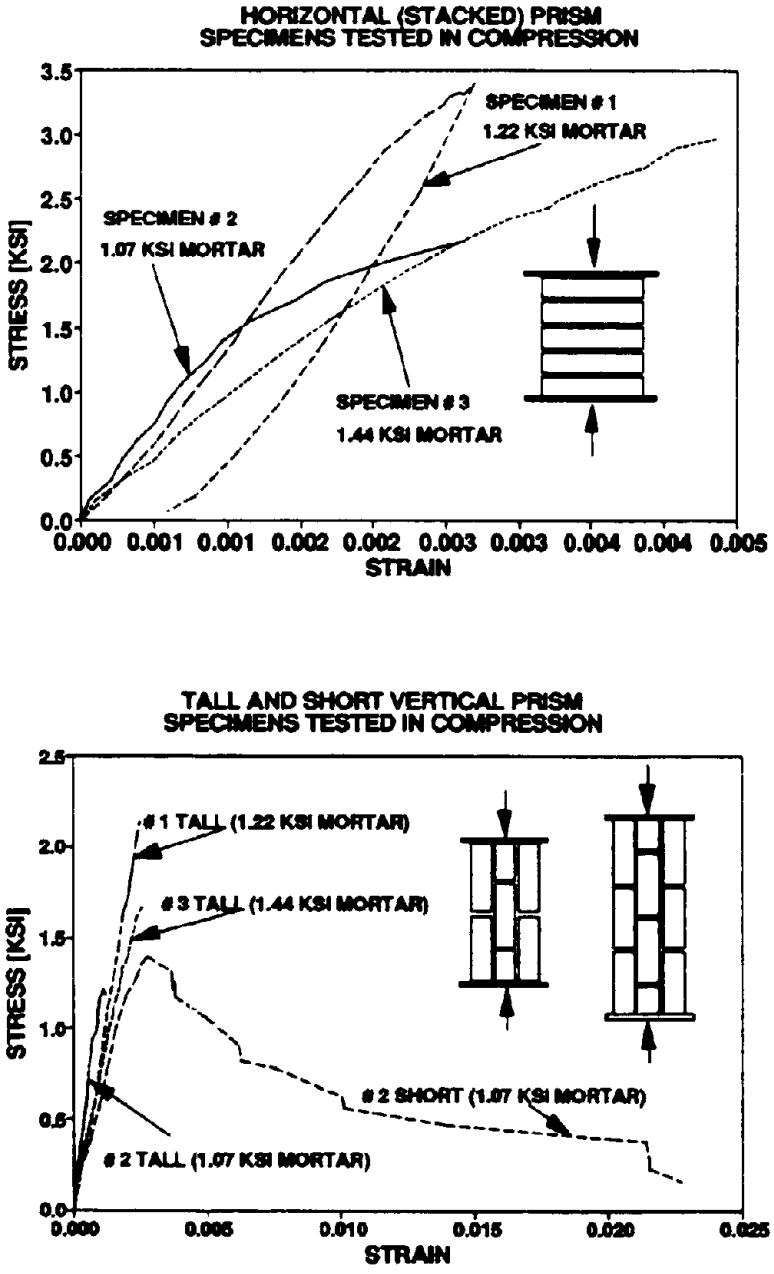

Fig. 2.5 Compression test results for brick specimens

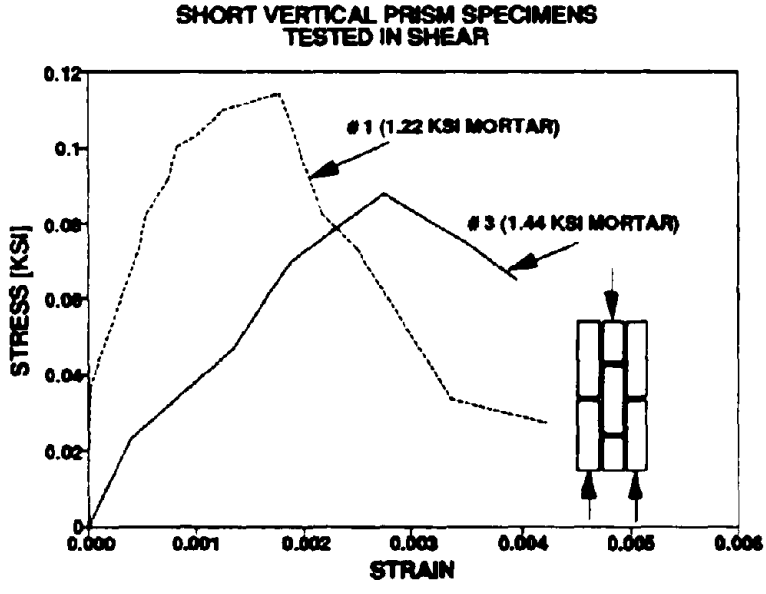

Fig. 2.6 Shear test results for brick specimens

The plain bricks tested in compression (end-on-end) resulted in an average strength of 3.55 ksi. Modulus of rupture tests were carried out to assess the tensile capacity of the materials. Three tests were carried out on plain bricks with modulus of rupture values of 0.4, 0.63 and 0.9 ksi. Modulus of rupture tests were also carried out on prism specimens with values of 0.085 and 0.12 ksi. The material properties are shown in Table 2.1

Table 2.1 Material Properties

	Specimen 1 Ordinary/ Repaired	Specimen 2 Retrofitted	Specimen 3 Ordinary/Enhanced Repair
MORTAR STRENGTH	1.22 ksi	1.07 ksi	1.44 ksi
PRISM STRENGTH			
Stacked Prism (f'_m)	3.40 ksi	2.20 ksi	2.90 ksi
Parallel Test (f'_{m90})	2.15 ksi	1.22 ksi	1.65 ksi
Modulus of Rupture (f'_t)	0.120 ksi		0.085 ksi
Shear Strength (cohesion)	0.115 ksi		0.09 ksi
Shear Angle	41.0 deg.		44.4 deg.
FERROCEMENT			
Mortar Compressive Str.	4.08 ksi	4.15 ksi	3.70 ksi
Mesh: tensile yield str.	60.70 ksi	60.70 ksi	60.04 ksi
Rebars: tensile yield str.			68.34 ksi

Ferrocement

Ferrocement may be regarded as a special type of reinforced concrete that is characterized by a small thickness and reinforced with small scale weld wire mesh. It differs from conventional reinforced concrete because of its closely packed reinforcement within the matrix. Ferrocement behaves rather like a composite material that can act in out-of-plane bending, in plane shear, and membrane action. Ferrocement is advantageous over sprayed reinforced concrete (shotcrete) as small but strong thicknesses can be formed into complex shapes without the use of any

formwork. Welded wire mesh with pitches varying between 0.25" to 2" may be used. However, due to small cover, it is necessary that the mesh be galvanized. A spacing of 0.5" was used for the mesh in the present study. The mesh was anchored onto the brick wall by concrete anchor bolts. Specimen 2 used 1.25"x0.25" bolts whereas Specimen 3 used longer 2.25"x 0.25" bolts to accommodate the thicker ferrocement measured. The anchor bolts had a tensile pull-out strength of 1.0 kip. Mortar used for the experiment was prepared out of water, rapid hardening Type III Portland Cement and sand that was passed through a #8 sieve. The ratio of the mix for water:cement:sand was 1:2:4. Compression tests were done on specimens of dimensions 3"x 6" prepared while coating the infill wall with the ferrocement mortar, the results being summarized in Table 2.1.

2.4 Test Rig Construction

Fig. 2.2 shows the stabilizing frame that was designed and constructed to resist any accidental out-of plane forces, transverse to the plane of the test specimens, of not less than ±10% of the in-plane test load applied to the infilled-frame specimen.

A truss system composed of WT sections for the vertical members and Unistrut for the horizontal and diagonal members, was chosen as the most economical solution for building the stabilizing frame.

W8x15 members, cut in half lengthwise, were used in order to create the WT4x7.5 upright members of the stabilizing frame. Holes were drilled into the web and flange of the WT section to enable the Unistrut bracing members to be bolted directly to the uprights.

Provisions had to be made to ensure that the test specimen remained plumb and square during the test cycle. To accomplish this, guide wheels were designed to roll against the top beam of the test specimen. Four of these wheels were fabricated, and two were attached to the stabilizing frame, on each side of the test specimen.

Each specimen was put in turn into position between the stabilizing frame and connected to the lower pin connections of the bottom W14x257 base beam. The base beam was anchored securely to the strong floor and the bolts were torqued to 600 ft-lb. For the second specimen, an additional 55-kip MTS servo-controlled actuator was used against the base beam to prevent slip.

The columns of the specimen were also connected to the two pin connectors of the top W14x257 beam and all bolts were torqued. The four guide wheels were adjusted for each test so that there was a one-eighth inch total clearance between the wheel and the web of the top W14x257 beam. Plumb bobs were hung from each end of the test frame to ensure that the frame was vertically oriented prior to testing.

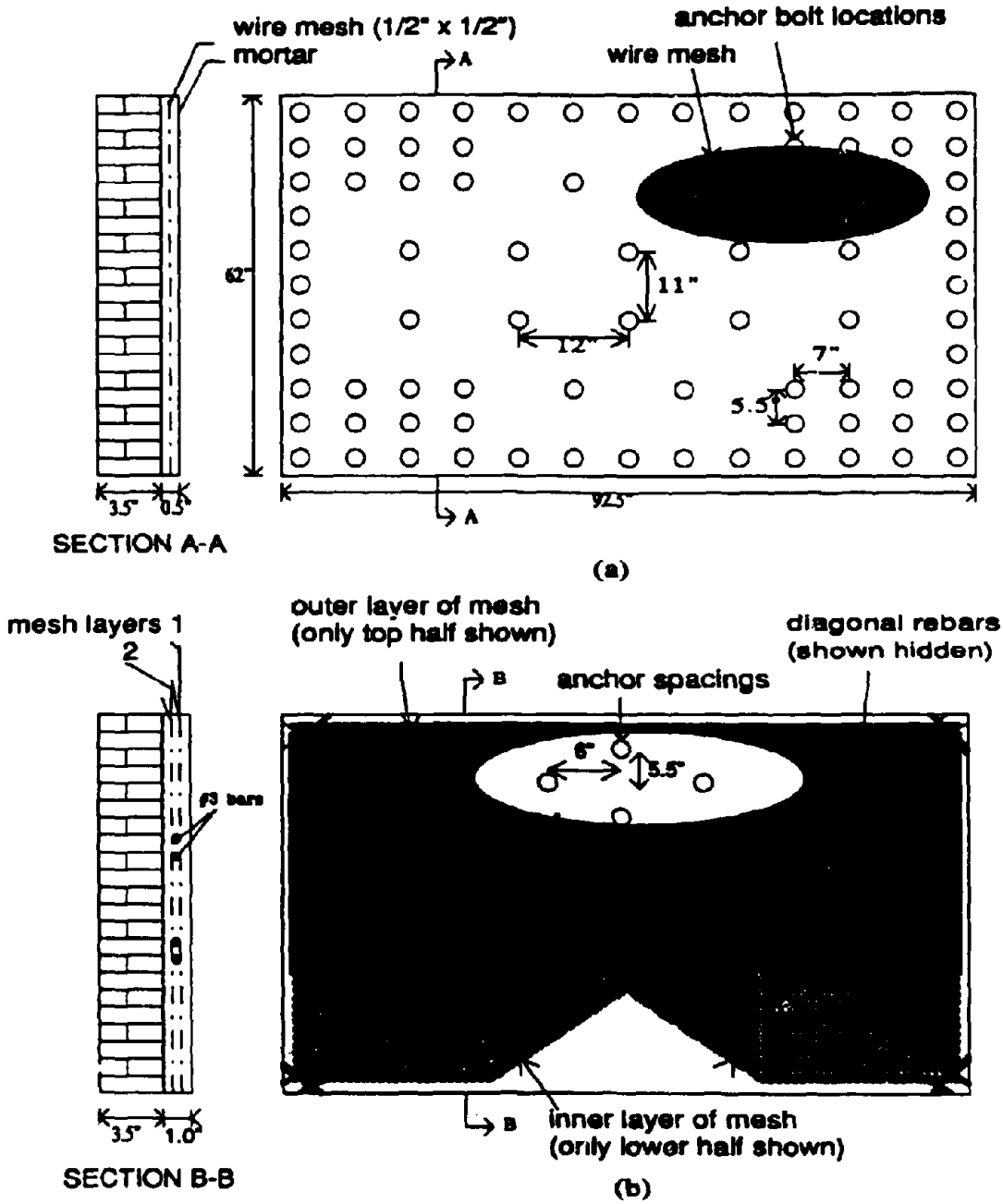

Fig. 2.7 Ferrocement overlays used: (a) ordinary overlays for Specimens 1 and 2 ; and (b) enhanced overlay for Specimen 3

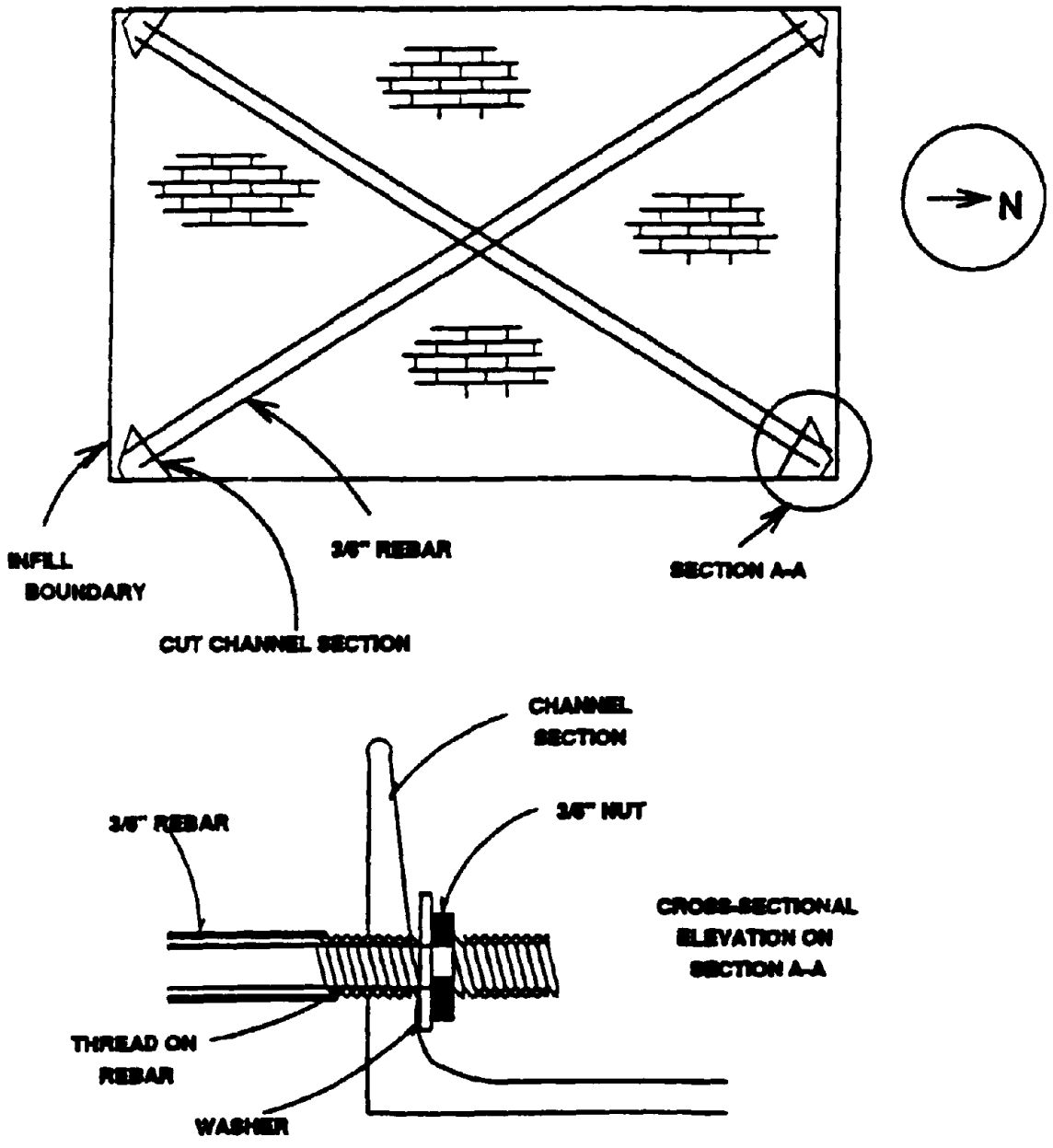

Fig. 2.8 Arrangement and identification of rebars within the infill panel for Specimen 3

SECTION 3 STEEL FRAME BEHAVIOR

3.1 Introduction

This section presents only the results for first frame that possessed (new) undamaged semi-rigid angle connection. The specimen is shown in Fig. 3.1. Fully reversed cyclic loading was applied to the upper and lower W8x21 beams at a frequency of 0.01 Hz, with a data sampling rate of 1 Hz for each of the 36 channels. In this study it was considered necessary to firstly obtain an understanding of the behavior of the steel frame prior to testing the infilled frames.

3.2 Hysteretic Response of the Bare Frame Specimen

The force-drift response for the bare frame is shown in Fig. 3.2. As can be seen, the specimen is elastic up to and including the ±1.00% drift sub-test. After that, degradation starts to be evident as the slope of the curve decreases. The end of the test is clearly shown by the two sharp breaks in the curve in the lower left-hand portion of the graph. The theoretical moment vs. joint rotation response of the bare frame test can be seen in Fig. 3.3. In order to convert the load on the specimen to moments in the beams and columns, a computer model of the bare frame was run for a lateral load of one kip. From all the four graphs, it can be seen that the joints are elastic up to and including the ±0.50% interstory drift test. Following this limit, significant hysteresis within the cycles is apparent indicating that the angle connections had yielded. Continued strength increase beyond a moment of 300 kip-in is due to strain-hardening of the plastic hinges that form in the angle.

From the raw test data, the moments at each strain gage locations were computed. Since the bare frame specimen had no infill, the theoretical moments could be determined based on statics. The theoretical vs. measured moments for both the beam and the column, for the first cycle of both the ±1.00% drift and the ±2.00% drift test are shown in Figs. 3.4 and 3.5. As can be seen, the theoretical and measured moments match quite well, especially in the beam. In the column, even though the measured moments are slightly offset from the theoretical moments, they do form a straight line in themselves, indicating that there is some further redistribution of moments amongst the joints. It is considered that on the basis of the agreement between the theoretical

moments calculated from statical equilibrium and the experimental moments inferred from beam bending strains, that this approach can be used to determine beam moments and hence contact stresses when the brick infill panel is present.

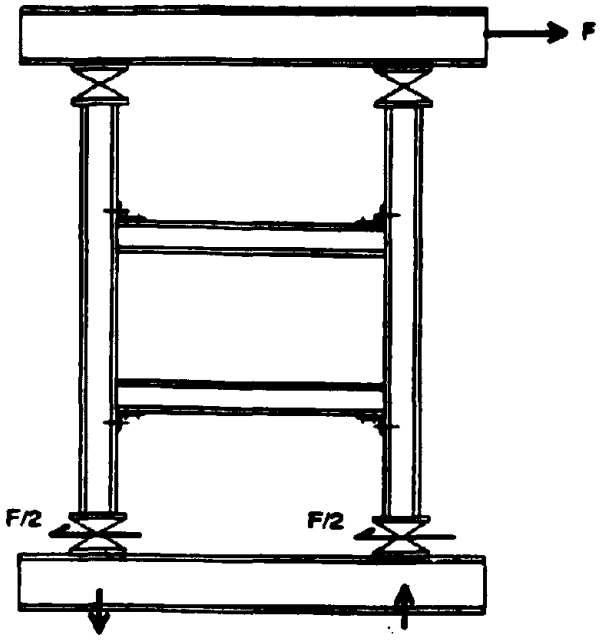

Fig. 3.1 Bare frame

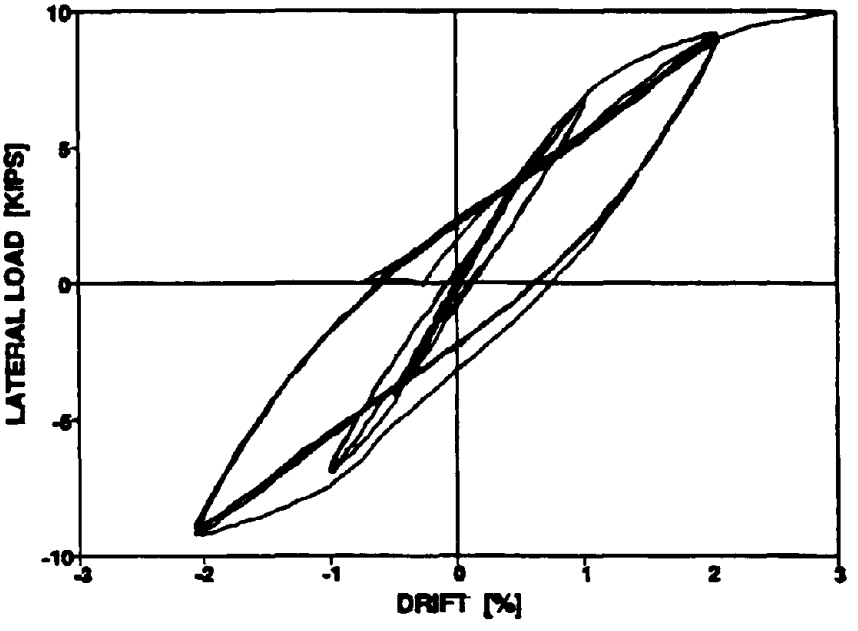

Fig. 3.2 Lateral load-drift response of bare frame specimen

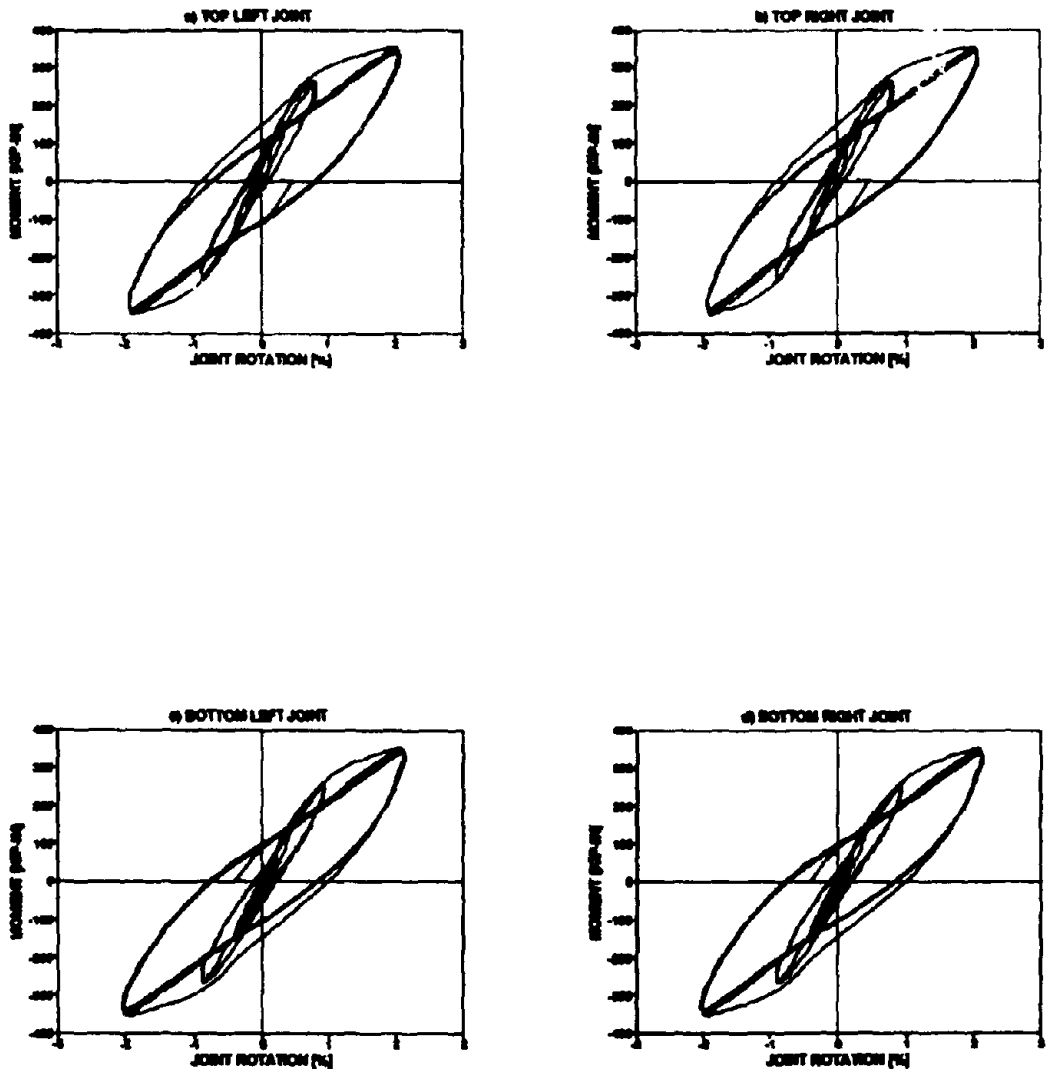

Fig. 3.3 Joint rotation response of the bare frame specimen

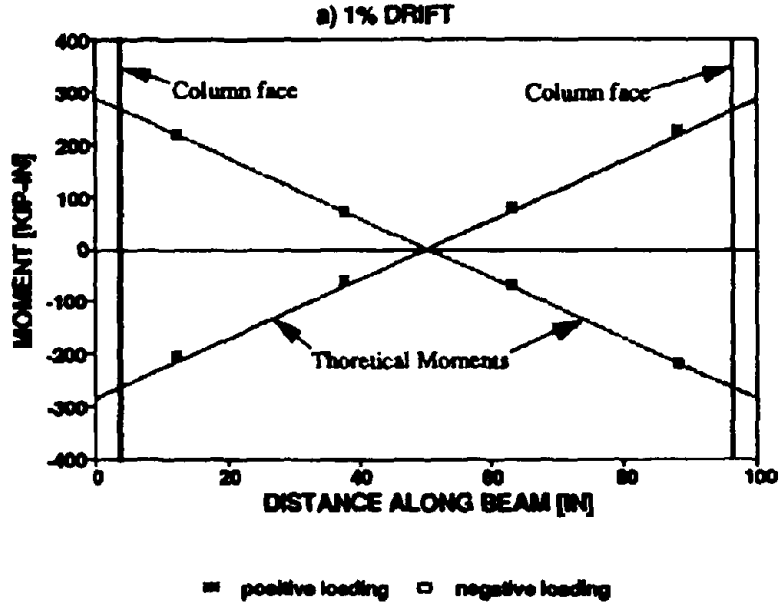

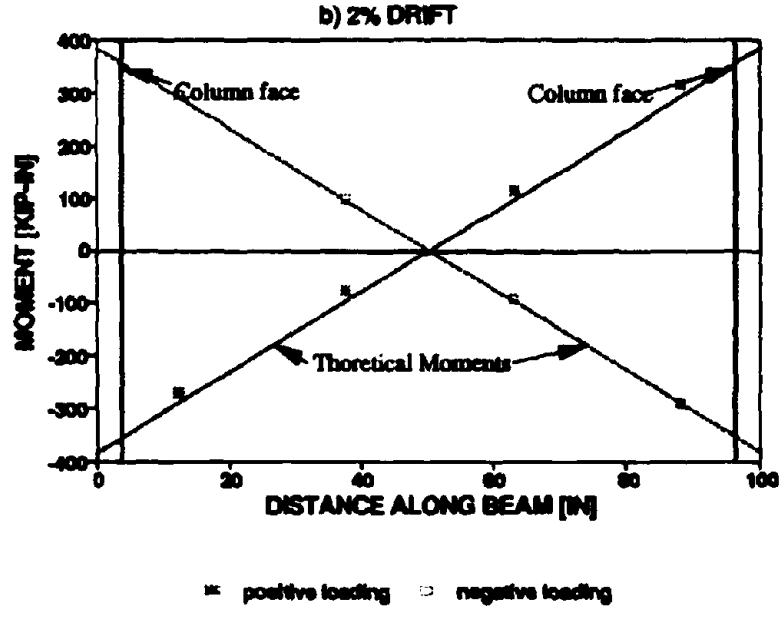

Fig. 3.4 Implied bending moments along the bottom beam (Specimen 1)

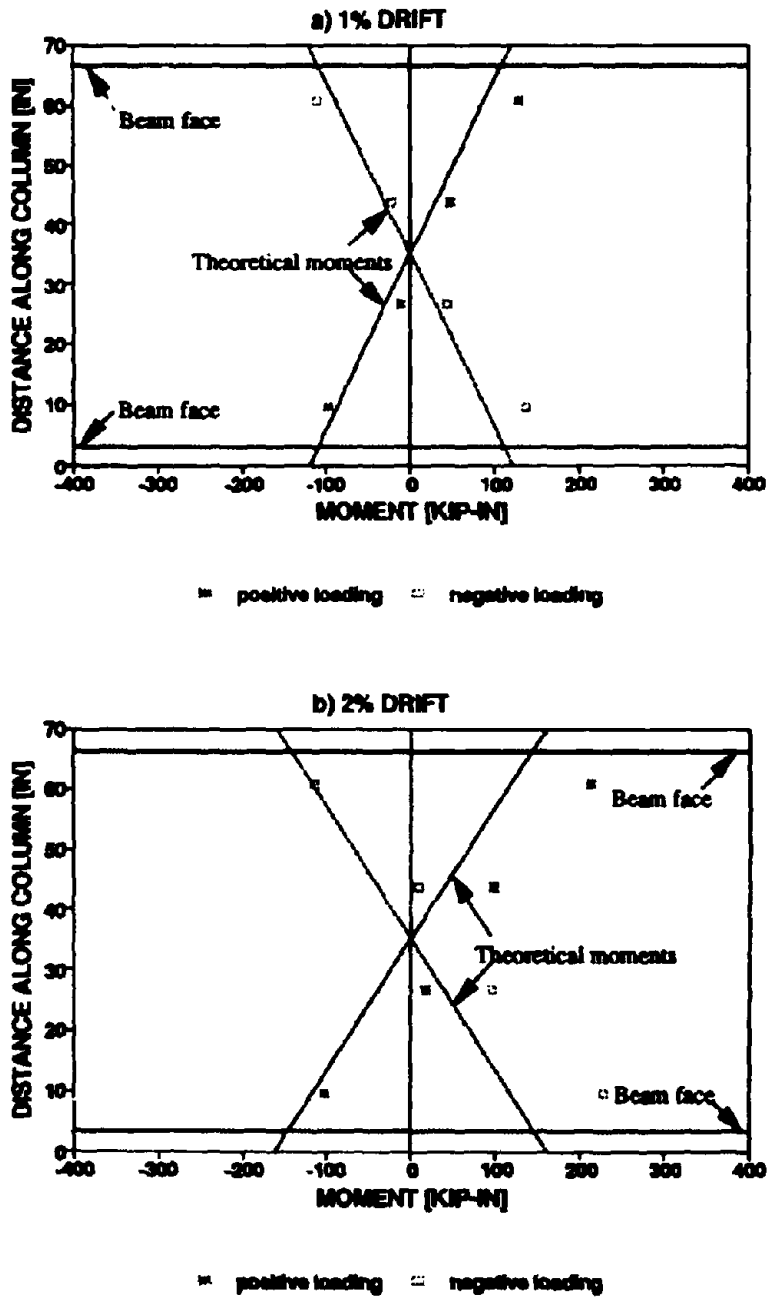

Fig. 3.5 Implied bending moments along the right column (Specimen 1)

SECTION 4

EXPERIMENTAL RESULTS FOR THE INFILLED FRAME SPECIMENS

4.1 Introduction

This section presents the results for each of the frames when tested with the presence of the brick infill. The first brick infilled specimen (Specimen 1) was initially tested, and then repaired with ferrocement and retested. Following this, Specimen 2 was retrofitted and tested. Specimen 3 was tested using diagonal rebars initially, repaired with an enhanced ferrocement overlay which contained the diagonal rebars and retested.

A 55-kip MTS servo-controlled hydraulic actuator, with a ±12 inch stroke, was used for Specimen 1 and a 250 kip actuator used for Specimens 2 and 3. An externally mounted load cell and internal displacement transducer automatically monitored the readings for the applied actuator force and stroke. Universal swivels on each end of the actuator allowed it to pivot during the test set-up and during the test itself. The actuator was controlled by an MTS 436 Control Unit with a function generator in drift control.

All transducers were routed into an amplifier and into an OPTIM MEGADAC data acquisition system, which had a 128 channel capacity. The raw data was then fed into a Compaq 386/20 microcomputer for analysis and reduction, using the OPTIM OPUS 5000 software.

Testing consisted of applying two completely reversed cycles between drift limits of ±0.25%, ±0.50%, ±0.75%, ±1.00% and ±1.50% using a sine wave input for interstory drift control at a cycling frequency of 0.01 Hz and a data sampling rate of 1.0Hz. Between each sub-test of two cycles, the infill was inspected for cracks in the mortar/bricks and the cracks were highlighted by a white chalk marker for easy identification in photographs.

4.2 Experimental Results for Specimen 1

4.2.1 Ordinary Infill Test

During the first sub-test(±0.25% drift), small microcracks could be observed in the mortar beds. During subsequent testing at larger drift amplitudes these cracks opened more widely and could

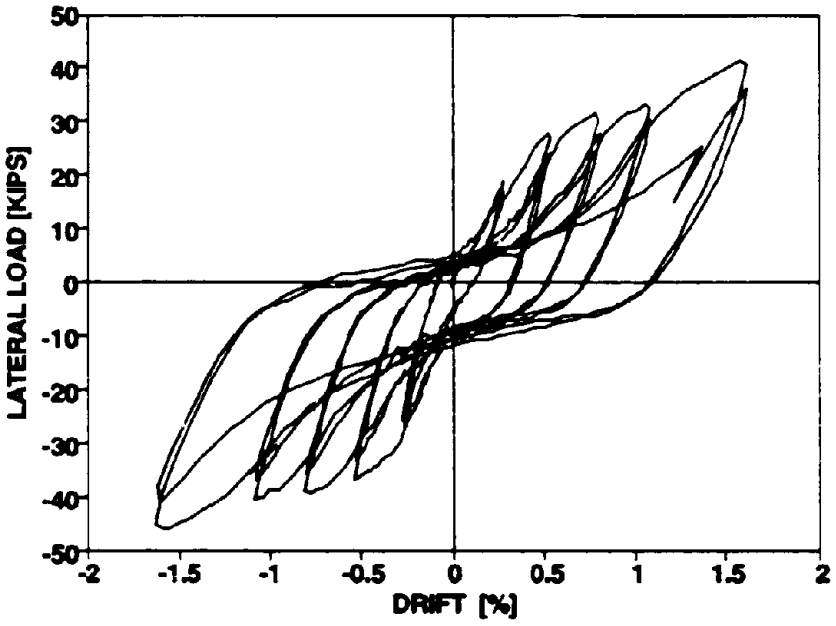

Fig. 4.1 Lateral load-drift response of ordinary infilled frame (Specimen 1)

easily be seen opening and closing along the compression diagonal during forward and reverse motion of the test specimen. During later stages of testing, new cracks formed at a steeper angle to the horizontal. These cracks appeared to be the beginnings of the formation of a secondary strut mechanism. At the completion of the last sub-test, the brick infill was still intact although the bond between the mortar and the infill did break along the top beam and the upper left portion of the infill.

Load Interstory-drift Response

Fig. 4.1 shows the load versus interstory drift of the ordinary infilled frame test for Specimen 1. It can be seen that there is a progressive increase in lateral load as the drift amplitude increased. On the second cycle of load at each drift limit there is a small loss in strength due to narrowing of the hysteresis loops. Less energy was also dissipated on the second cycles.

Joint Rotation Response

The load vs. joint rotation graphs of the top and bottom right joints shown in Fig. 4.2 (a) and (b) indicates the panel peak drift percentages corresponding to the first peak of each loading cycle. Two graphs show a similar response as that of the load vs. interstory drift results. For the top right joint, a noticeable shifting of the joint rotation is seen after the ±0.50% drift test. This is not seen in the bottom right joint most likely because of the fact that the infilled specimen is stronger in one direction and the joint response is greater for that particular direction. As in the load vs. interstory drift graph, there is a slight irregularity in the second cycle of the last (±1.50%) test, for each of the two instrumented joints. It is apparent that when the entire specimen shifted in the strong-floor holes, the load dropped temporarily and then reloaded to its original loading path.

Distribution of Moments

For the infilled frame test, six more pairs of strain gages were added to both the lower beam and right column. This was necessary because it was not known how the frame would react with an infill placed inside of it. It was hoped that the strain readings could help determine the response of the beam/column knowing the response of the bare frame. Figs. 4.3 (a) and (b) indicates the

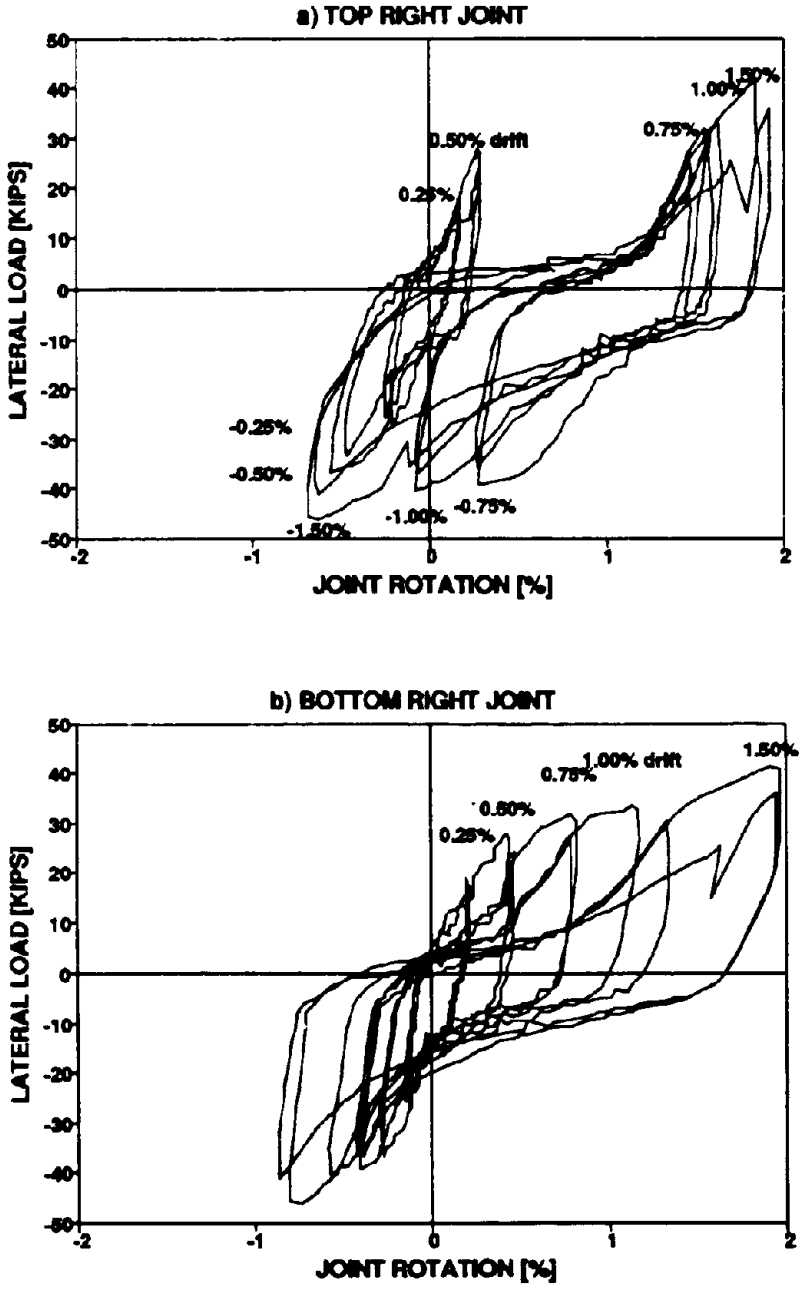

Fig. 4.2 Joint rotation response of ordinary infilled frame (Specimen 1)

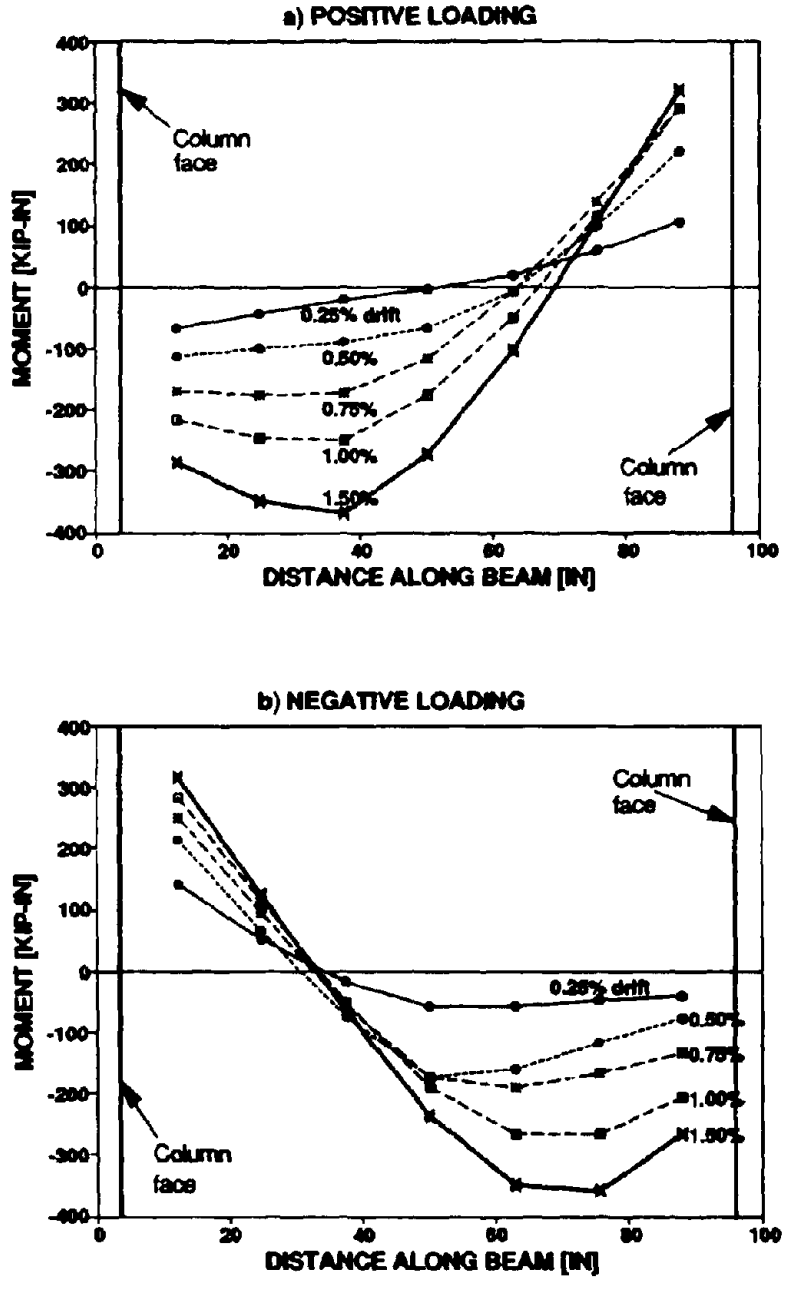

Fig. 4.3 Implied moments along bottom beam of ordinary infilled frame (Specimen 1)

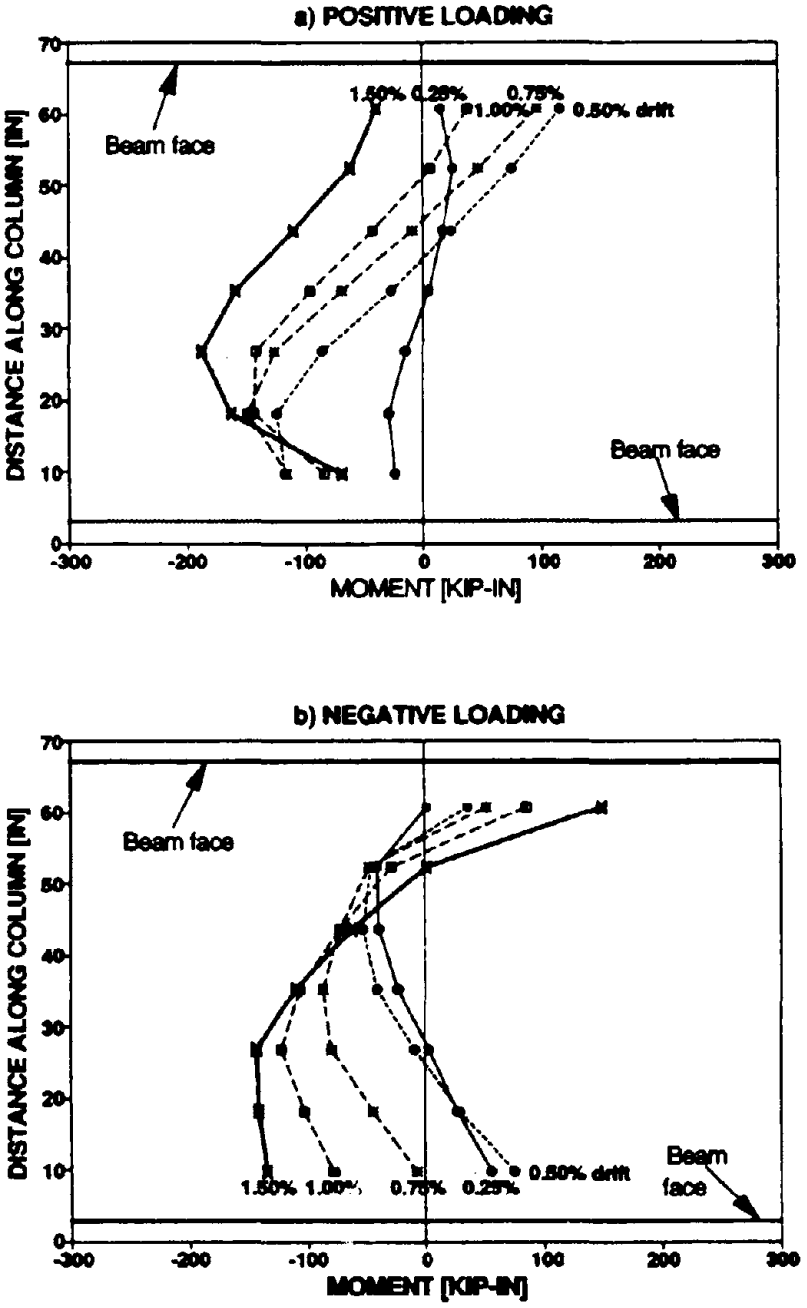

Fig. 4.4 Implied moments along right column of ordinary infilled frame (Specimen 1)

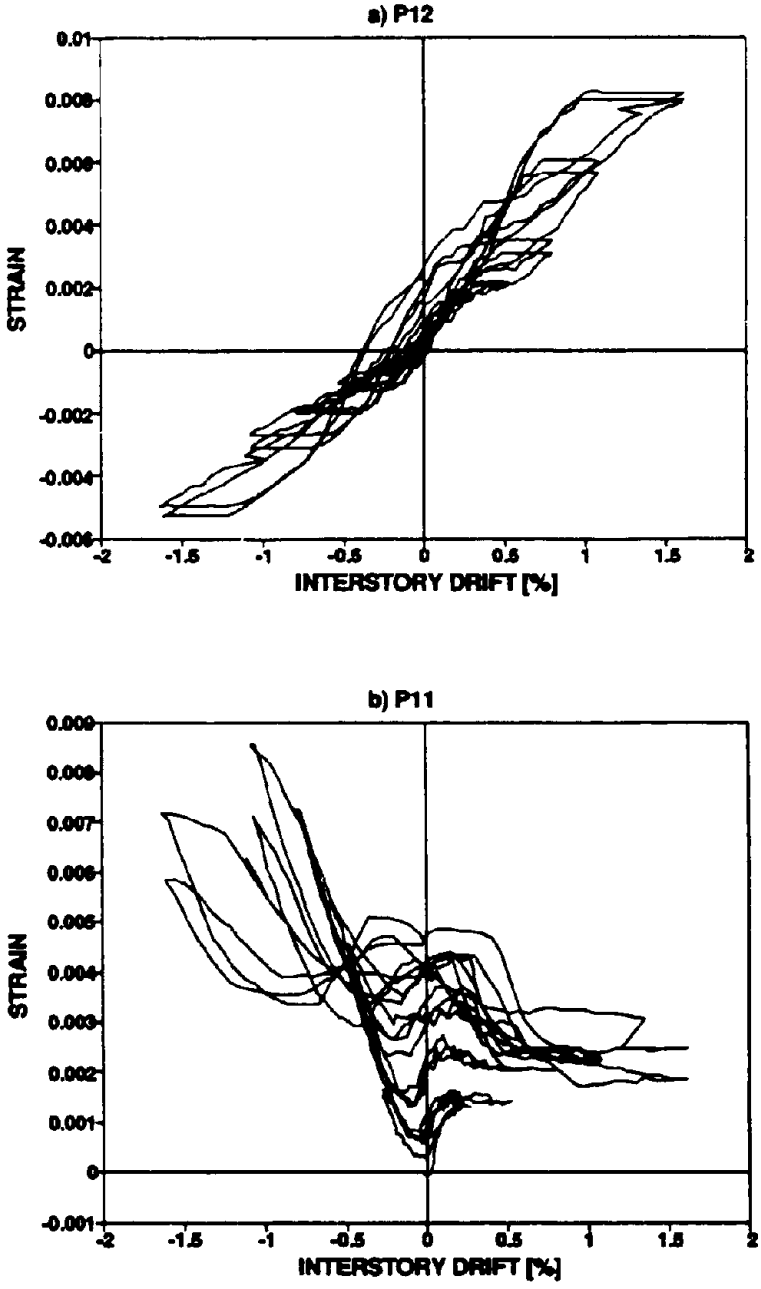

Fig. 4.5 Strain history of top right joint (Specimen 1)

moments for the bottom beam for positive and negative loading. Figs. 4.4 (a) and (b) indicates the moments for the column for positive negative loading.

Central and Corner Strains

Strain is defined as tension positive and equal to the change in length with respect to the gage lengths. Figs. 4.5 (a) and (b) indicates the strain histories of the infill panel as recorded by the strain gages P12 and P11. There is more activity on one side of the axes than on the other side indicating that the cracks opened more widely when loaded in the direction of positive drift.

4.2.2 Experimental Results for Specimen 1 after Repairing with Ferrocement

Visual Testing Observations

Cracks along the diagonal from the previous test on the infilled steel frame tested were clearly evident before testing commenced. Therefore, careful attention was paid to these cracks which were transmitted to the ferrocement during the testing of the repaired specimen. At the completion of the final cycle at a drift of ±1.5%, a wide diagonal crack could be seen in the center of the ferrocement coating. This was largely due to out-of-plane buckling of the coating between the anchors. Two additional cracks formed through the coating: one was vertical; another was horizontal. At the completion of the bare frame testing, there appeared to be no sign of fracture occurring in the joint angles due to low cycle fatigue.

Load-Interstory Drift Response

The lateral load-interstory drift response of the repaired infill specimen test is shown in Fig. 4.6. The purpose of the ±0.25% drift cycle was to examine the initial stiffness of the repaired infill. For the ±1.5% drift cycle the strength can be compared with the results at the end of the testing. This will be discussed later. Under the second cycle of loading, there was a significant strength loss due to damage in the infill coating.

Joint Rotation Response

From the load vs. joint rotation response (Figs. 4.7 (a) and (b)) it can be seen that the top rotation

is relatively smaller than the bottom. The top joint appears to be moving less probably due to some extra stiffening and strengthening in that corner of the infill However, it is evident that significant hysteresis can be seen that indicates the angle connections had yielded.

Distribution of Moments

From the raw test data, the moments at each gage location were computed when either maximum positive loading or maximum negative loading was applied. The figures indicate that at high drift limits the curved shape of the bending moment diagram increases indicating an increase in the secondary contact stresses. Figs. 4.8 (a) and (b) indicate the measured bending moments of the bottom beam for negative and positive loading. Figs. 4.9 (a) and (b) indicates the measured bending moment for the right column for negative and positive loading. This appears to be due to the dilation of the masonry at large shear strains.

4.3 Experimental Results for Specimen 2

The retrofitted specimen (Specimen 2) was tested in a similar fashion to the repaired specimen (Specimen 1). However a few important differences in the testing procedures were carried out. Sub-tests were run which consisted of one trial test (±0.25% drift limit), one complete reversed cycle of ±0.25% drift limit test and two complete reversed cycles of ±0.50%, ±0.75%, ±1.00% drift limit test. Finally, four complete reversed cycles at a ±1.5% drift limit test were run. This loading history was the same as the combined effect on the bricks of the pre and post-repair loading history used previously on Specimen 1.

Visual Testing Observations

During the testing of the retrofitted specimen, observations were made of both the brick masonry and ferrocement coating. As the tests progressed and the interstory drift limit increased, the cracks in the ferrocement coating side clearly came into view. Initially micro-cracking commenced in the compressed corners. At the ±0.75% drift limit, an obvious crack could be seen at the bottom left corner of the ferrocement coating. During later tests, the cracks could be easily seen opening and closing during the forward and reverse motion of the test specimen and maximum opening was about 1/4 inch. For the cycles with the ±1.00% drift limit, cracks in the

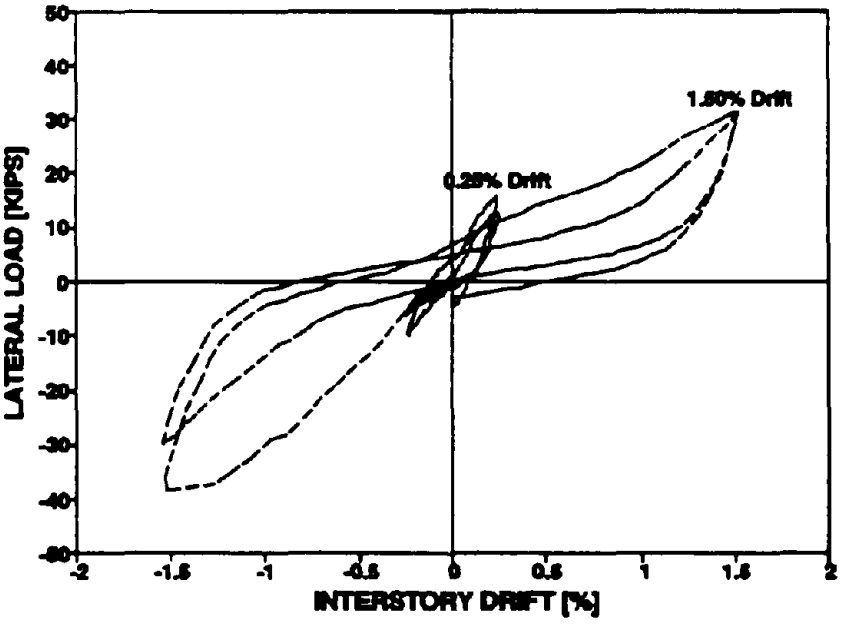

Fig. 4.6 Lateral load-drift response of repaired infilled frame (Specimen 1)

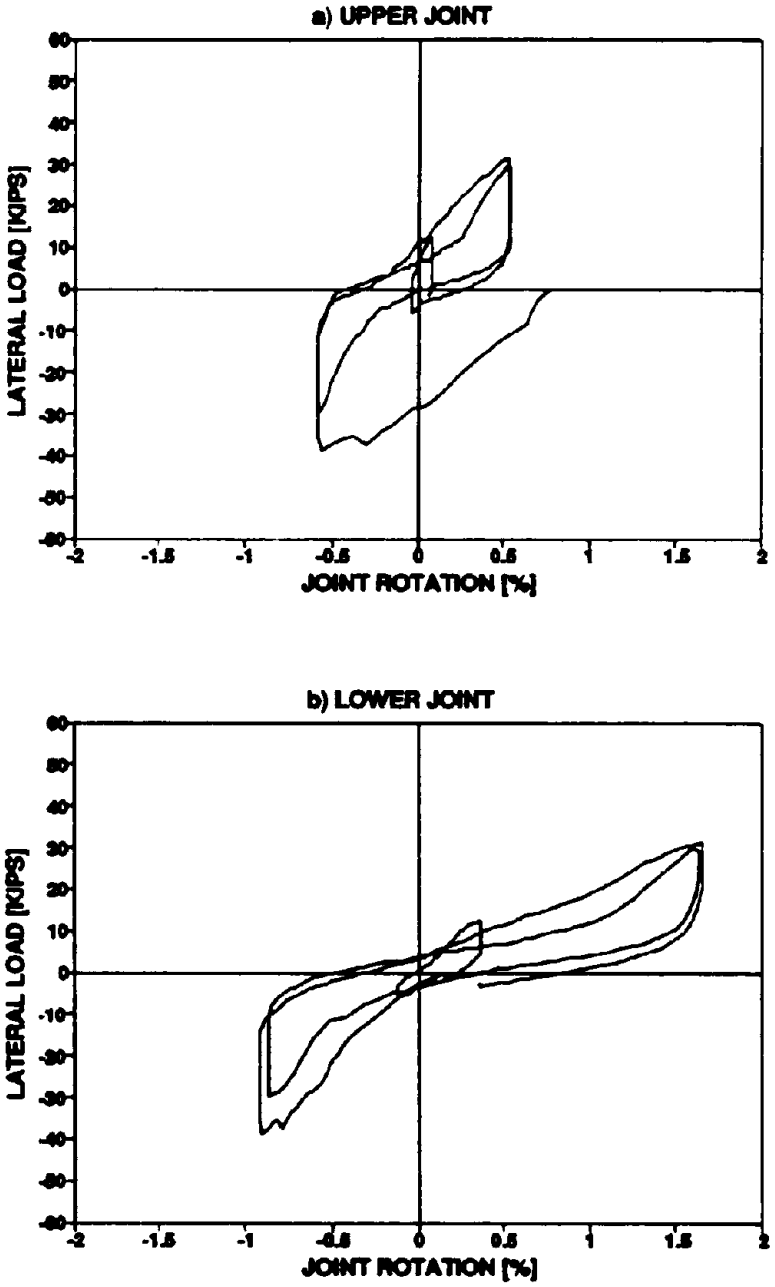

Fig. 4.7 Joint rotation response of repaired infill (Specimen 1)

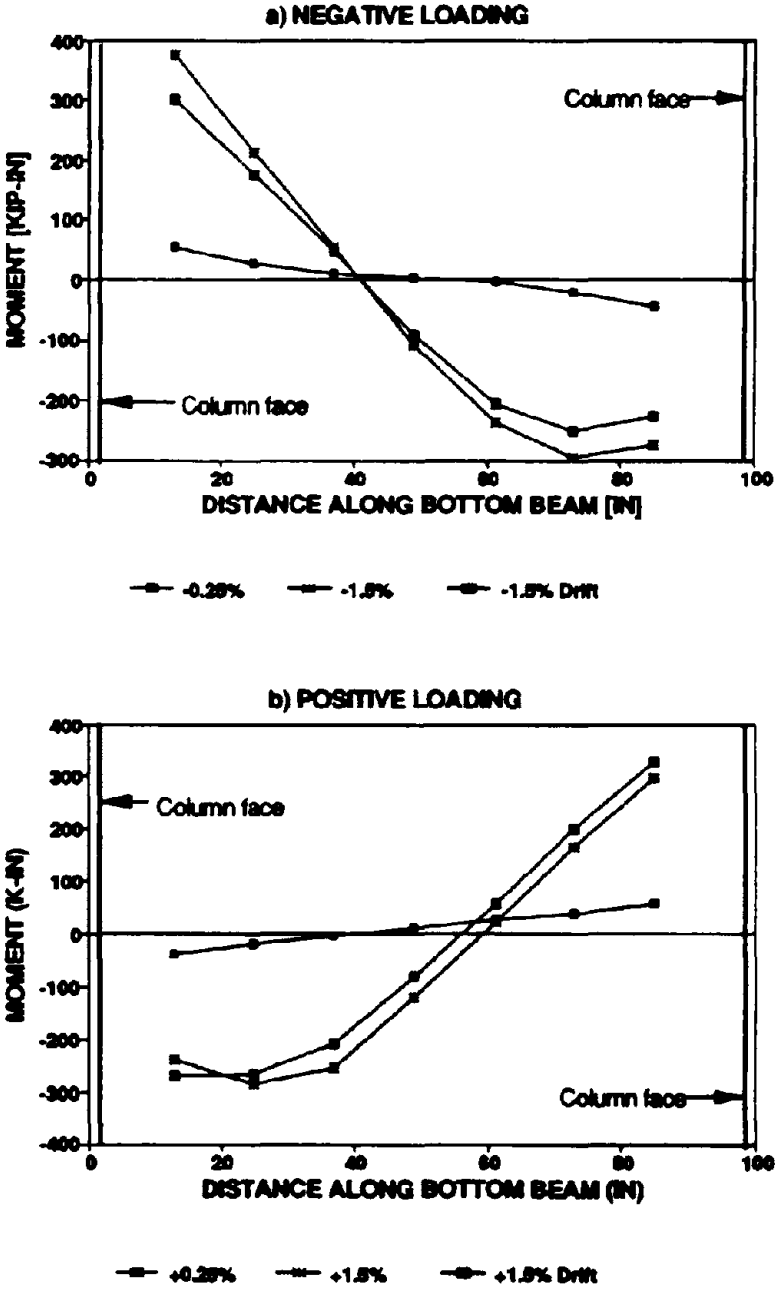

Fig. 4.8 Implied moments on the bottom beam of the repaired infill (Specimen 1)

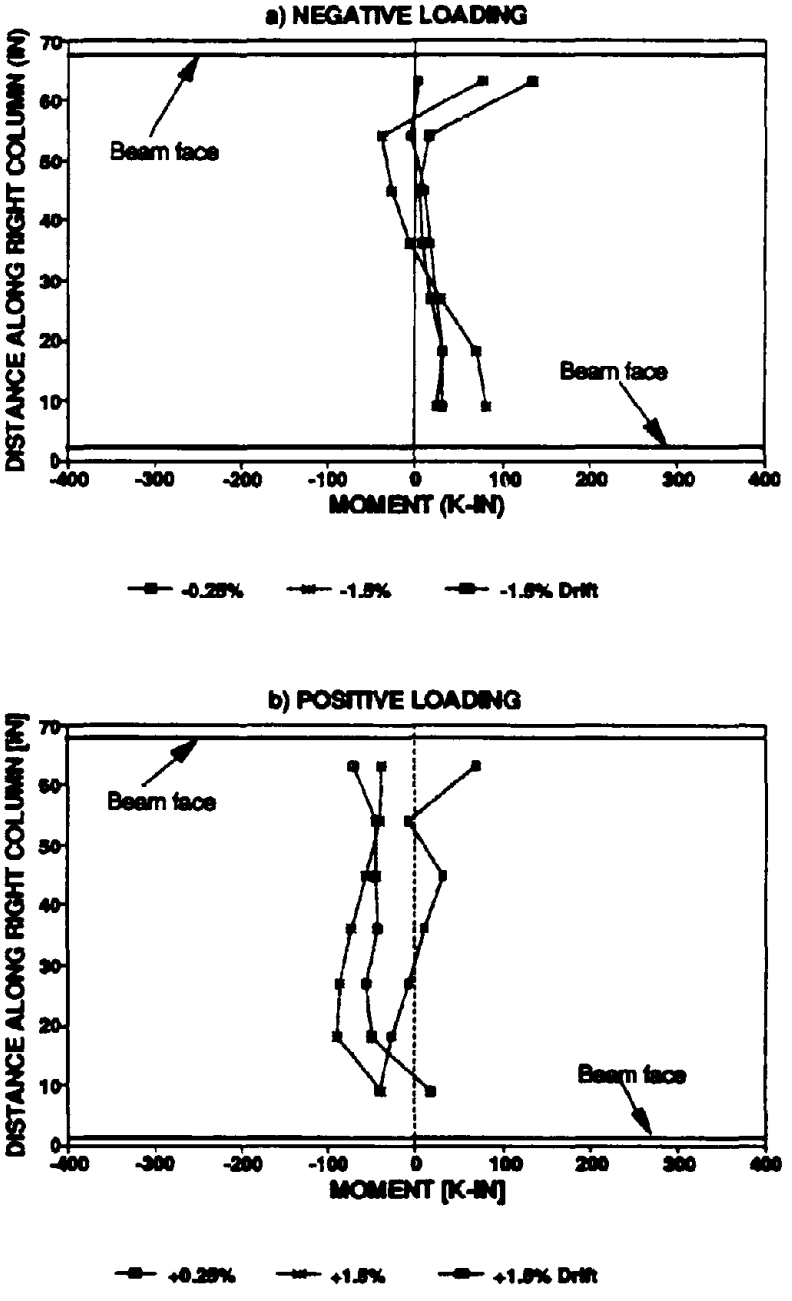

Fig. 4.9 Implied moments along the right column of the repaired infill (Specimen 1)

center of the ferrocement panel appeared and some mortar chips and dust started to fall from the edges of the coating. The whole infill panel started to offset laterally in the out-of-plane direction. During the first cycle with the ±1.5% drift amplitude, the cracks in the center of the infill panel coating grew very wide with a large diagonal opening resulting in exposure of the wire mesh. More cracks appeared and more mortar fell from the coating side during the next 3 cycles during the ±1.5% drift limit test. At completion of the infill testing, the whole infill panel had "walked" out-of-plane by 1.5 inches and 1.0 inch at the right hand column side and one inch on the left hand column side, respectively. As the infill panel moved laterally out of plane, the lateral load could not be transmitted directly into the ferrocement. By the commencement of the final four cycles at the drift of ±1.5%, only the bricks were in direct contact with the upper and lower beams.

On the brick side of the panel, only fine cracks could be seen at the completion of testing. It was evident that the presence of the ferrocement distributed the cracking throughout the masonry in contrast to the one or two diagonal cracks that opened in the repaired infill specimen.

At the completion of the final bare frame test, the areas around the beam and column connections appeared to be undamaged and in good condition. Clearly, all damage in the bare frame tests was concentrated in the semi-rigid bolted connections.

Load-Interstory Drift Response

The load-interstory drift response of the retrofitted specimen test is shown in Fig. 4.10. It is evident that there is a consistent amount of degradation in strength which is of the order of -15%, -10% and -5% for each cycle at a given drift amplitude. However, the overall response shows an increase in strength as the drift amplitude was increased.

Joint Rotation Response

Fig. 4.11 (a) and (b) shows the load vs. joint rotation response for the top and bottom joints of the retrofitted infill test. The panel peak drift percentages for both these graphs are shown corresponding to the first peak of each loading cycle. These two graphs show that a similar response as that of the load vs. interstory drift results. It should be noted that the reduction of

joint rotations occurs when the joint is closing in on the panel, whereas in the reverse direction the diagonal strut helps to open the joint more than the drift angle.

Distribution of Moments

For the retrofitted infilled frame test, seven pairs of strain gages were added to the upper beam. This was considered necessary because it was not known how the top beam of the frame would behave. The strain gages of both the lower beam and right column were kept the same as the previous tests. The measured bending moments for the top and bottom beam for negative loading is shown in Figs. 4.12 (a) and (b); and for positive loading is shown in Figs. 4.13 (a) and (b). The bending moments for the right column for negative and positive loading are shown in Fig. 4.14 (a) and (b).

Diagonal and Vertical Strains in the Corner of the Infill Panel

The strain vs. drift graphs for the corner portion of the coated infill are shown in Fig. 4.15 and Fig. 4.16. As expected from Fig. 4.15 it can be seen that under positive drift, the top right and lower left joints are under tension and compression, respectively. Corner crushing was visually observed when the drift was increased from ±1.0% to ±1.5%. Here the corner strains have increased from about -0.003 to either -0.006 or -0.010 for the top right and bottom right joints, respectively. Such a strain magnitude would normally indicate crushing in the masonry.

4.4 Experimental Results for Specimen 3

The experimental set-up was the same as that for the previous two specimens except that a slight modification was made near the beam-column joints at the angle seat. A cut channel section was fillet welded onto the horizontal leg of the angle connections. Two 3/8" holes at a distance of 3" apart were drilled on the outer flange of each channel section. Two #3 rebars, with their ends threaded over a length of 6", with a 5/16" thread were passed through the two holes in the channel section. These rebars were set up diagonally across the infill panel. The yield force of the threaded portion of the rebars was measured as 7.3 kips. This implies a stress of 66 ksi. in the unmachined portion of the deformed bar. The ends were connected in such a way that the rebars acted only in tension. In compression, the rebars were designed to move freely into the

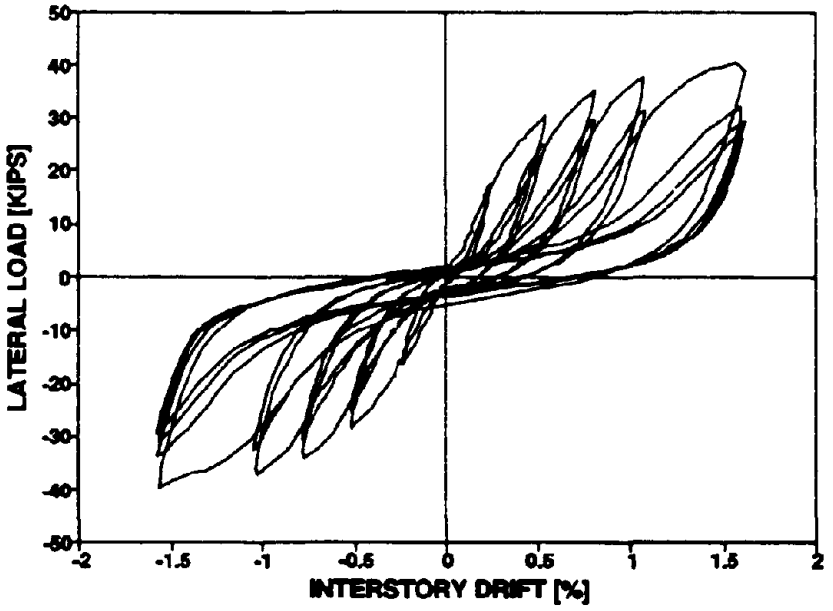

Fig. 4.10 Lateral load-drift response of retrofitted infill (Specimen 2)

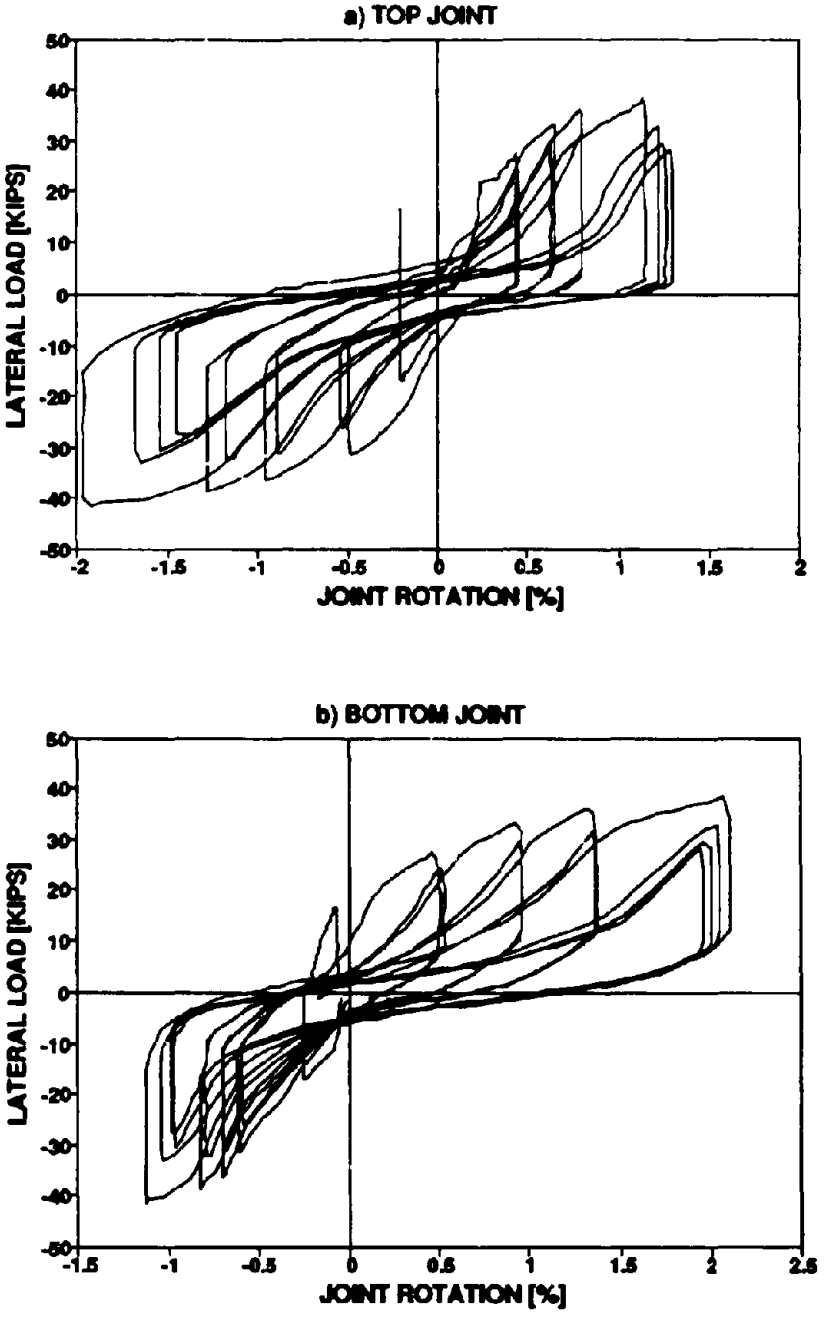

Fig. 4.11 Joint rotation response of retrofitted infill (Specimen 2)

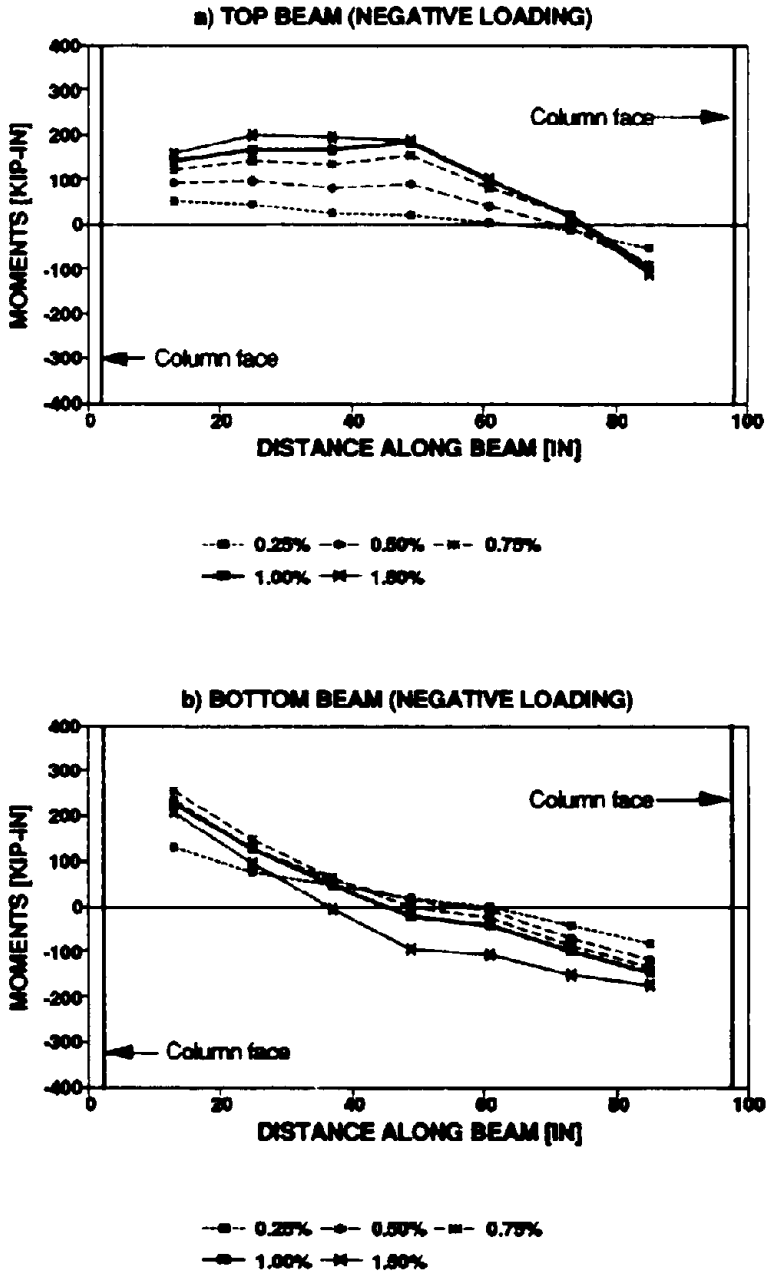

Fig. 4.12 Implied beam moments for negative loading (Specimen 2)

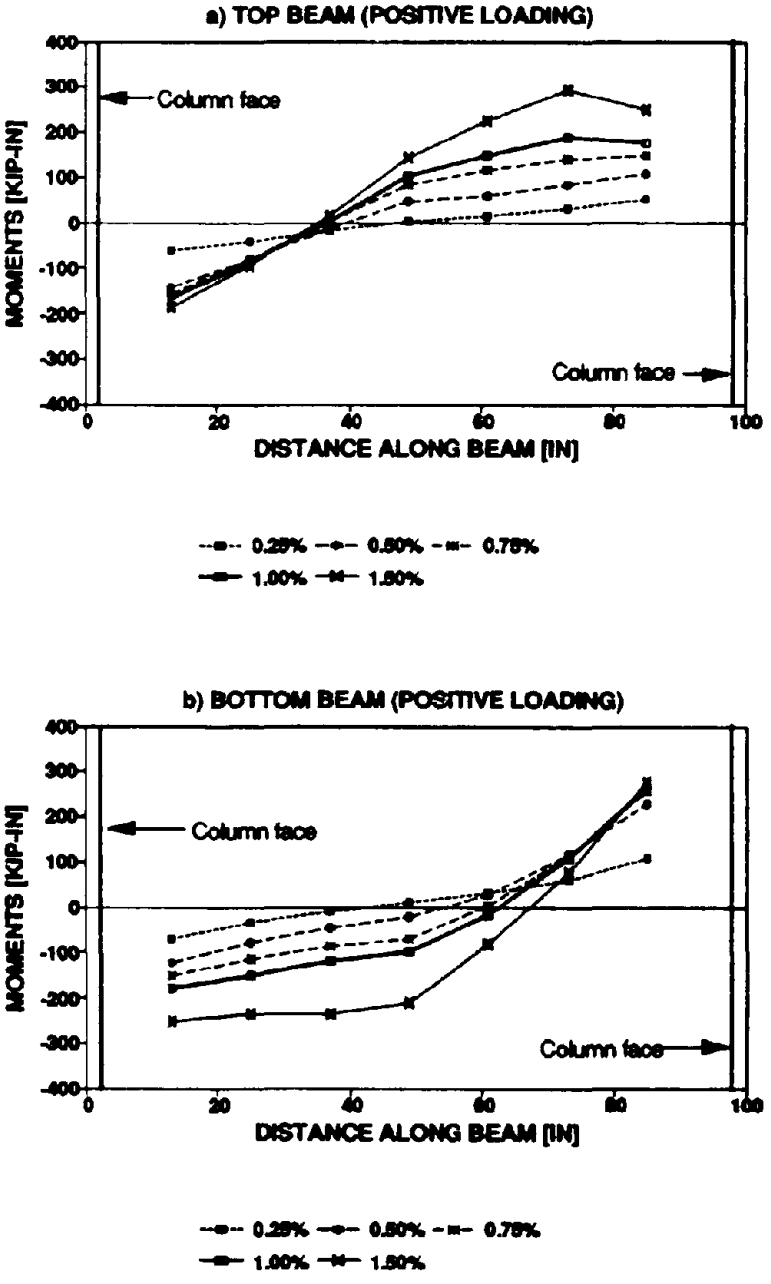

Fig. 4.13 Implied beam moments for positive loading (Specimen 2)

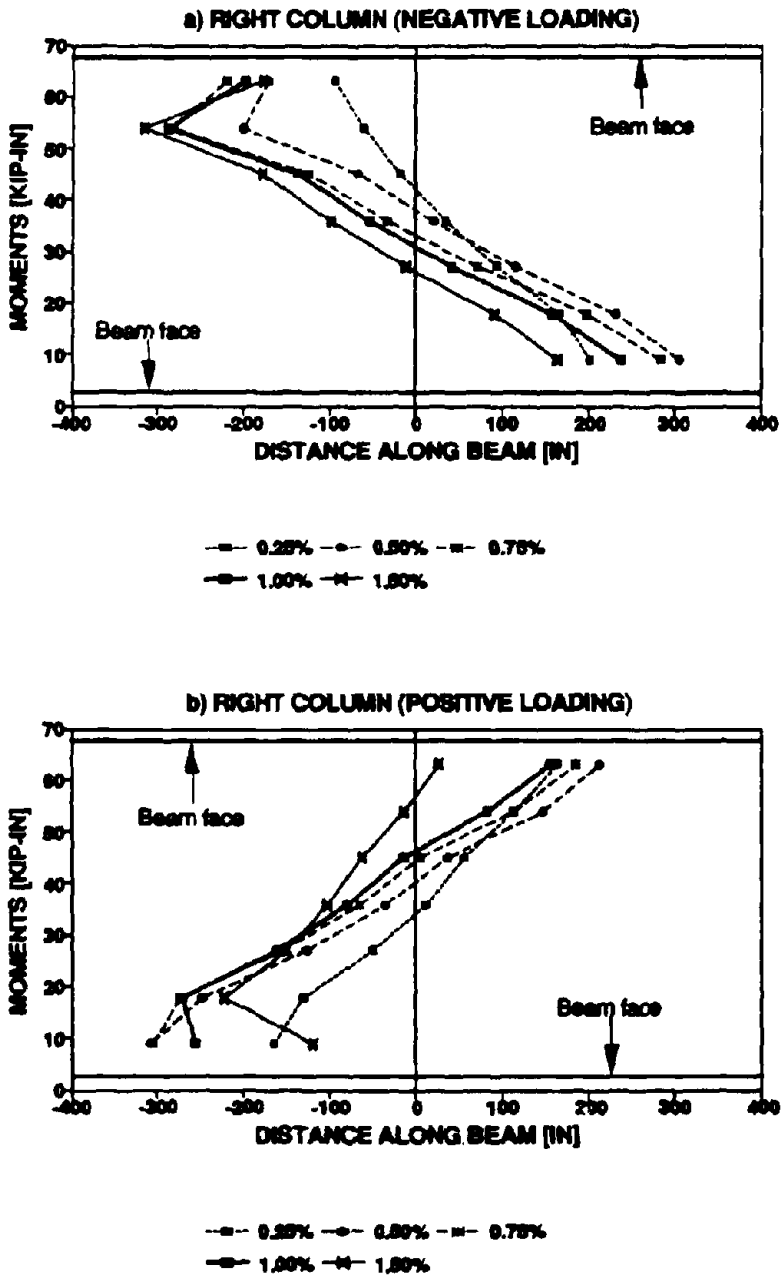

Fig. 4.14 Implied moments along the right column for Specimen 2

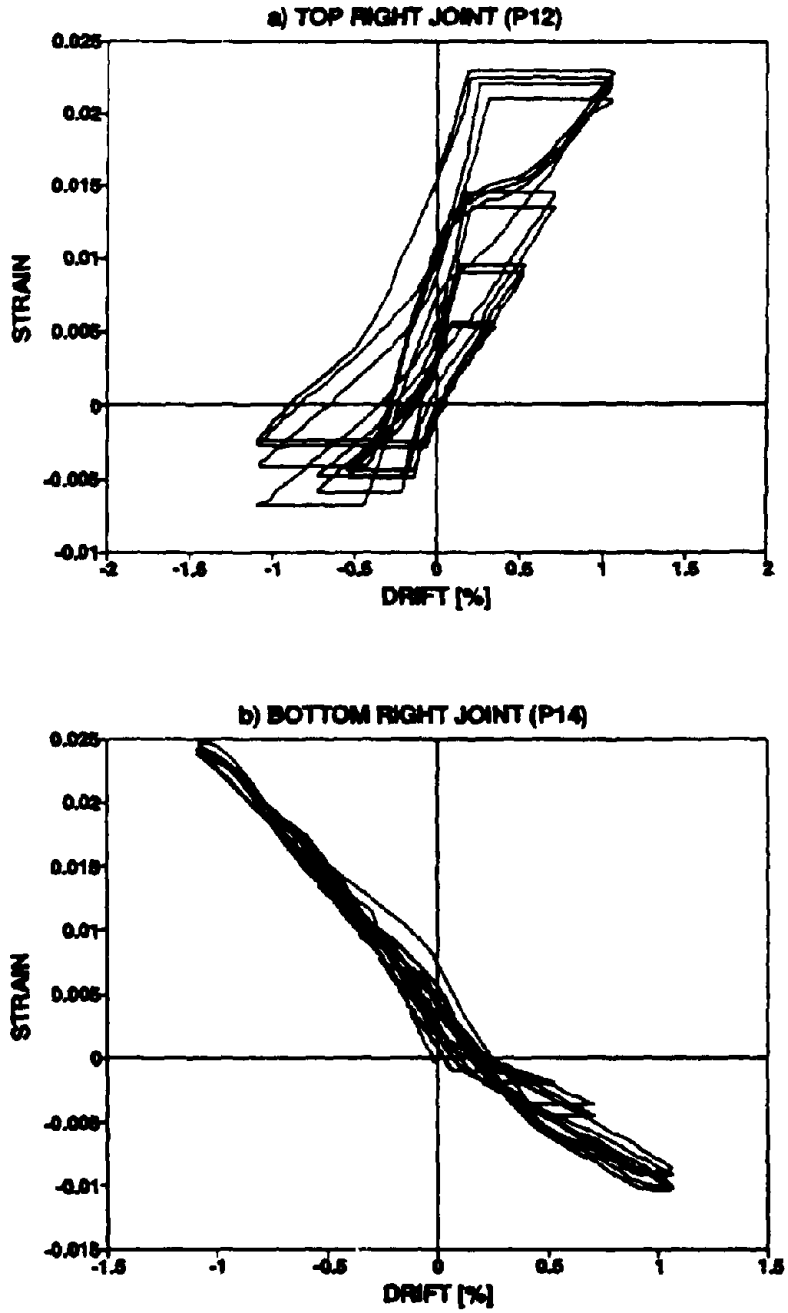

Fig. 4.15 Diagonal strains at corners of infill for Specimen 2

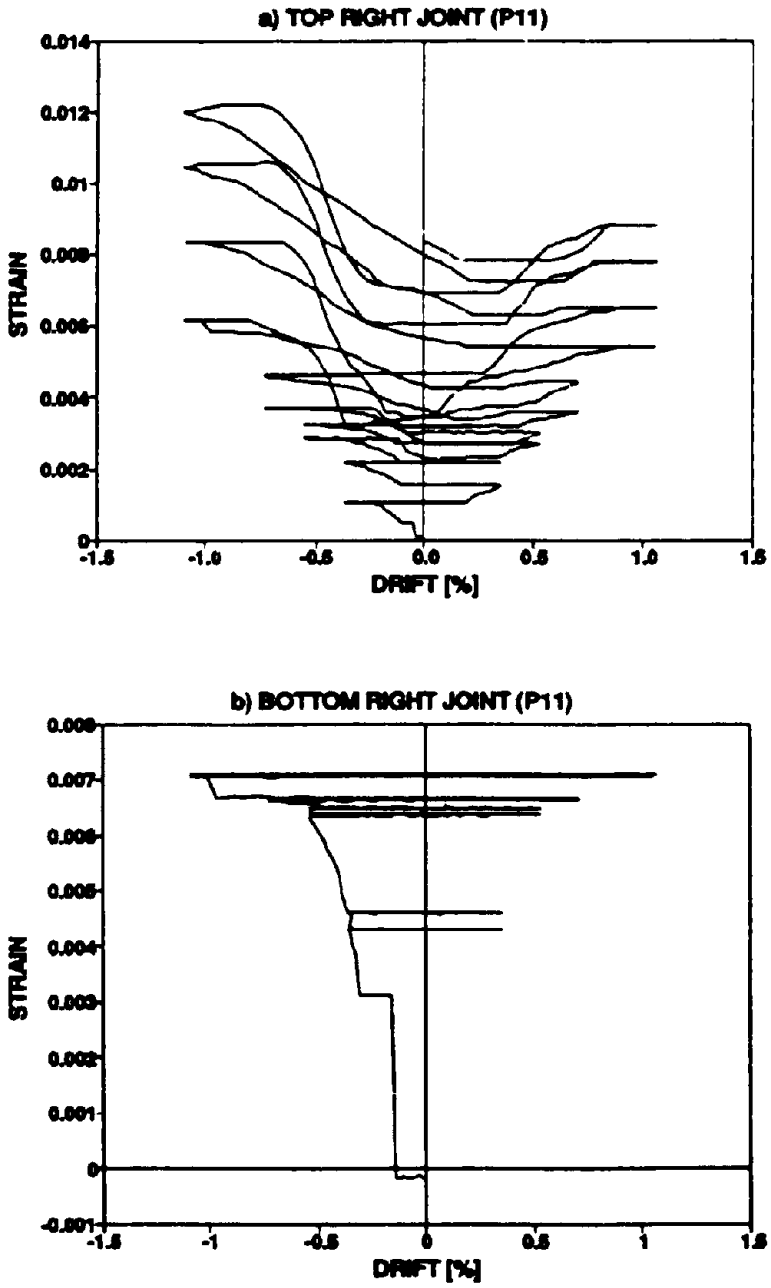

Fig. 4.16 Vertical strains at corners of infill for Specimen 2

fabricated cut channel section and not take any load.

An instrumentation check was done on Specimen 3 prior to the first test, by subjecting the frame to a complete reversed cycle of ±0.25% drift. Following this, testing was performed in three distinct phases as follows:

Phase I: One pair of rebars (from the top left to bottom right corner) were tightened a little to test for rebar action under negative (push) actuator forces. The frame was loaded with two complete reversed cycles at a drift amplitude of ±1.5%.

Phase II: All the rebars were tightened up at their ends and the frame was then subjected to one complete reversed loading cycle at a drift amplitude of ±1.5%.

Phase III: The enhanced ferrocement coating was applied to the infill. As described in Section 2.4, the previously yielded diagonal rebars were replaced with a new set of rebars which were sandwiched between an inner and outer layer of wire mesh, as shown in Fig. 2.3 (b). Following an initial ±0.25% drift subtest, six completely reversed cycles of loading were applied to a drift amplitude of ±1.5%.

4.4.1 Results for Phases I and II

Fig. 4.17 (a) and (b) shows the experimental load-drift results for Phase I and II testing. It can be seen that in Phase I, under reverse loading the tensile contribution from the diagonal rebars added 18 kips to the apparent shear strength capacity of the panel system. If the component of lateral load contributed by the diagonal rebars at yield is equal to about 12.56 kips, then it is evident that the diagonal tension in these bars also provided some confining action to the diagonal compression strut, thus enhancing the strength capacity of the masonry infill.

Following the initial stage of testing, the yielded diagonal reinforcement was tightened and new bars placed along the other diagonal. It is evident from the results that some additional strength (about 9 kips) was provided under positive loading, but as expected, little difference was noted under reverse loading due to fracture of one of the bars. At the completion of the Phase II testing, there was a considerable amount of compression cracking near the infill corners. However, outside these zones, there was only minimal evidence of cracking with a few fine micro-cracks detectable along the tension diagonals.

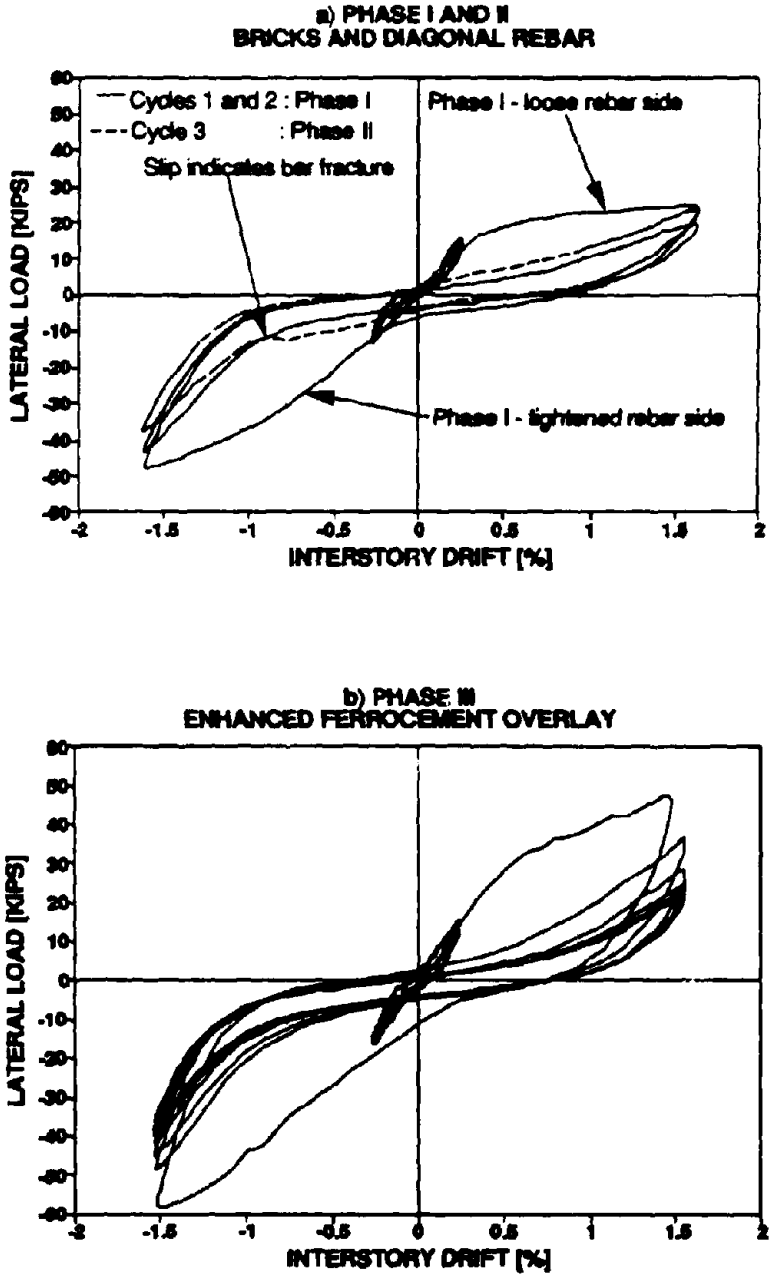

Fig. 4.17 Lateral load-drift response of Specimen 3

4.4.2 Phase III Results

The load-interstory drift response of Specimen 3 for the ordinary infill and the repaired infill are shown in Figs. 4.17 (a) and (b). The hysteresis curves show relatively more energy absorption when compared to Specimens 1 and 2.

Figs. 4.18 (a) and (b) shows the load vs. joint rotation response for the top and bottom joint of the repaired infilled frame test. The panel peak drift percentages for both these graphs are shown corresponding to the first peak of each loading cycle.

The measured bending moments of the top and bottom beams: for the ordinary infill plus rebar are shown in Figs. 4.19 and 4.20 and for the repaired infill in Phase III are shown in Figs. 4.21 and 4.22.

Figs. 4.23 to 4.24 shows the strain histories of the left and right columns for the inner and outer face of the columns in the case of the ordinary infill plus rebars and Figs. 4.25 to 4.26 shows the same in the case of the repaired infill.

Figs. 4.27 to 4.28 shows the strain histories of the rebars for the ordinary infill plus rebars. Figs. 4.29 to 4.30 shows the strain histories of the rebars for the repaired infill. It is clear from these graphs that the rebars have yielded.

4.4.3 Discussion of Visual Observations in Phase III

The photographs show the different stages involved in the testing of Specimen 3 with the enhanced ferrocement overlay.

Fig. 4.31 shows the lower corner of the beam-column joint (connected by a semi-rigid connection) on the side of load application. The photograph shows the stage during the second ±1.5% drift cycle during which part of the rebar connector (the fabricated channel) broke apart from the semi-rigid connection. This could be due to improper application of the fillet weld to attach the section to the connection. As seen, the bars are slack and the frame is being pulled away by the actuator, which indicates a positive loading cycle.

Fig. 4.32 shows the farther end of the coated side. The rebars 1 and 2 are in tension and hence

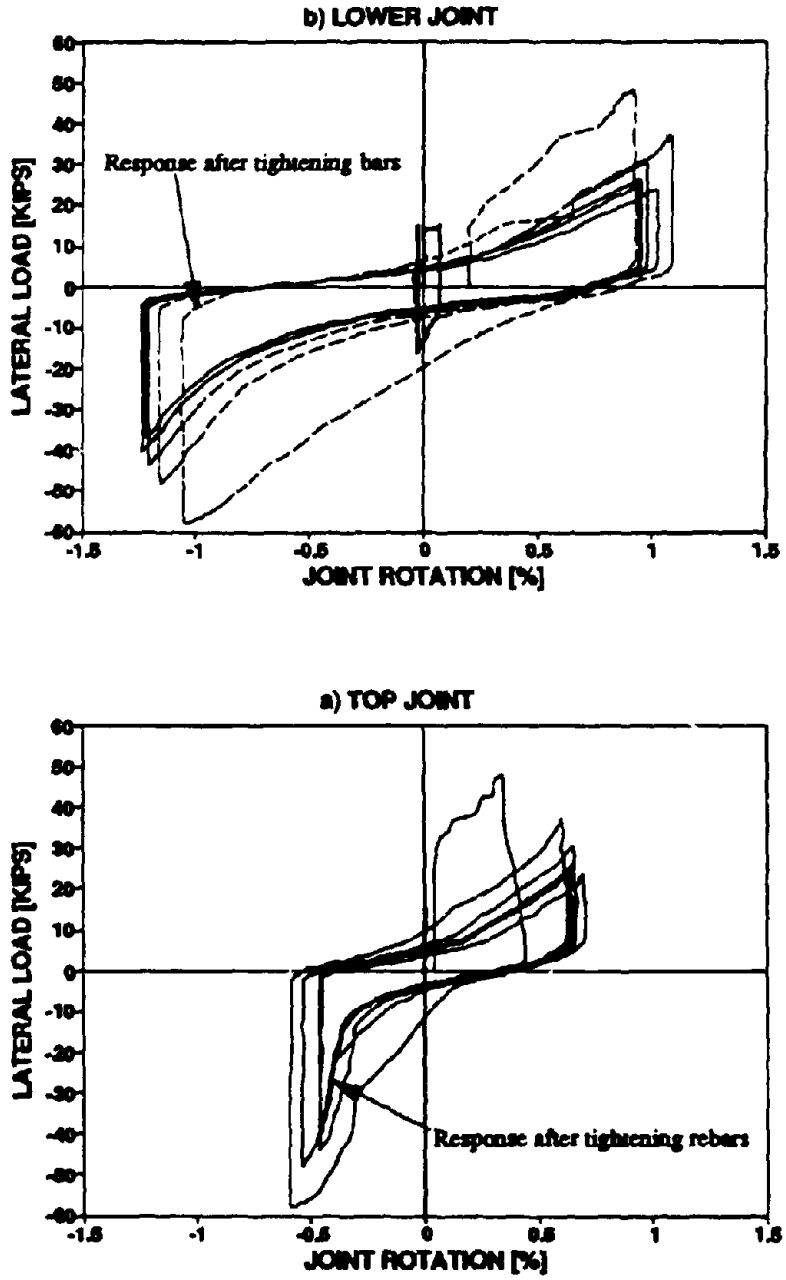

Fig. 4.18 Joint rotation response of Specimen 3 (Phase III)

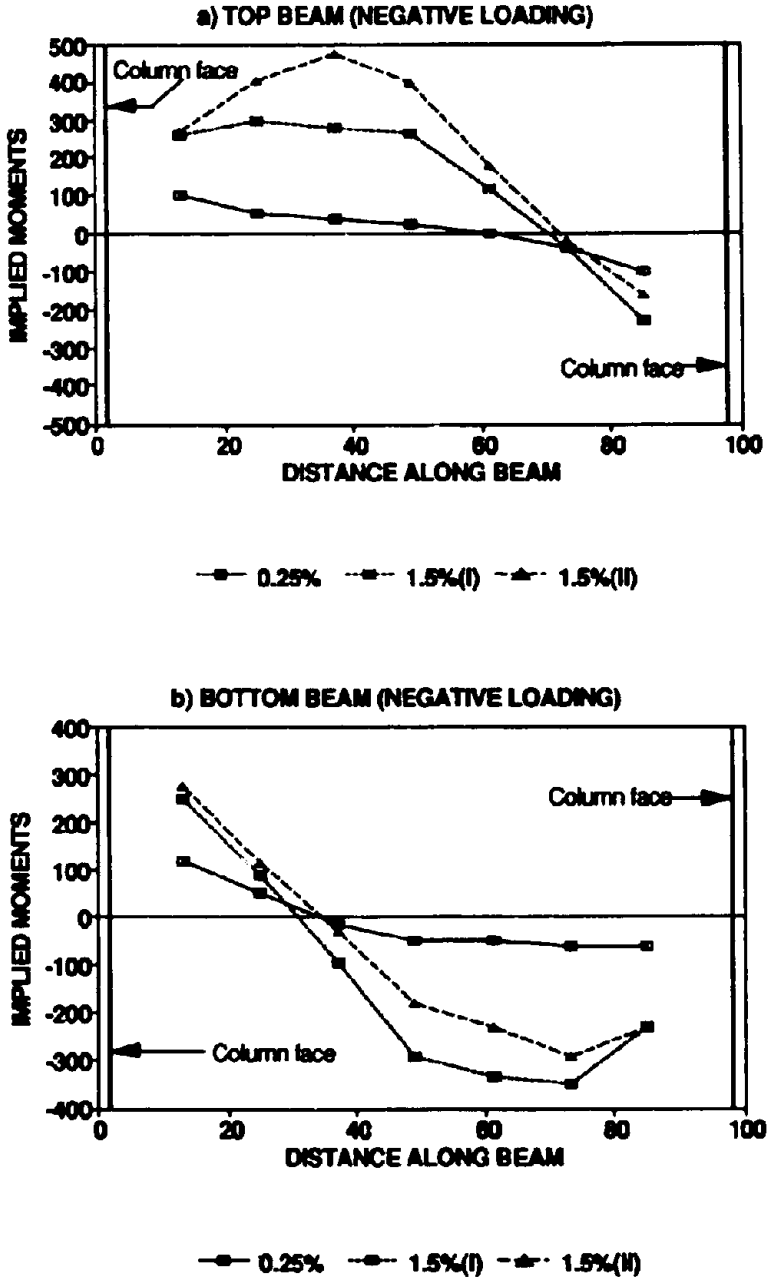

Fig. 4.19 Implied bending moments for negative loading of Specimen 3 (Phase I and II)

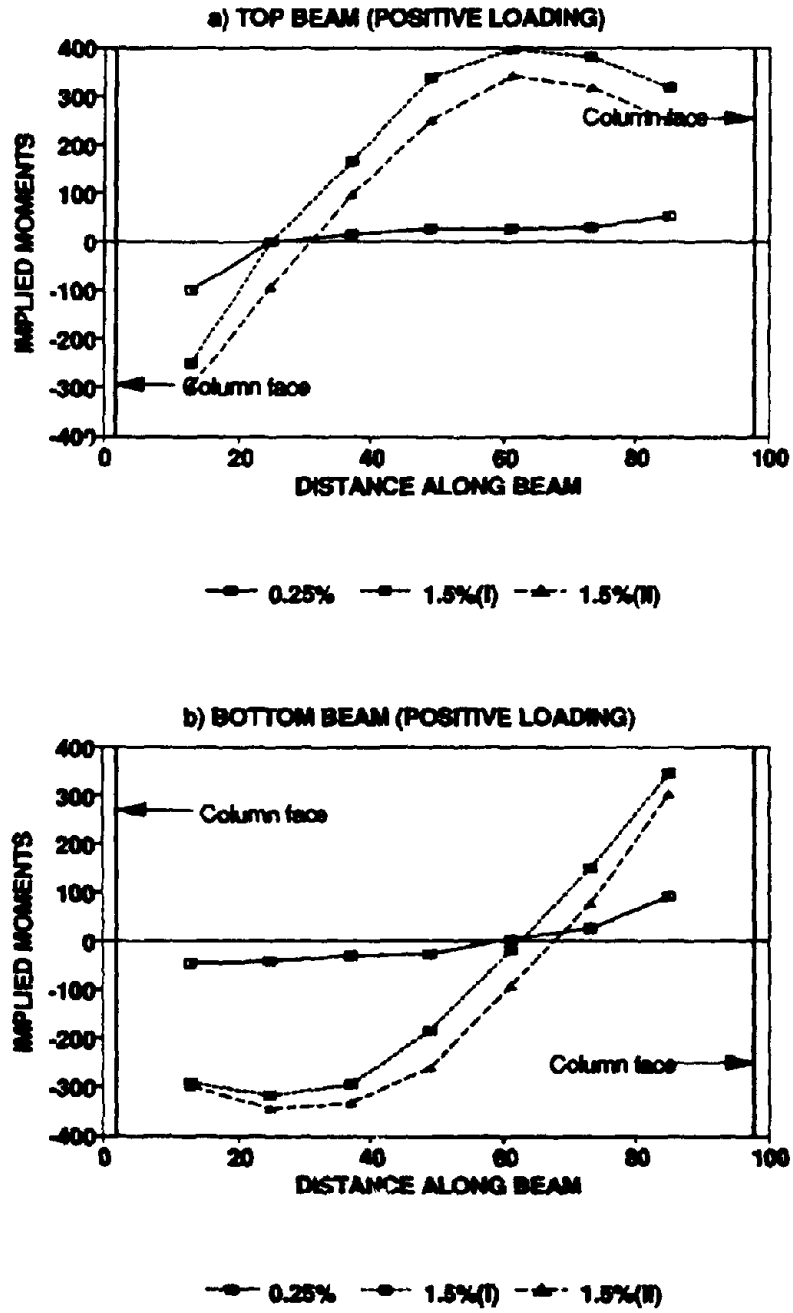

Fig. 4.20 Implied bending moments for positive loading Specimen 3 (Phase I and II)

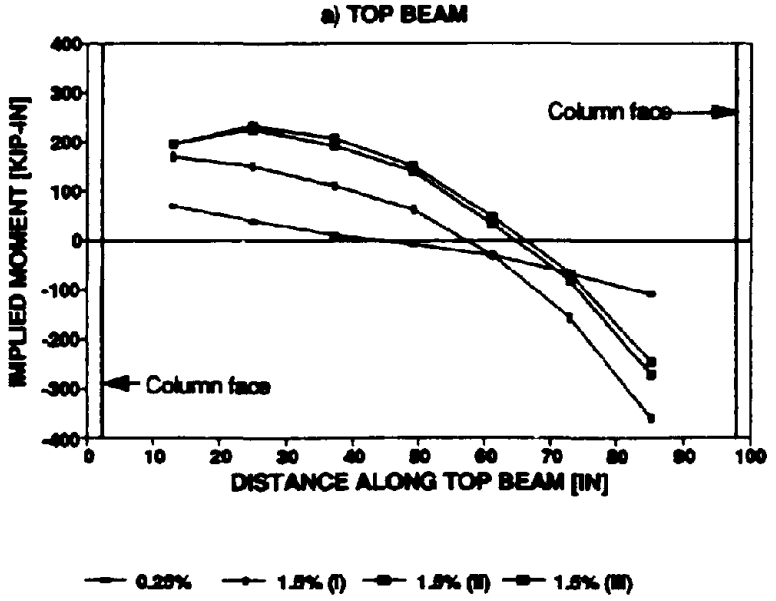

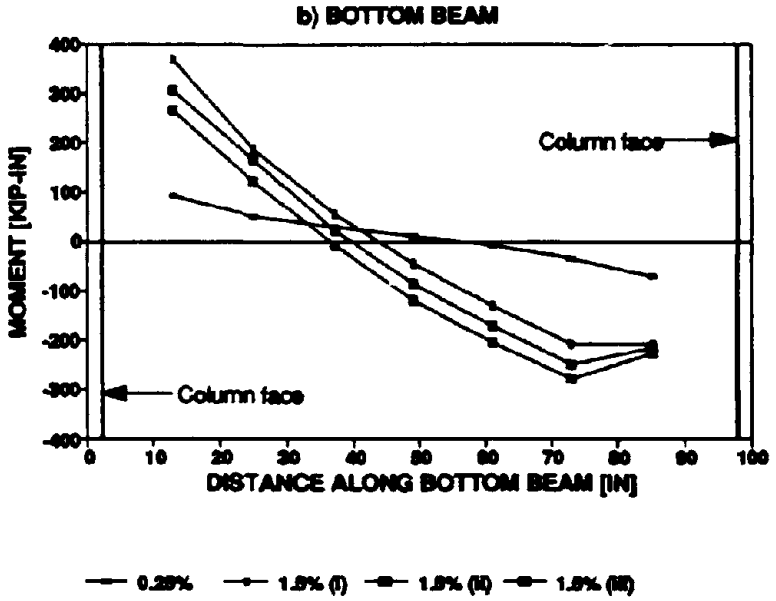

Fig. 4.21 Implied bending moments for negative loading of Specimen 3 (Phase III)

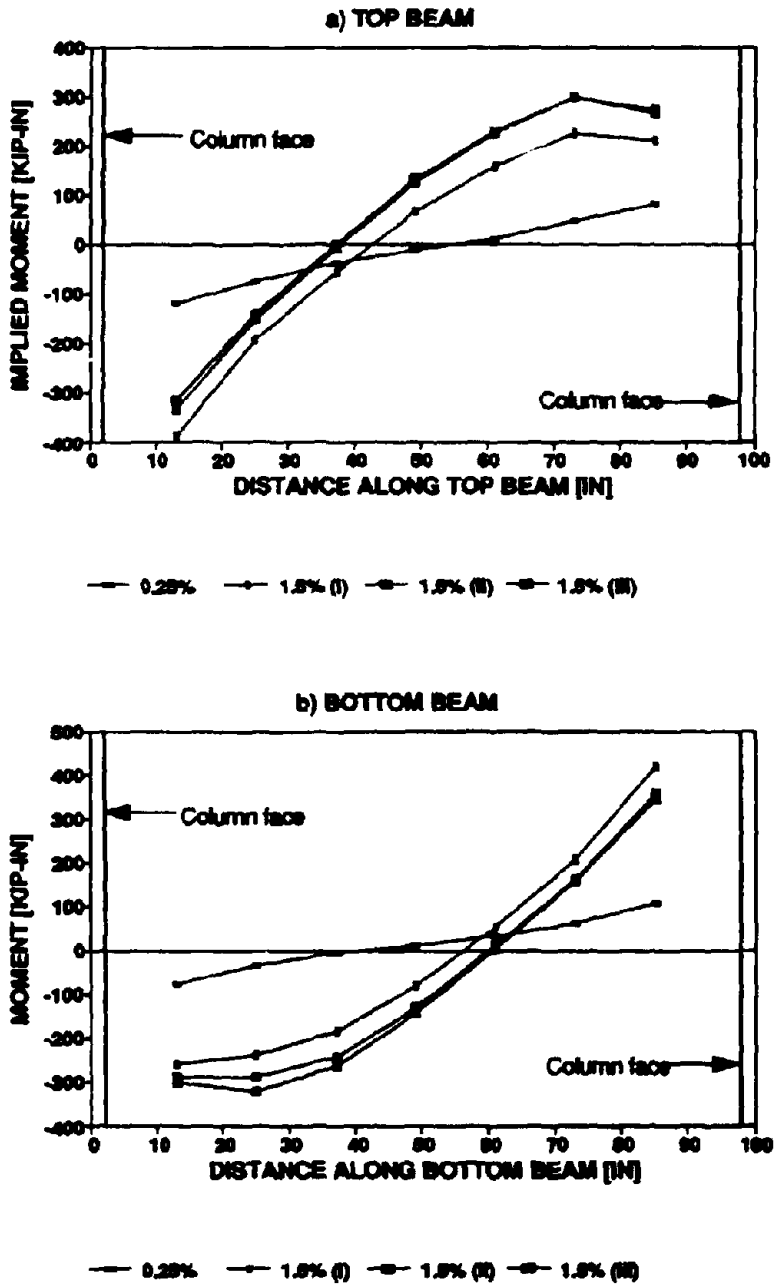

Fig. 4.22 Implied bending moments for positive loading of Specimen 3 (Phase III)

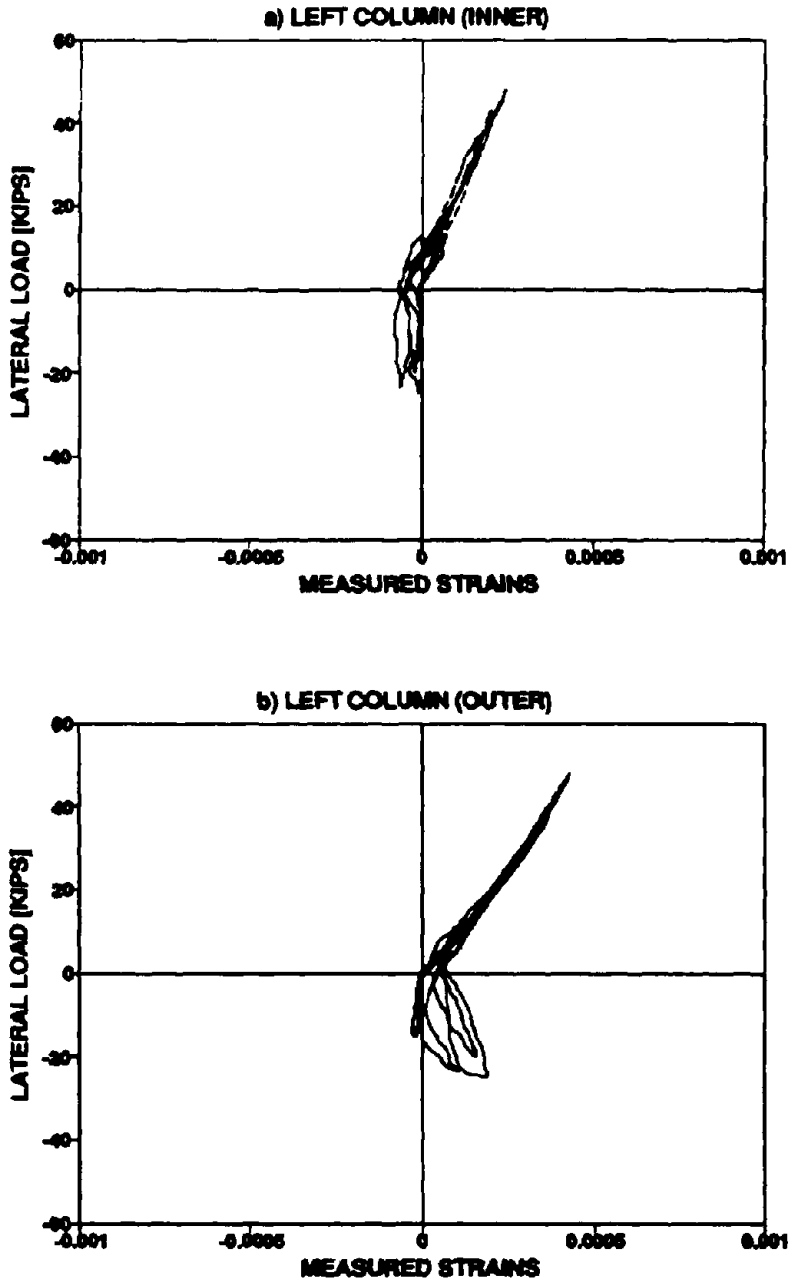

Fig. 4.23 Strain history of left column of Specimen 3 (Phase I & II)

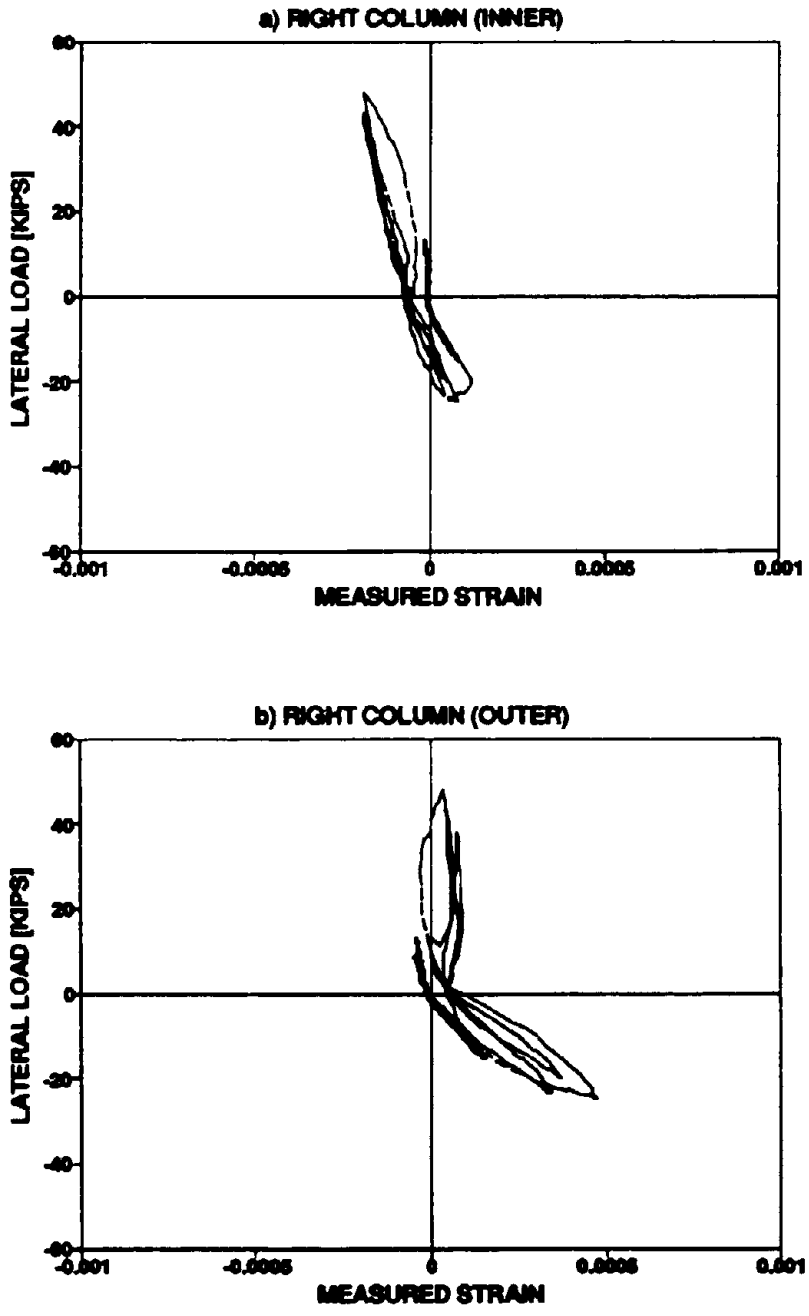

Fig. 4.24 Strain history of right column of Specimen 3 (Phase I & II)

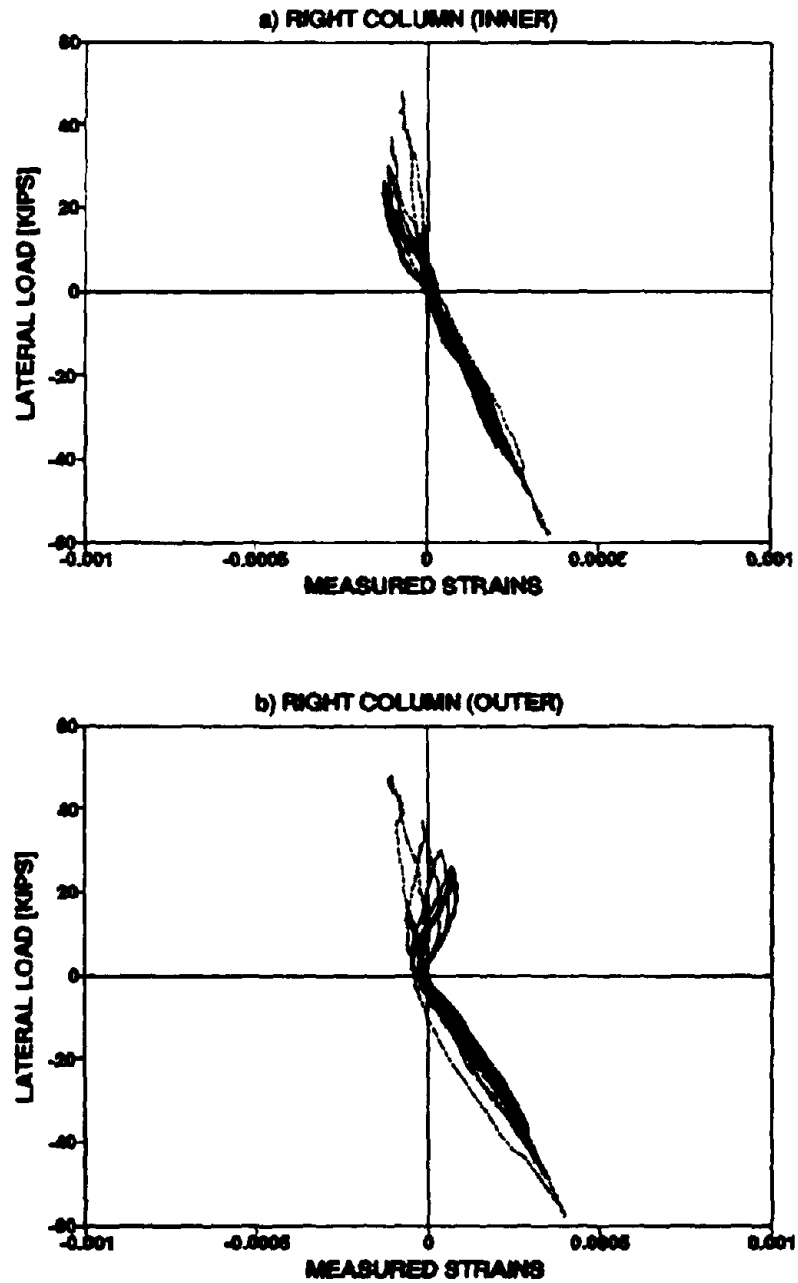

Fig. 4.25 Strain history of right column of Specimen 3 (Phase III)

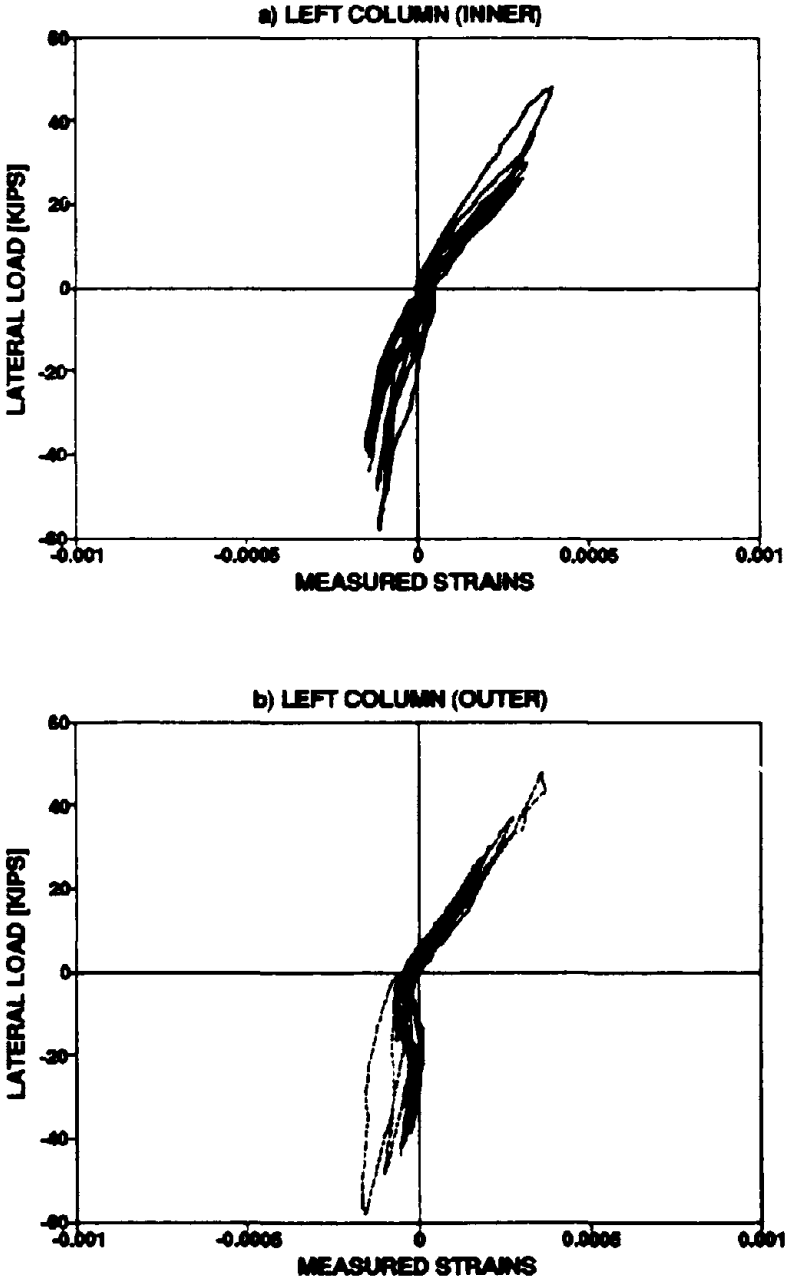

Fig. 4.26 Strain history of left column of Specimen 3 (Phase III)

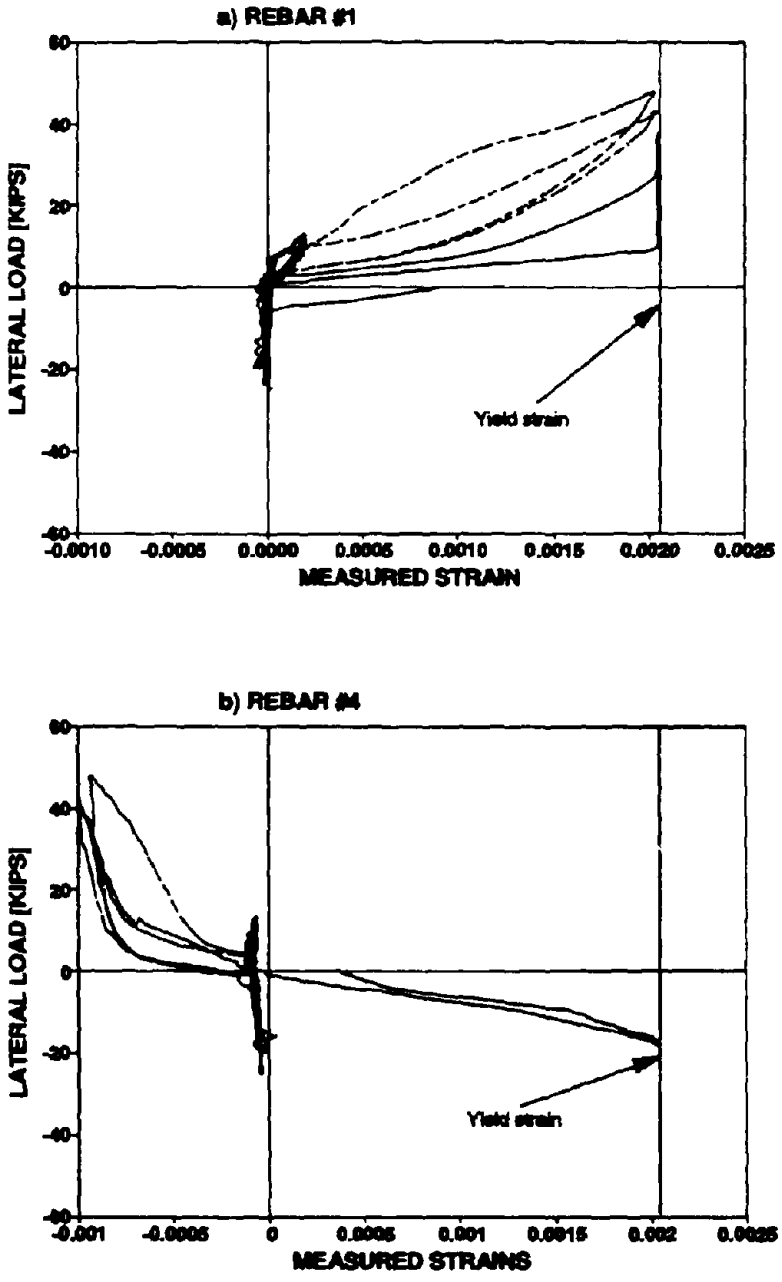

Fig. 4.27 Strain history of rebars of Specimen 3 (Phase I & II)

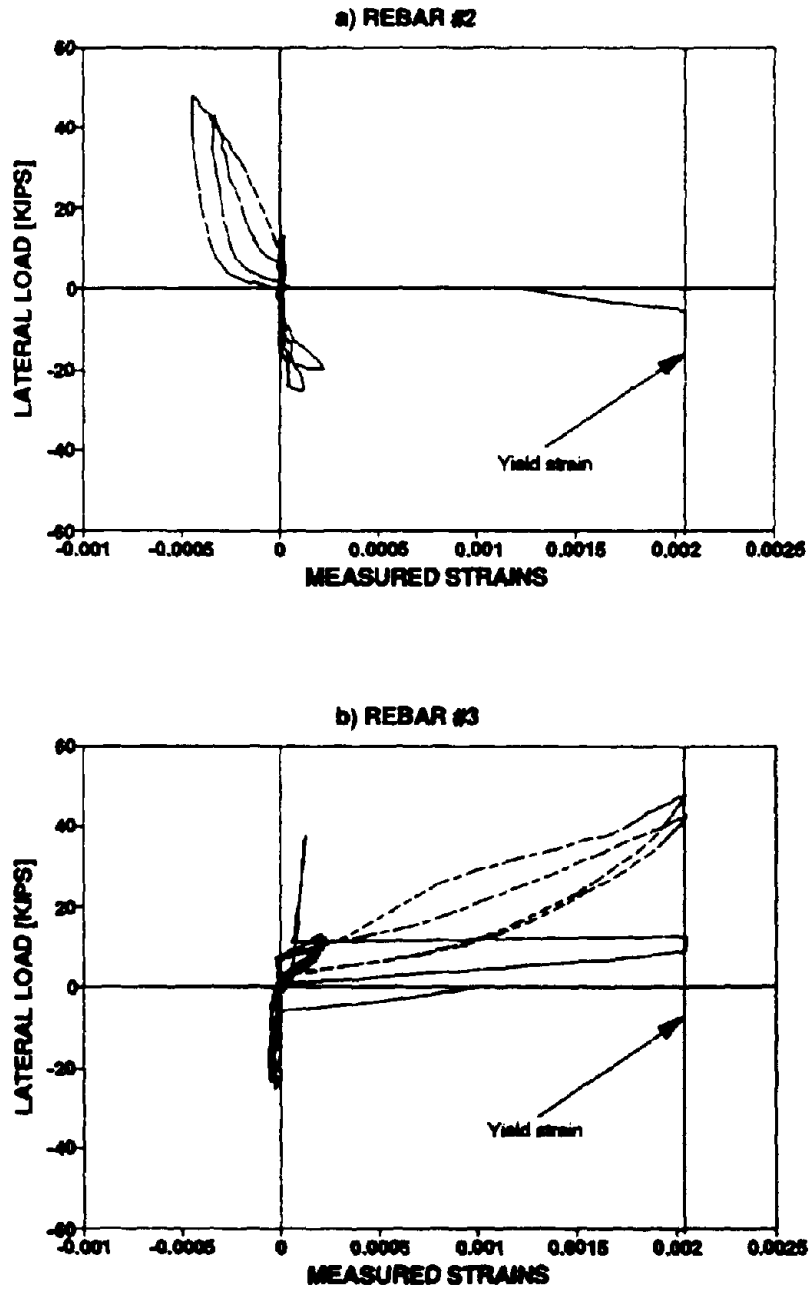

Fig. 4.28 Strain history of rebars of Specimen 3 (Phase I and II)

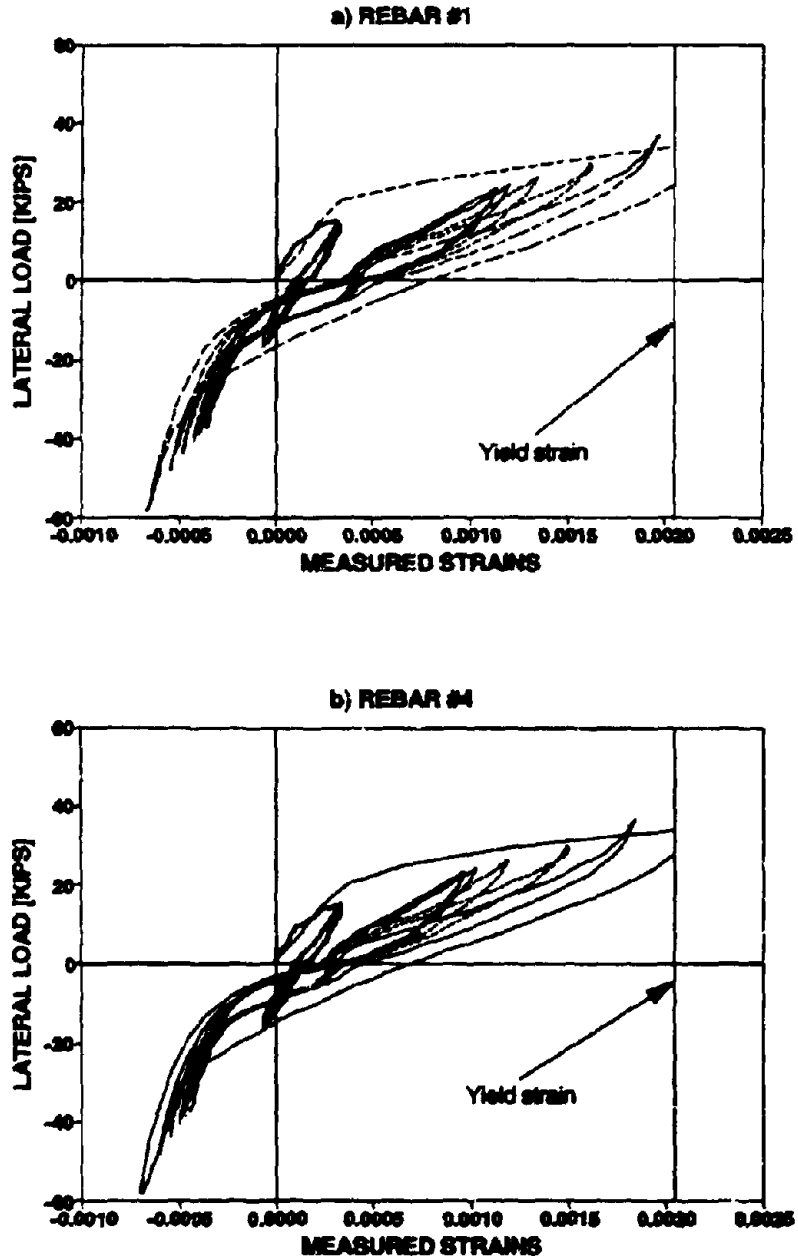

Fig. 4.29 Strain history of rebars of Specimen 3 (Phase III)

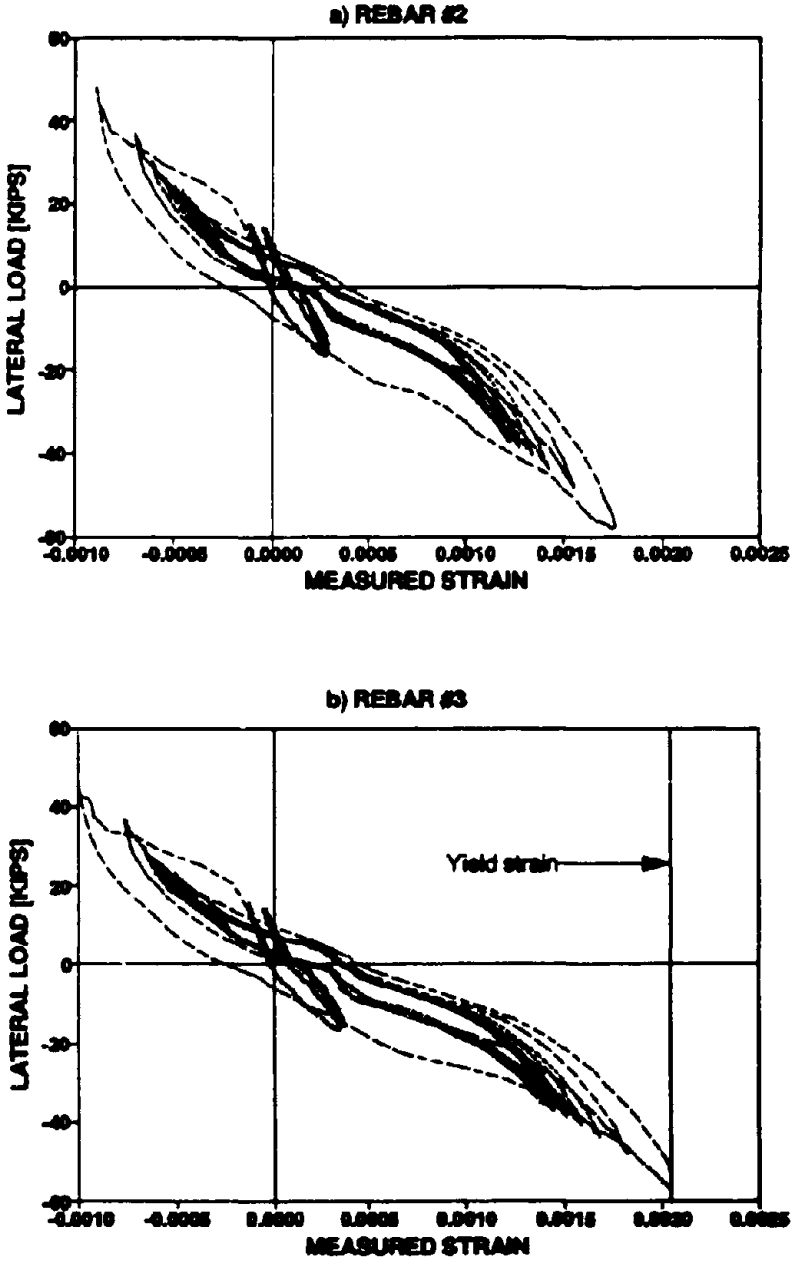

Fig. 4.30 Strain history of rebars of Specimen 3 (Phase III)

they are taut at their ends. At the tension face, there is boundary separation, whereas at the compression face, there is minimal crushing as this is only the second cycle in the whole series of tests.

Fig. 4.33 shows the beginning of the next compression cycle. The rebars 1 and 2 are slack and move into the rebar connectors freely.

Fig. 4.34 shows the final stage of the compression cycle on rebars 1 and 2. They are moved as much as an inch into the outer area of the rebar connectors on opposite ends of the compression diagonal.

Fig. 4.35 shows the pattern of cracks formed on the ferrocement after the test was complete. Evidently they have been more intense on the side away from the point of load application. There are little cracks distinctly visible on the diagonals indicating that the rebars were successful in limiting cracks.

Fig. 4.36 shows the side of the brick infill that had no coating applied to it. Clearly there are very few visible cracks on the masonry bricks. The corners show the mortar was used in repairing the crushed portion of the bricks at the corners.

During the first cycle to ±1.5% drift a significant number of hairline cracks spread along the coating, mainly on the side farther away from the face of application of the load. There was also movement of the coating away from the panel by a fraction of an inch around the corners. It was evident that the diagonal rebars behaved as intended by design during both the tension and compression cycles. There was also no observed buckling at the center of the infill panel as in the case of earlier tests on Specimens 1 and 2.

During the fourth cycle of loading, spalling of the cover concrete off the ferrocement coating at the corners commenced. This was restricted to a small area close to the channel sections. The top layer of mesh was exposed and the rebars were visible at these corners.

During the fifth cycle of loading, bending of the diagonal rebars when under tension at their anchorages was observed. The bending was towards the brick face and this caused the skewing at the junction of the channel section (where they were connected). This helped the bricks to

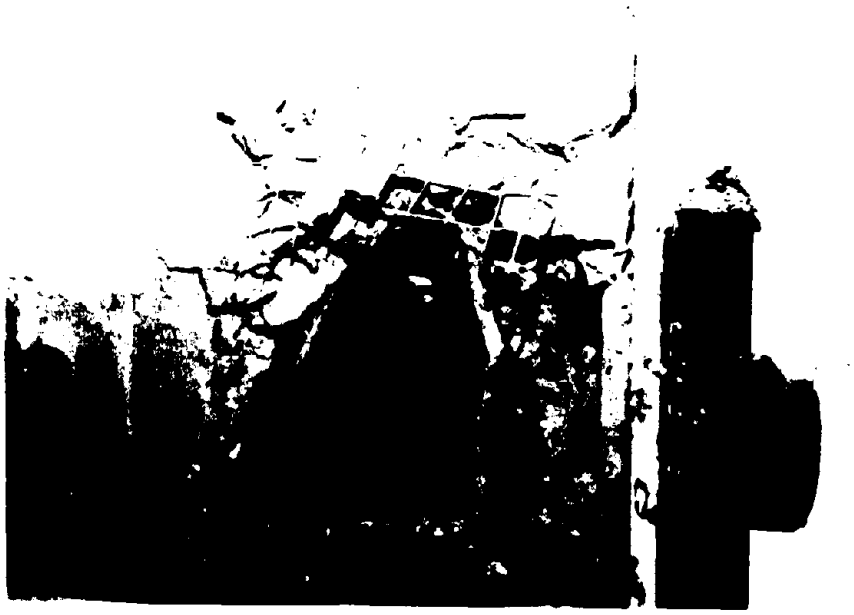

Fig. 4.31

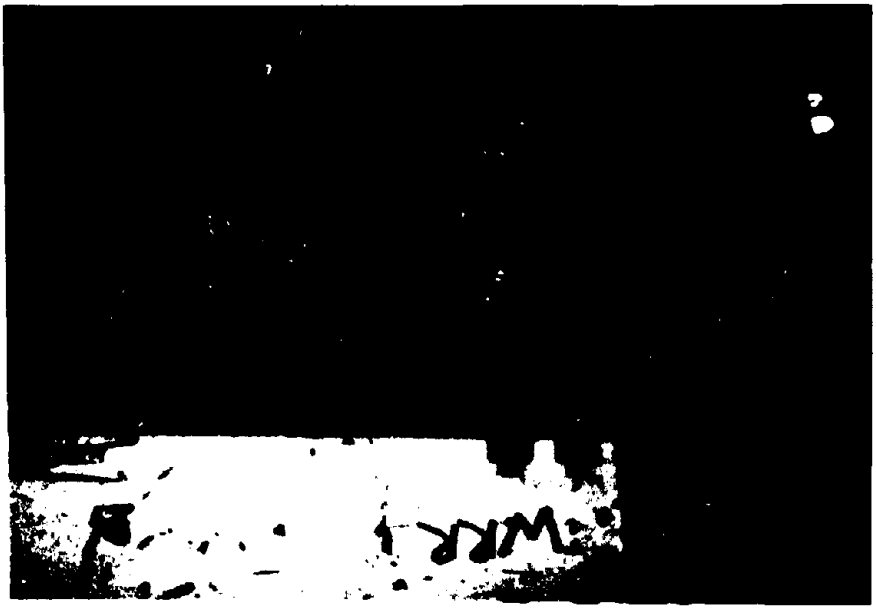

Fig. 4.32

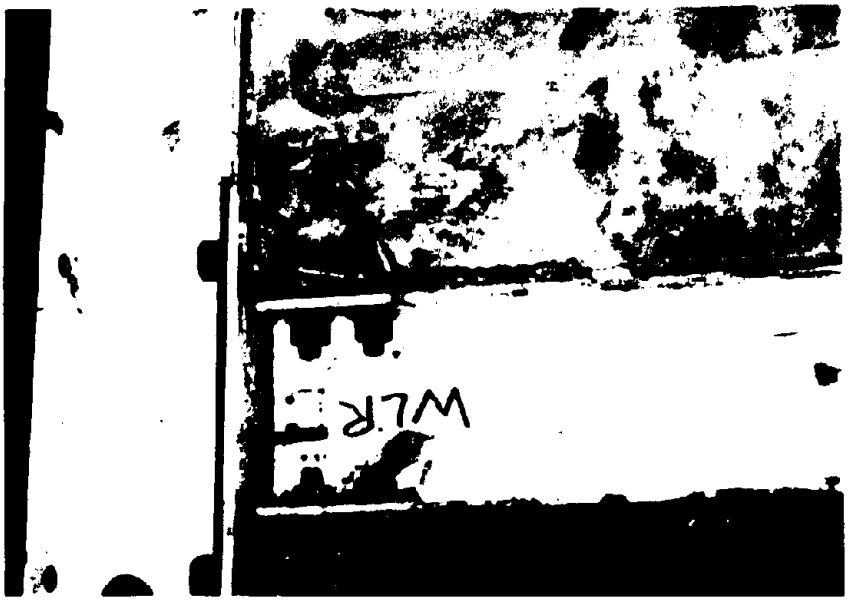

Fig. 4.33

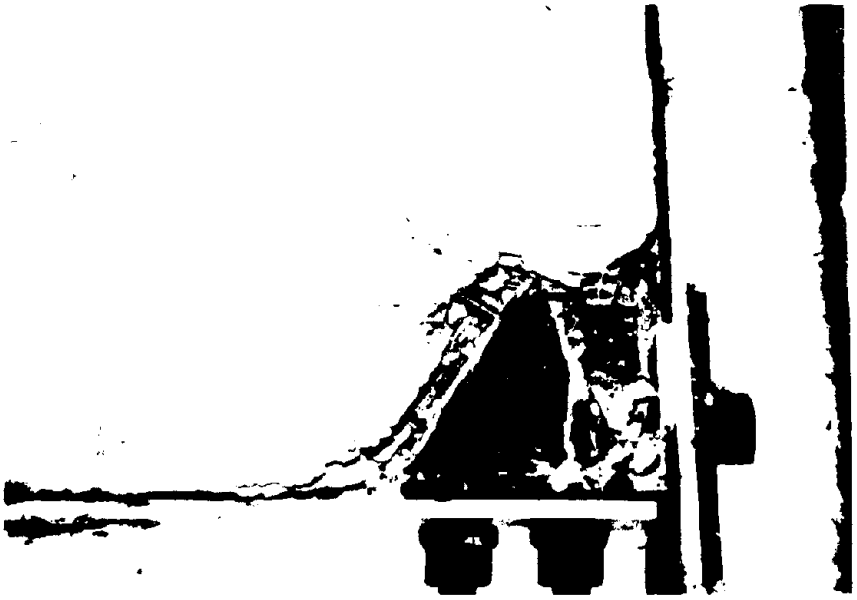

Fig. 4.34

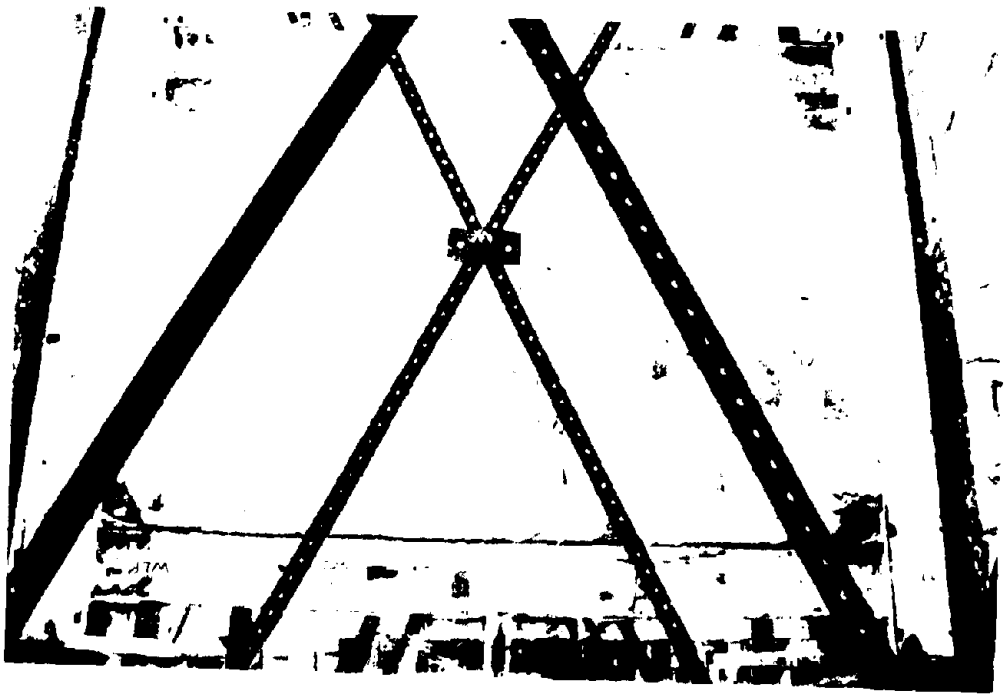

Fig. 4.35

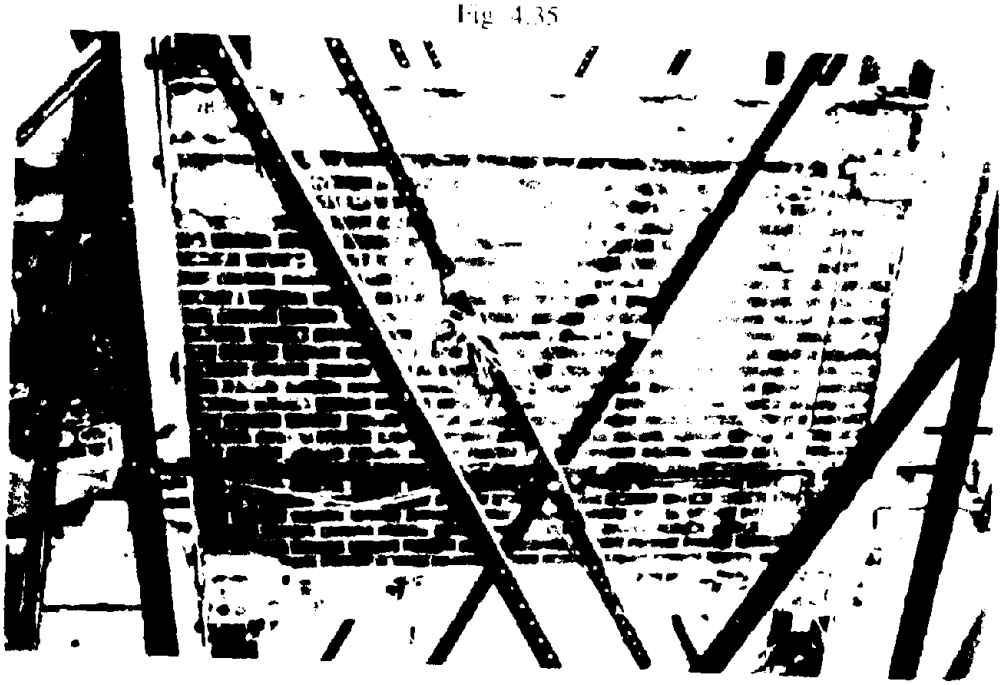

Fig. 4.36

"walk" out of the frame by 7/8ths inch at the end of testing. The bricks however were still connected to the ferrocement overlay, and the out-of plane integrity was not jeopardized. Testing was terminated on completion of the sixth cycle at the 1.5% drift amplitude as a result of a fracture in a pair of the diagonal rebars near the anchor nut. At the completion of testing, there was considerable compression crushing at the infill corners. However, outside theses zones there was only minimal evidence of cracking with a few fine micro-cracks detectable along the tension diagonals.

4.5 Discussion of Results

Corner crushing and diagonal cracking due to shear appeared to be the major form of failure in the testing of the first specimen using ordinary infill prior to repair/retrofitting. The inclusion of ferrocement proved that the ductility capacity of the masonry can be further improved marginally but introduced some lateral "walking out" of the frame under repetitive cycles of loading as observed in the repaired and retrofitted Specimens 1 and 2. The inclusion of an additional layer of reinforcing mesh and diagonal rebars in Specimen 3 demonstrated that the ductility capacity of the structure can be further improved as a whole. This has been further exemplified by the test results. A comparative hysteretic energy absorption of the three specimens will clearly distinguish the advantages of using an enhanced ferrocement overlay. This has been further dealt with in Section 5.

SECTION 5
AN EVALUATION OF THE TEST RESULTS

5.1 Introduction

In this section the experimental results are evaluated. Force-drift relationships are derived for the net infill performance, and based on that component of resistance, the hysteretic energy observed during each cycle of the tests are compared. The contact stresses induced on the infill frame are also evaluated. These stresses demonstrate that a complex inelastic stress field exists within the infill panel that changes throughout testing. Due to this complexity, analytical modeling is outside the scope of this experimental study, and is left for a future investigation. However, this section concludes with a comparison of the observed strengths with simple engineering code-based assessments.

5.2 Net Infill Contribution to the Frame Resistance

When the infill was present, a diagonal strut action formed and the truss action of the system as a whole was mobilized. Therefore, the net response of the infill was thus obtained by subtracting the bare frame load for a given drift from the gross infill frame response. It is, therefore, assumed that

$$F_{INFILL} = F_{TOTAL} - F_{STEEL\text{-}FRAME} \tag{5-1}$$

where $F_{STEEL\text{-}FRAME}$ = the force resisted by the steel frame after the bricks had been removed including the effects of the end diagonal braces.

Figs. 5.1 to 5.6, respectively, show the net performance of the infills at the ±1.5% drift amplitude for Specimens 1, 2 and 3. It should be noted that the net hysteresis loops for drift amplitudes less than 1.5% could not be derived as the steel frame performance at these lesser amplitudes was not known precisely due to the absence of appropriate base frame test results. The pinched appearance of the loops between drifts of ±1% is due to damage inflicted on the infill during previous loading cycles. Nevertheless, it is evident when comparing the overall

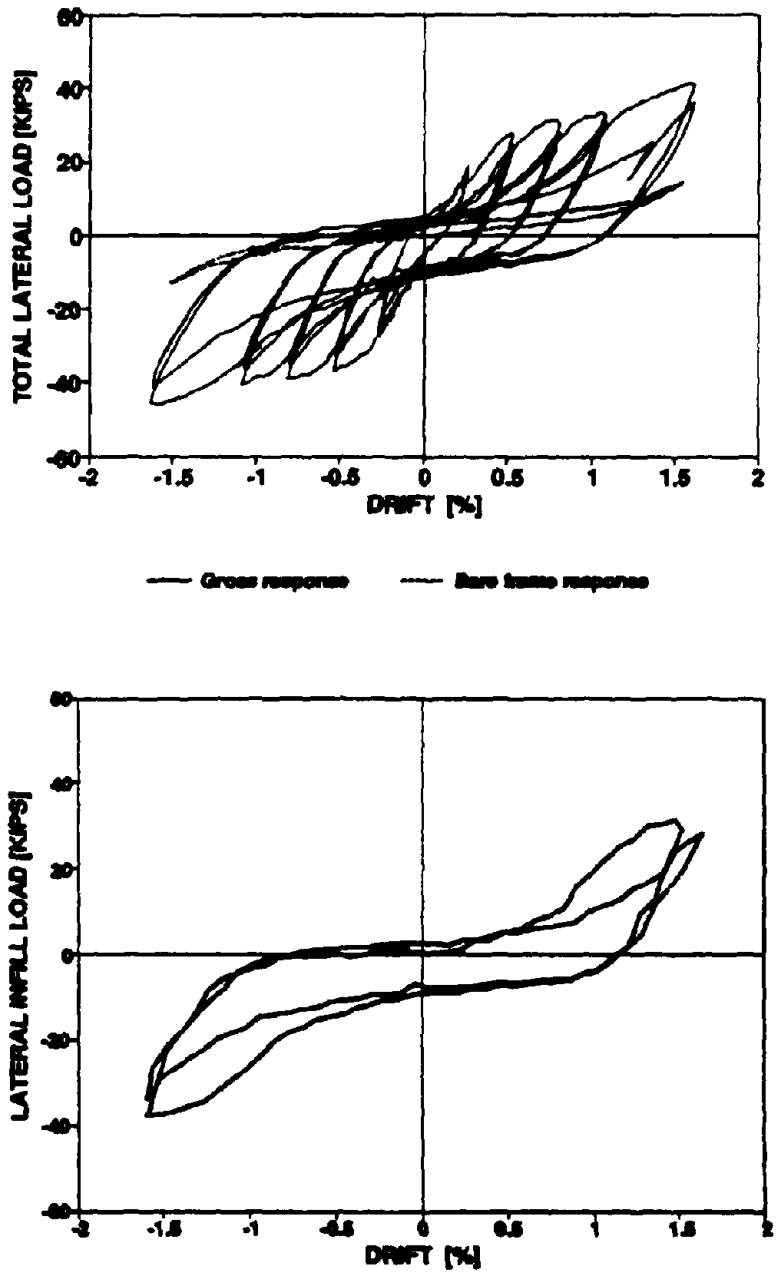

Fig. 5.1 Total and net infill response for Specimen 1

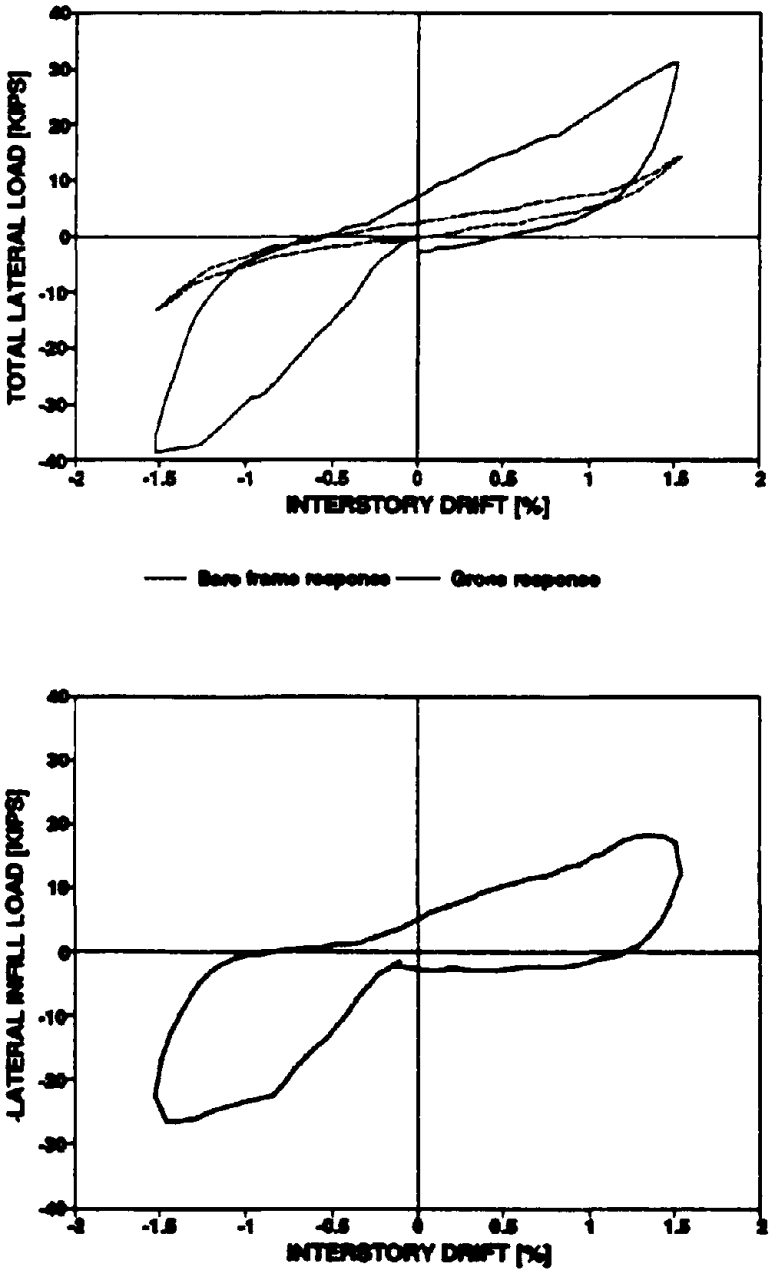

Fig. 5.2 Total and net response for Repaired Specimen 1

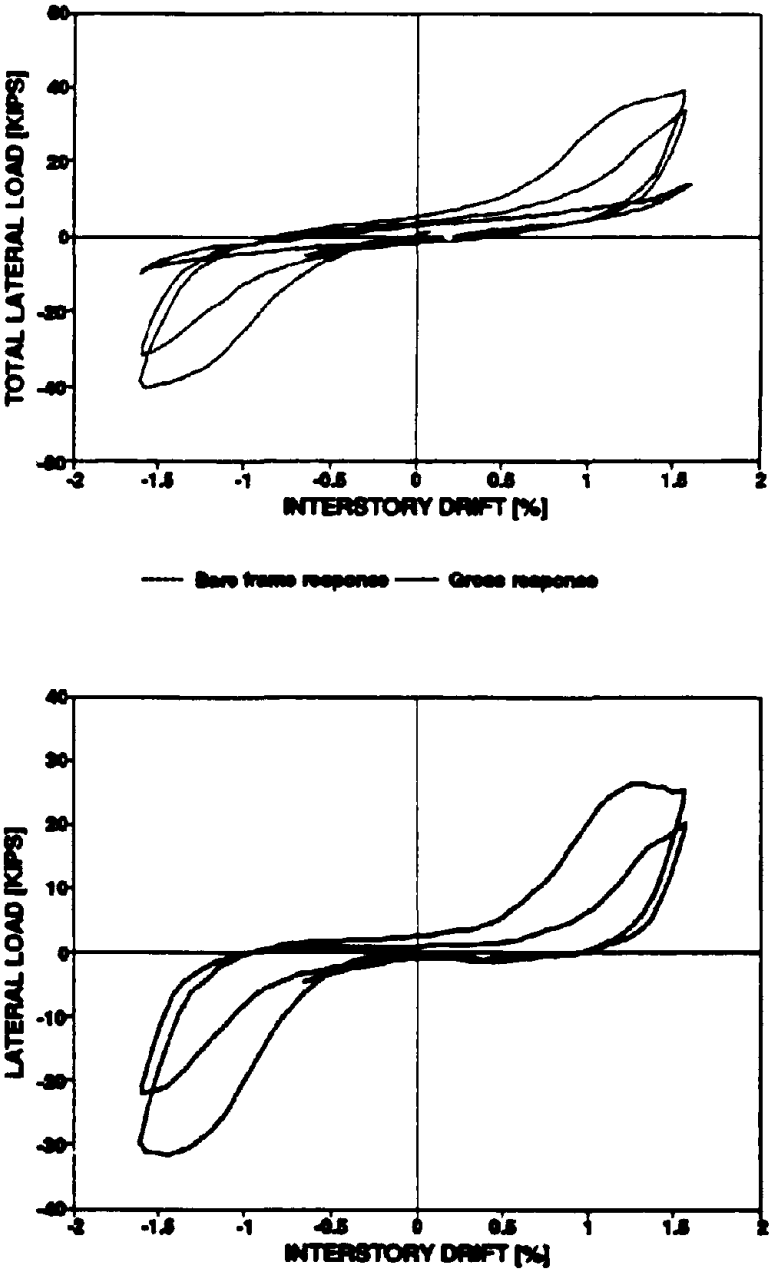

Fig. 5.3 Total and net response for Retrofitted Specimen 2

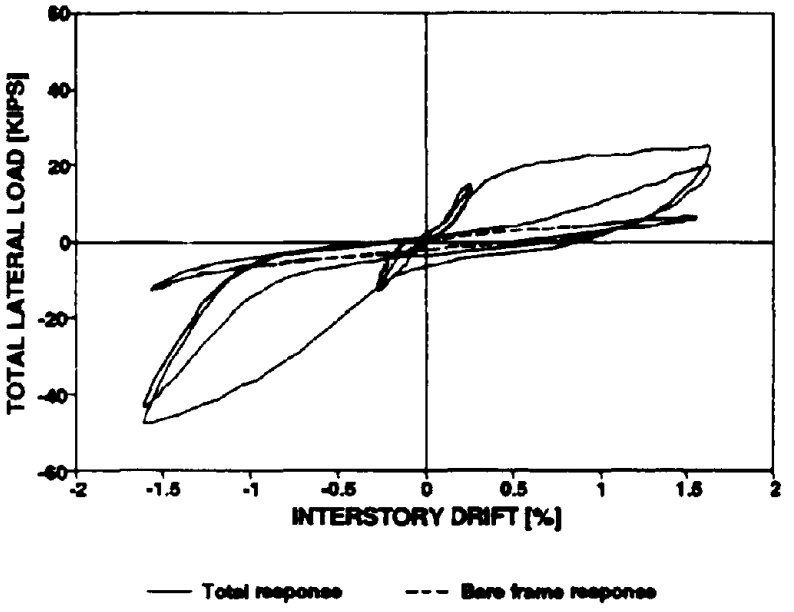

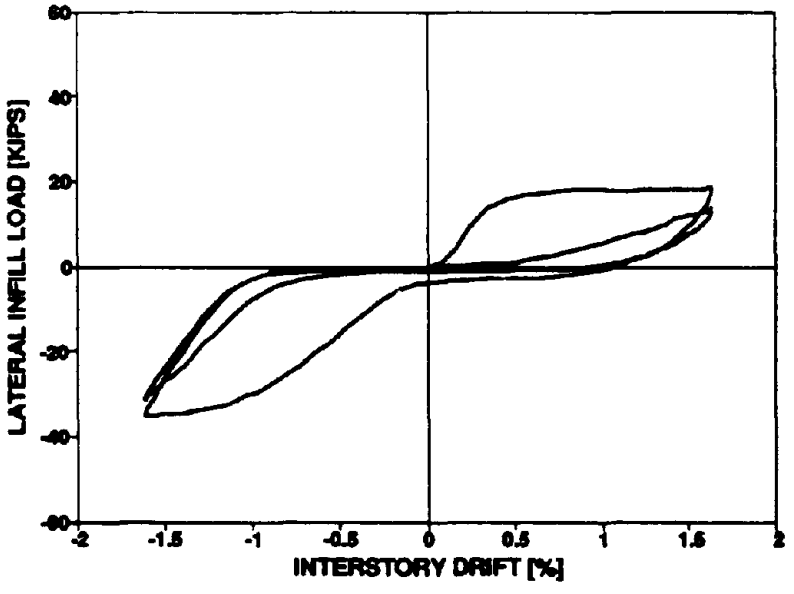

Fig. 5.4 Total and net infill response for Phase I of Specimen 3

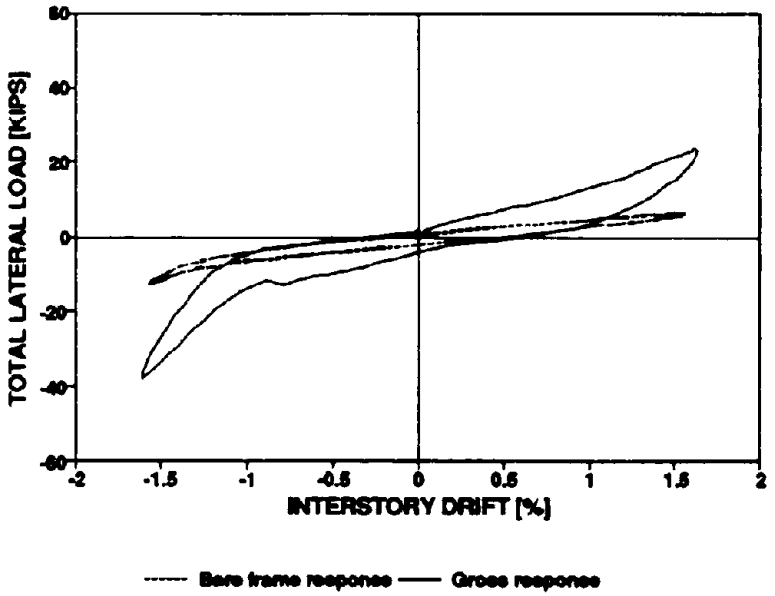

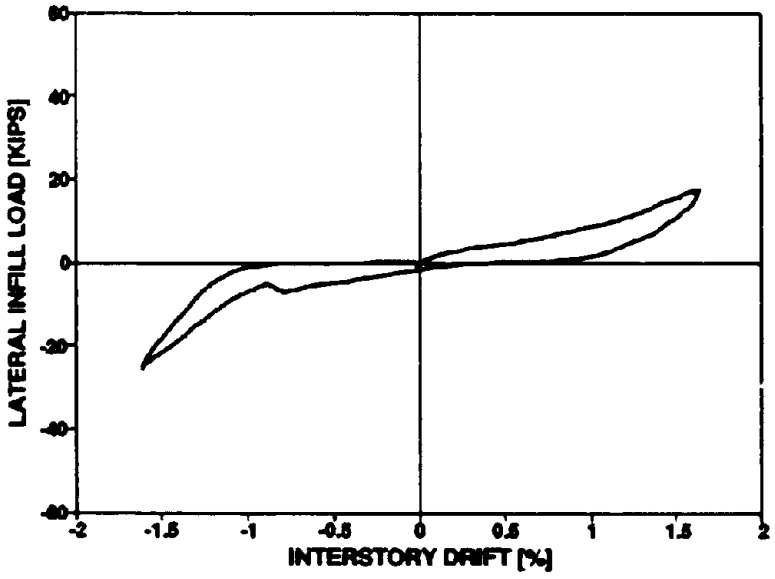

Fig. 5.5 Total and net response for Phase II of Specimen 3

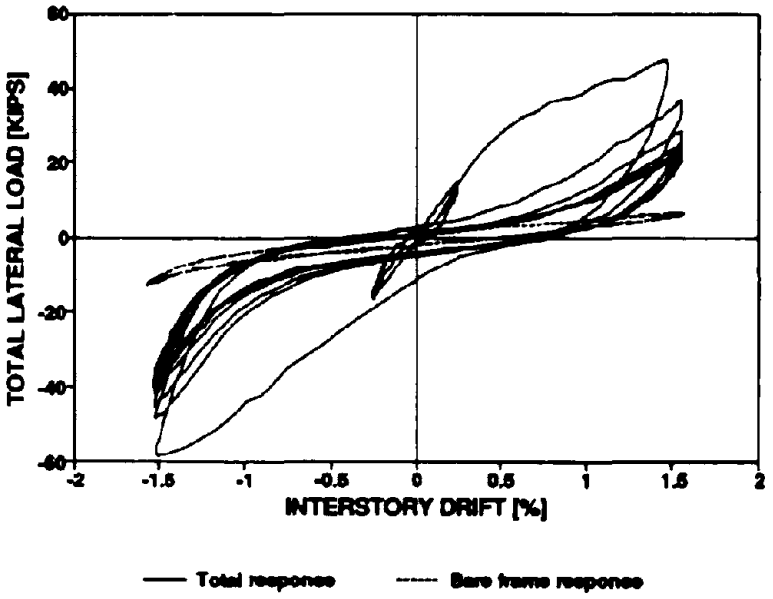

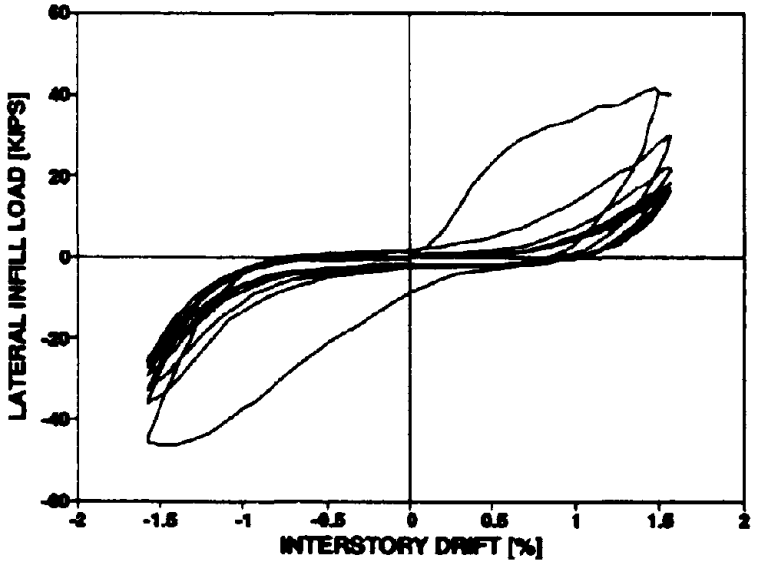

Fig. 5.6 Total and net response for Phase III of Specimen 3

performance, as well as the net infill performance between 1% and 1.5% drifts, the behavior is mostly elasto-plastic. However, on successive loading cycles at the ±1.5% drift amplitude, the pinched appearance becomes more exacerbated due to additional sliding shear that takes place. The peak strength at the end of each cycle also drops off with an apparent logarithmic type of decrement.

By comparing the performance of Specimens 1 and 2, it is possible to obtain some insights into the effects of the application of the ferrocement overlays. Both of these overlays were similar, one being applied to the damaged Specimen 1 (the repair), the other as a retrofit to Specimen 2. When comparing Figs. 5.1 and 5.2, it is evident that the ferrocement repair has had only a marginal benefit in the form of delaying strength deterioration of the infill. It is of interest to sobserve that due to the weaker masonry, Specimen 2 is still not as strong as Specimen 1 prior to repairing.

Figs. 5.4 to 5.6 show the net infill response for the three phases of testing Specimen 3. It is evident that the monotonic curve for Phase I is essentially elasto-plastic in nature for the ordinary brick infill under forward loading, while under reverse loading strain-hardening of the engaged diagonal rebars led to a bi-linear response. A similar bi-linear response is evident for Phase III which includes the enhanced ferrocement overlay. Under reversed cyclic loadings, it can be observed that there is a steady drop off in the peak strength with each cycle of loading. However, the hysteretic loops appear to have stabilized after five cycles of loading in Phase III. The hysteretic performance of the infill shows evidence of a sliding shear mechanism.

5.3 Energy Absorption Capacity

The hysteretic energy absorption for Specimens 1, 2 and 3 are shown in Fig. 5.7. It is evident from the results that Specimen 3 with the enhanced ferrocement overlay (Phase III) absorbed the most energy during the first cycle of loading. Specimens 1 and 2 also absorbed similar amounts of energy on their first loading cycles. The effect of a sliding shear mechanism on the response can be better understood by considering hysteretic energy in each loop for the three phases of testing Specimen 3. Phase I and II are essentially the same testing situation, the only different is that in Phase II the diagonal rebars were also engaged under forward (positive) loadings. For

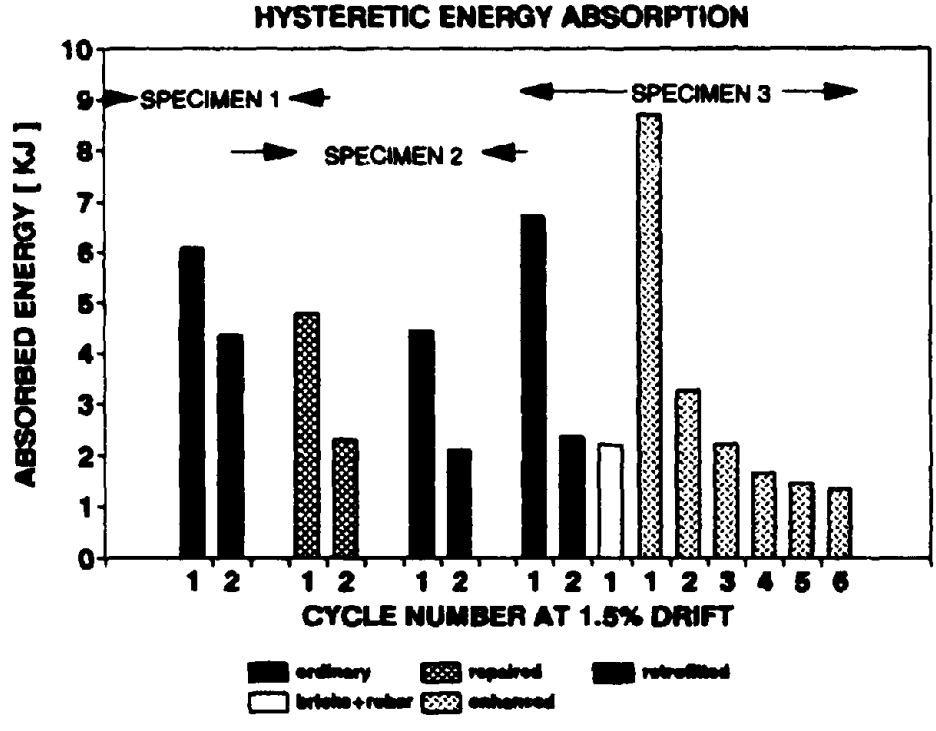

Fig. 5.7 Hysteretic energy absorbed by specimens

both the ordinary infill (Phase I) and the enhanced ferrocement repair (Phase III) it is evident that for the first cycle of loading, a considerable amount of energy was dissipated. Following a sudden drop off in energy dissipation capacity after these first cycles, subsequent cycles of loading show only a gradual decay in energy dissipation.

5.4 Contact Stresses

Contact stresses between the brick infill panel and the steel beams are calculated from the implied moments for each sub-test of the specimens for the final 1.5% drift cycle. The finite difference method was used which employed forward, central and backward differences at the appropriate nodes of the beams' strain gage pairs to obtain inferred contact stresses. From first principles, the load intensity (w) acting on a beam is related to its bending moment (M) by

$$\frac{d^2M}{dx^2} = -w \tag{5-2}$$

Using finite difference relations of the second order, the beam can be divided into (n) nodes and ($n-1$) equal segments of lengths (dx). At the left end of the beam, the following forward difference was used:

$$\frac{2M_i - 5M_{i-1} + 4M_{i-2} - M_{i-3}}{\Delta x^2} = -w_i \tag{5-3}$$

where i represents the node number. Backward differences were employed at the right end of the beam given by:

$$\frac{-M_{i-3} + 4M_{i-2} - 5M_{i-1} + 2M_i}{\Delta x^2} = -w_i \tag{5-4}$$

Along the other nodes, the following central difference relation was used;

$$\frac{M_{i-1} - 2M_i + M_{i-1}}{\Delta x^2} = -w_i \tag{5-5}$$

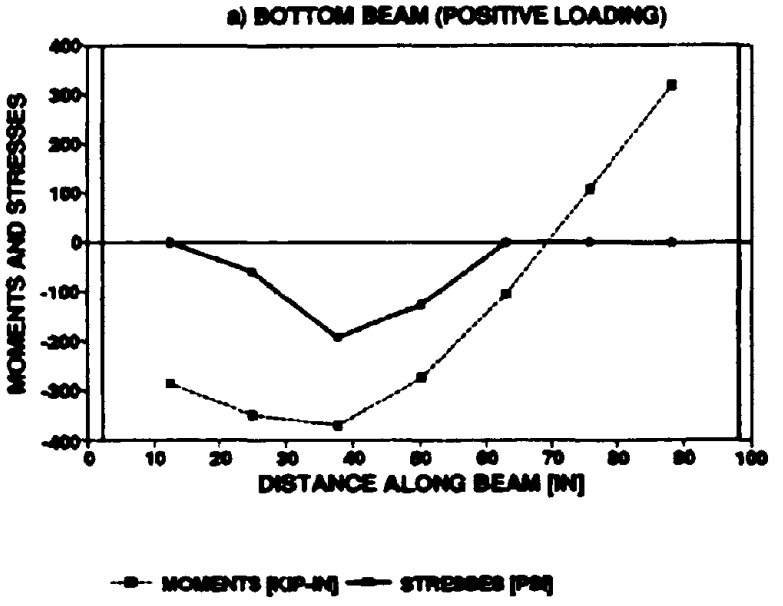

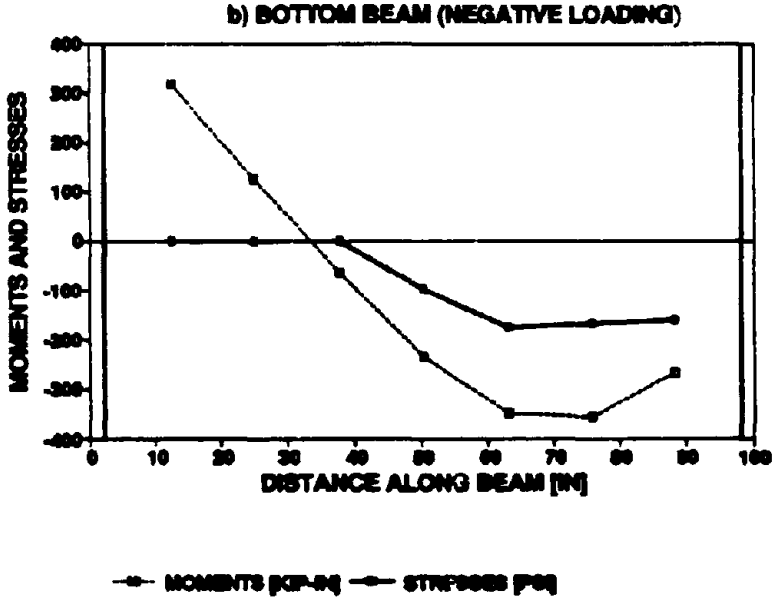

Fig. 5.8 Implied moments and stresses for Specimen 1

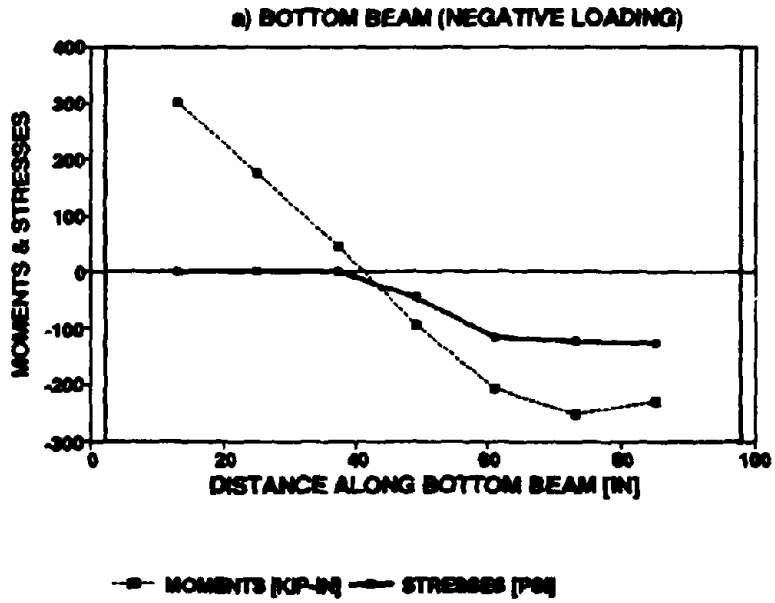

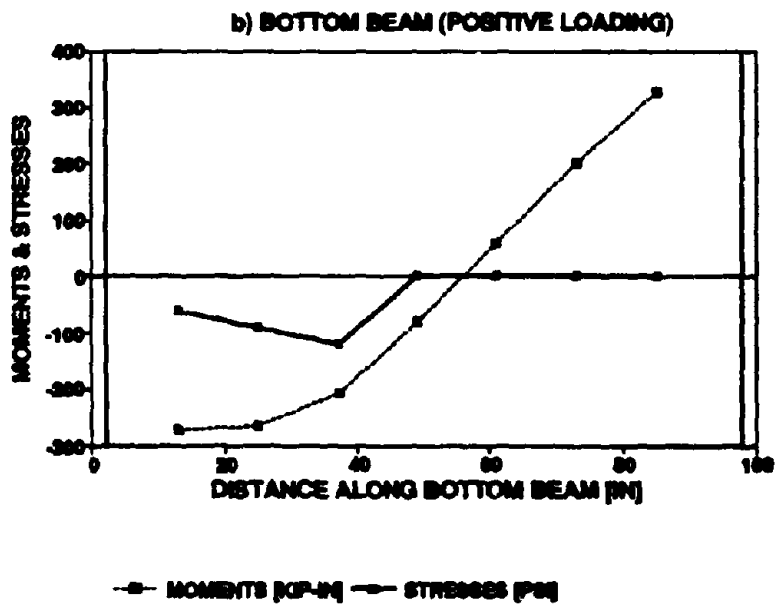

Fig. 5.9 Implied moments and stresses for Repaired Specimen 1

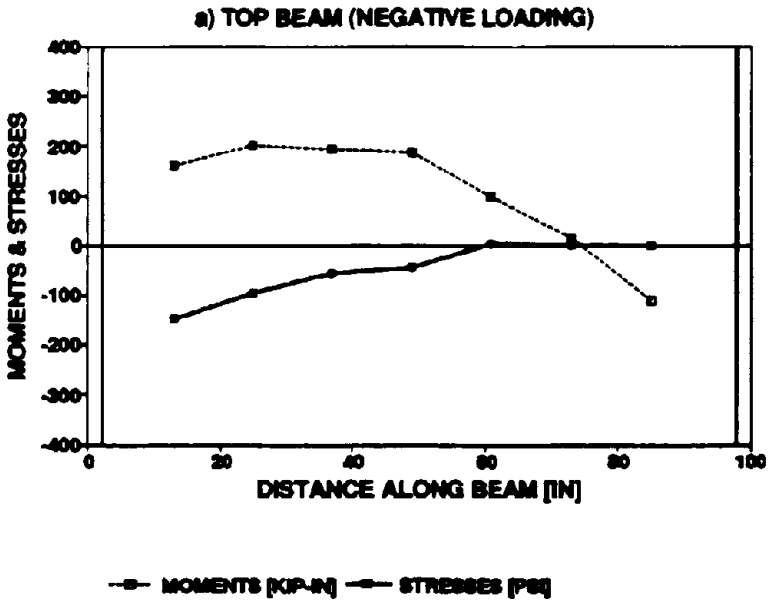

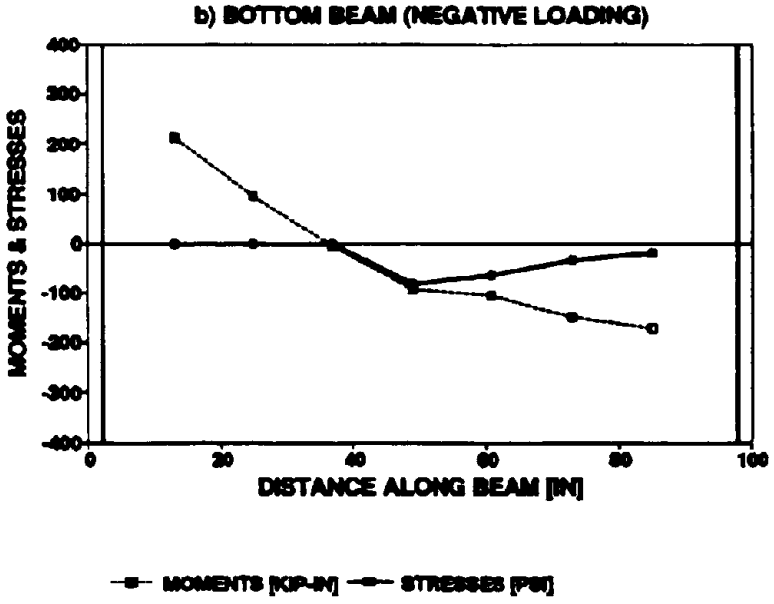

Fig. 5.10 Implied moments and stresses for Retrofitted Specimen 2

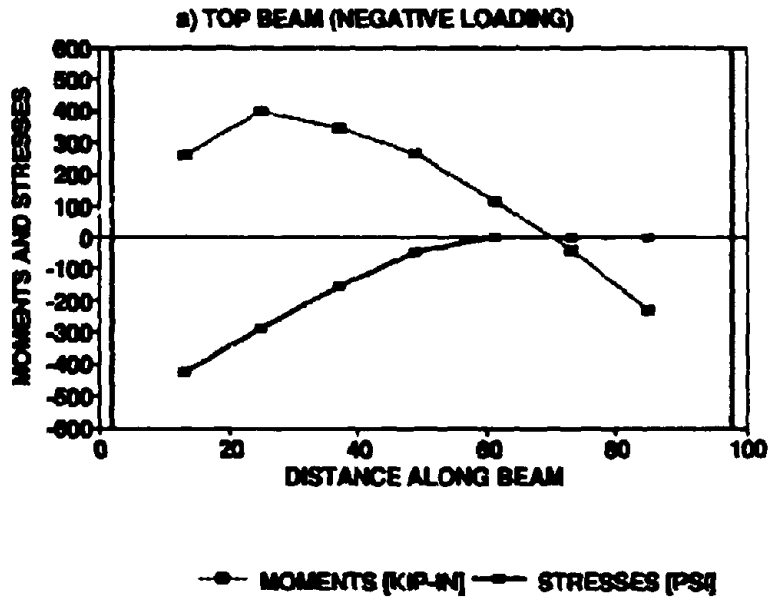

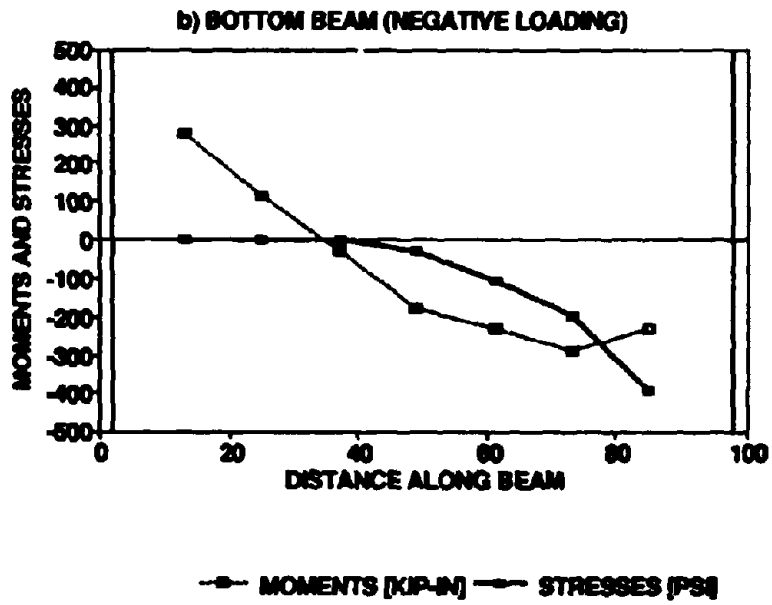

Fig. 5.11 Implied moments and stresses for Specimen 3 (Phase II)

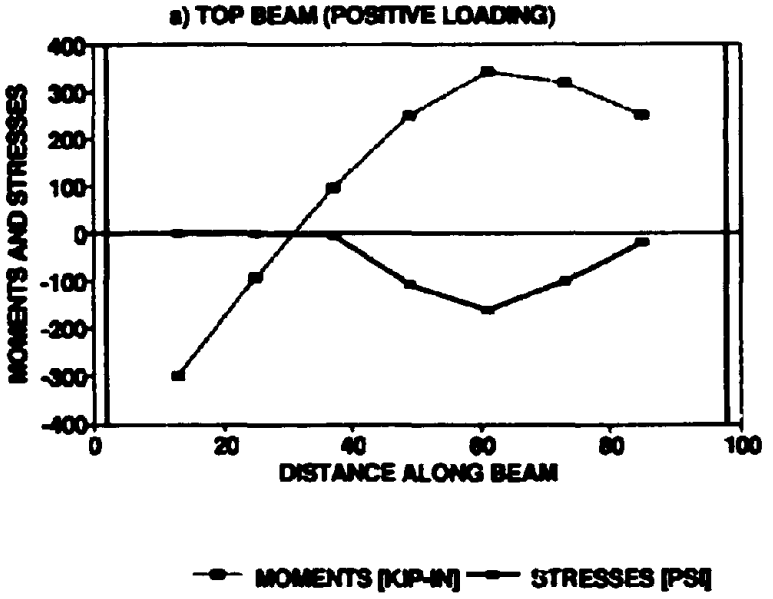

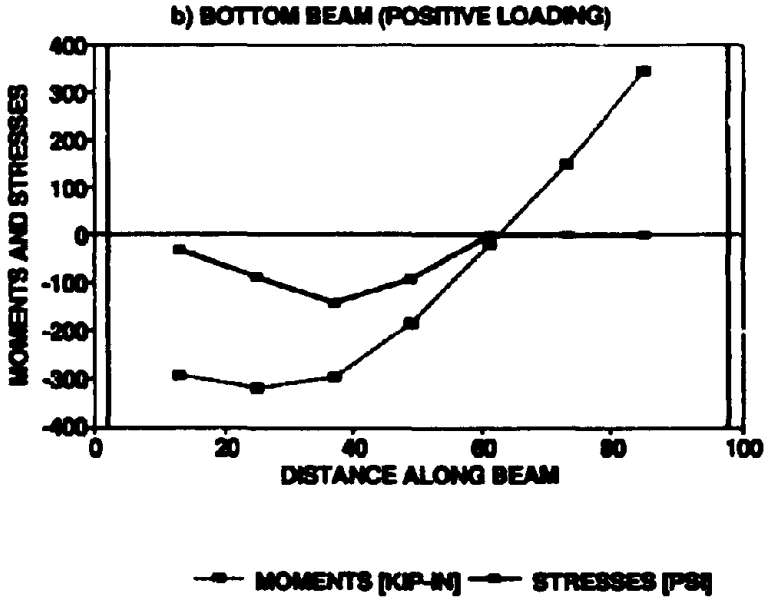

Fig. 5.12 Implied moments and stresses for Specimen 3 (Phase II)

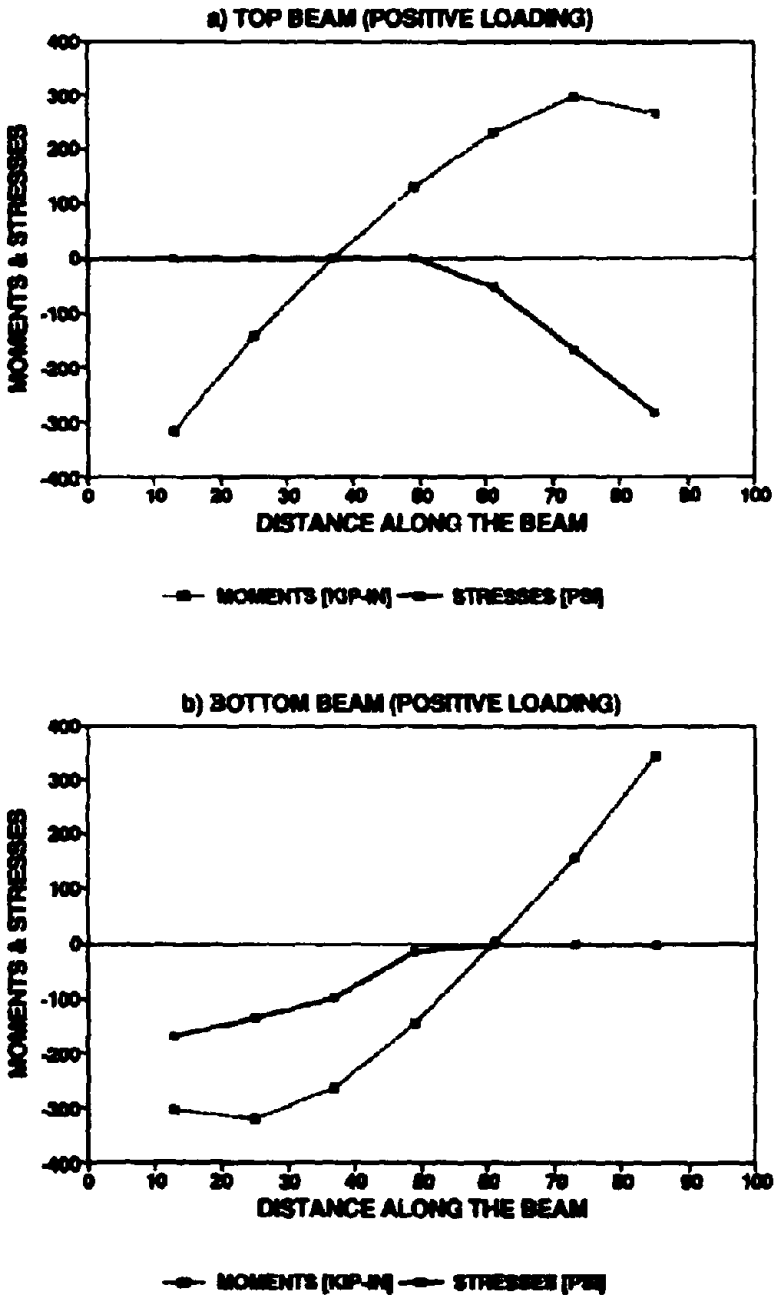

Fig. 5.13 Implied moments and stresses for Specimen 3 (Phase III)

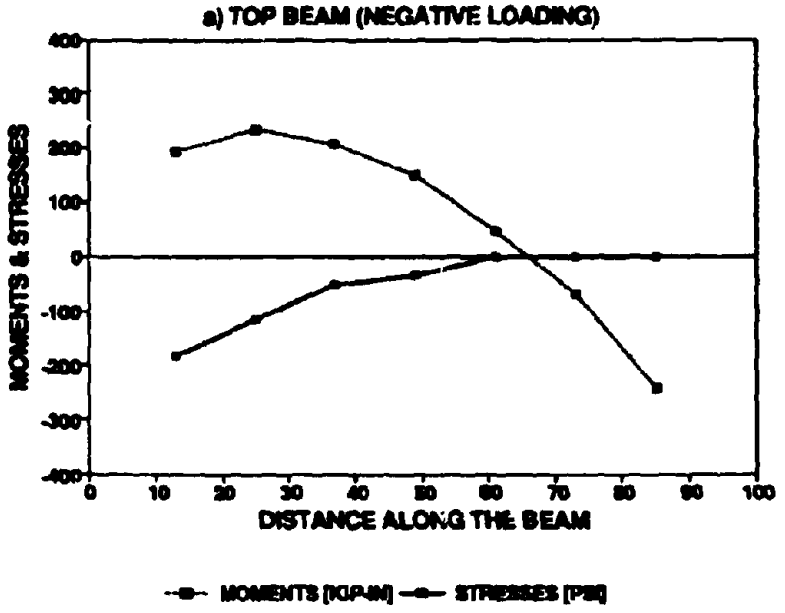

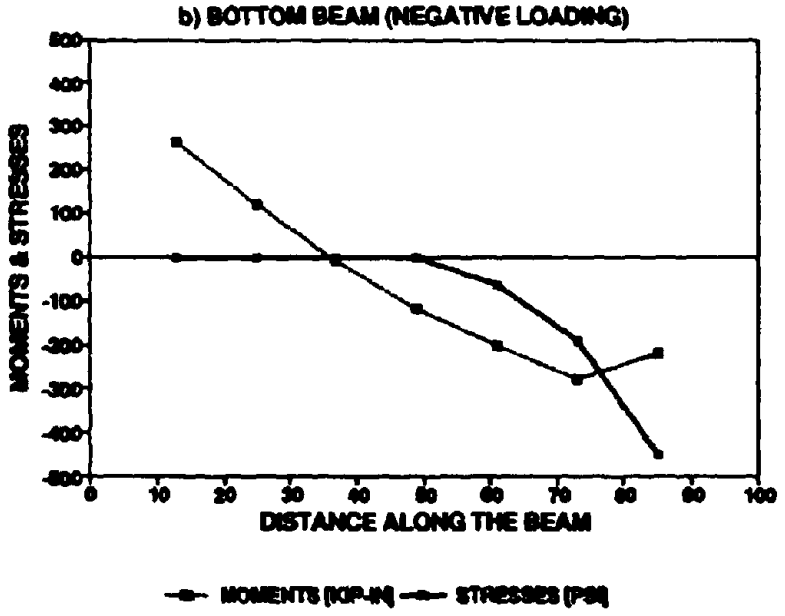

Fig. 5.14 Implied moments and stresses for Specimen 3 (Phase III)

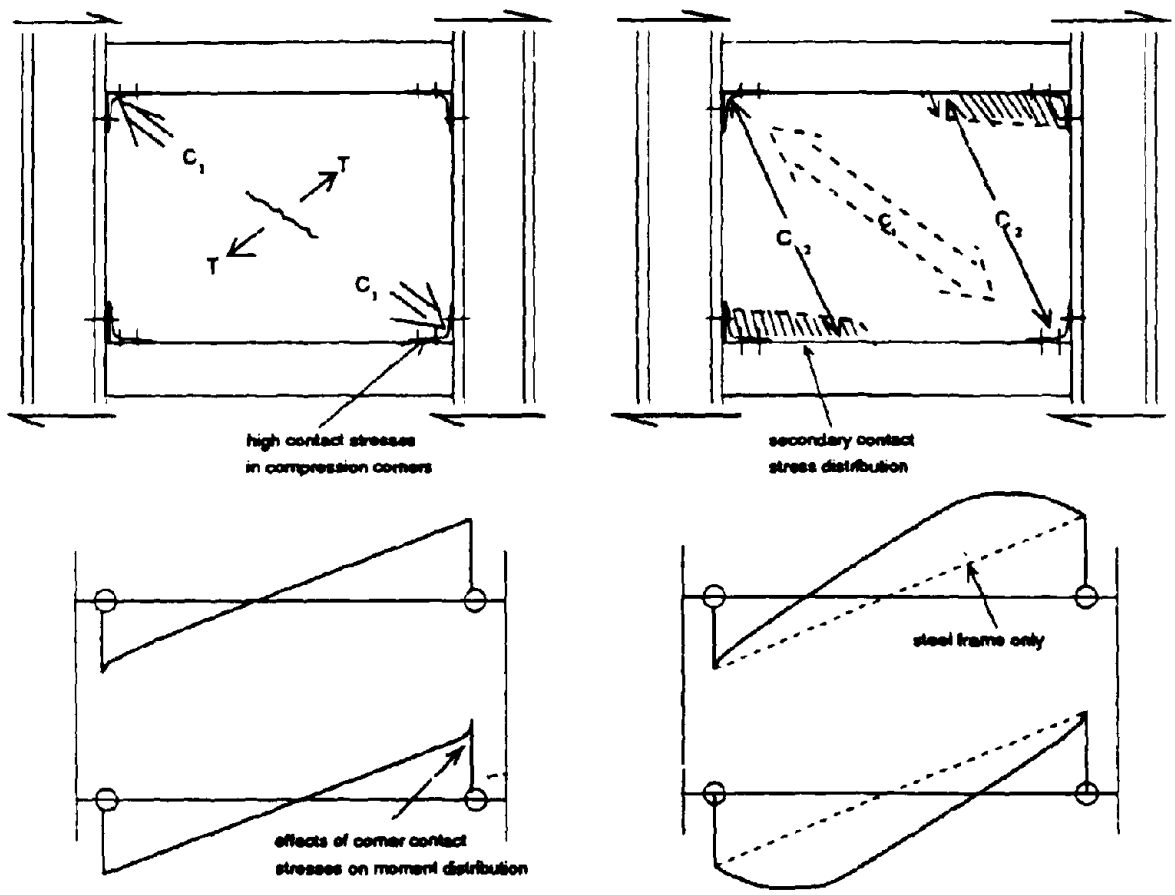

BENDING MOMENT DIAGRAM FOR BEAMS

Fig. 5.15 (a) Formation of initial corner-to-corner strut mechanism;
followed by (b) secondary strut mechanism following loss of diagonal tension capacity

Figs. 5.8 to 5.14 show a plots of implied moment and the corresponding contact stresses. It should be noted that the stresses are tension positive (in psi), and the bending moments (in kip-in) are plotted on the tension side of the beam.

The stresses induced in the mid-span vicinity of the beam are due to the formation of a secondary strut mechanism. The initial primary strut mechanism leads to high stress concentrations at the corners of the infill as shown in Fig. 5.16 (a). Following a few loading cycles at low drift amplitudes (see Figs. 4.3(a), 4.12, 4.13 and 4.19 - 4.22), it is evident that the infill looses its tension strength at the interior of the panel and is unable to sustain the corner-to-corner diagonal strut. Thus, secondary struts form as shown in Fig. 5.16 (b), which are primarily governed by Coulomb shear friction across the mortar interfaces. These secondary struts lead to the application of contact stress distributions such as those shown in Figs. 5.8 to 5.14. The formation of these secondary struts and subsequent additional cracking is due to the formation of a SR (shear rotation) mode of failure[8].

5.5 Infill Strength Assessment

From the foregoing discussion, it is evident that a somewhat complex form of resistance evolves during the course of cyclic testing. It is not within the scope of this report to model such behavior. This is the subject of ongoing research. However, it is of interest to determine the strength of the infills by applying commonly used engineering strength assessment techniques. Paulay and Priestley[6] have summarized the in-plane failure modes for masonry infilled frames. These include:

1. Tensile failure of the tension (windward) column resulting from applied overturning moments.
2. Flexural or shear failure of the columns.
3. Compression failure of the diagonal strut.
4. Diagonal tension cracking of the panel.
5. Sliding shear failure of the masonry along horizontal mortar beds, generally near the mid-height of the infill panel.

Frame Failure:

The first two failure modes are concerned with frame failure. In this study frame failure was

avoided by deliberately designing the beam and column members to be significantly stronger than the infill panel. This resulted in lateral load capacities of 204 and 337 kips for failure modes 1 and 2, respectively.

Diagonal Compression Failure:

For a compression failure of the diagonal strut, the method suggested by Stafford-Smith and Carter can be used, such that

$$V_c = \frac{2}{3} \alpha \, t \, h \, f'_{m90} \tag{5-6}$$

where f'_{m90} = masonry strength from the parallel prism test, h = height of the masonry (62.2"), t = thickness of the bricks (3.5") and α = the ratio of the panel height under compression which is given by

$$\alpha = \frac{\pi}{2}\left(\frac{4 E_m I_{col}}{E_m t h^3 \sin 2\theta}\right)^{\frac{1}{4}} \tag{5-7}$$

in which $\theta = \tan^{-1} h/b$ being the angle between the infill diagonal and the beam, E_m = elastic modulus of masonry (see Fig. 2.6), E_s = elastic modulus of the steel column (29,000 ksi) and I_{col} = second moment of area of the steel column (82.8 in^3). Using the above equations, $V_c = 145 \times f'_{m90}$ (kips) and $\alpha = 2.8 E_m^{-0.25}$.

Diagonal Tension Failure:

The lateral infill load (F_x) at which diagonal tension cracking is induced can be determined by considering Mohr's cycle of stress at the center of the panel. The lateral infill load must be kept in equilibrium by a vertical force such that

The respective horizontal (σ_x), vertical (σ_y) and shear (τ) stress at the center of the infill panel are

$$F_y = \frac{h}{b} F_x \tag{5-8}$$

$$\sigma_x = -\frac{F_x}{th} \tag{5-9}$$

$$\sigma_y = -\frac{F_y}{th} = \sigma_x \left(\frac{h}{b}\right)^2 \tag{5-10}$$

$$\tau = 1.5 \frac{F_x}{tb} = -1.5 \frac{h}{b} \sigma_x \tag{5-11}$$

From Mohr's circle shown in Fig. 5.16

$$\tan 2\theta = \frac{2\tau}{\sigma_x - \sigma_y} \tag{5-12}$$

Thus

$$\theta = \frac{1}{2} \tan^{-1} \left(\frac{3}{\frac{b}{h} - \frac{h}{b}} \right) \tag{5-13}$$

For the dimensions of the present problem $\theta = 37.334°$. The tensile stress can be computed from

$$\sigma_1 - \sigma_y = \tau \tan\theta \tag{5-14}$$

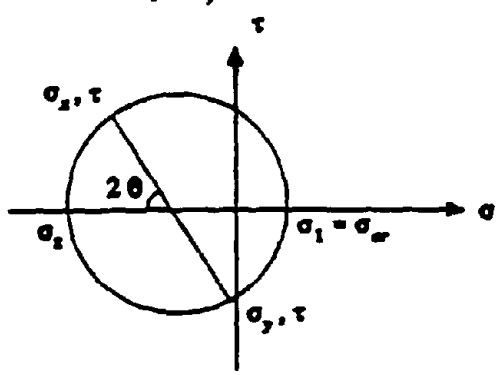

Fig. 5.16

Solving for cracking shear when $V_{cr} = F_s$ using Eqs. 5.9 to Eq. 5-11 in Eq. 5-14 gives

$$V_{cr} = \frac{\sigma_t t b}{1.5 \tan\theta - \left(\frac{h}{b}\right)} \tag{5-15}$$

For the dimensions of the present student, the cracking shear is

$$V_{cr} = F_s = 685\,\sigma_t \tag{5-16}$$

Sliding Shear Failure:

A Mohr-Coulomb failure criteria can be used to assess the sliding shear capacity

$$V_\tau = (\tau_o + \sigma_y \tan\phi)\, b\, t \tag{5-17}$$

where τ_o = cohesion strength given in Table 2.1.

$$V_\tau = \frac{\tau_o\, b\, t}{1 - \frac{h}{b}\tan\phi} = \frac{217.7\,\tau_o}{1 - 0.67\tan\phi} \tag{5-18}$$

Application:

The failure strengths for modes 3 to 5 are given in Table 5.1 for brick infills only. From the results listed in Table 5.1 it is evident that the sliding shear is critical, but closely associated with diagonal tension failure. However, each of these capacities are approximately 60% higher than the observed results in the present tests. This difference is perhaps due to the early onset of diagonal cracking associated with cyclic loading. In any case, each of the above analytical methods provide a poor assessment of strength. One improvement in the analysis may be to reduce the angle of internal friction to reflect the effects of cyclic loading. Using the value of $\mu = \tan\phi = 0.5$ as recommended in Paulay and Priestley, then $V_{sl} = 327\,\tau_o$. This gives shear strengths of 37.6 and 29.5 kips for Specimens 1 and 3, which indicate a predicted strength within -0.5% and +5% of observed results for Specimens 1 and 3, respectively.

TABLE 5.1 Basic Infill Panel Failure Model Capabilities

		Specimen	
		1	3
Mode 3: Compression Failure of Diagonal Strut			
E_m	ksi	1130	800
f'_{m90}	ksi	2.15	1.65
$\alpha = 2.89 E_m^{-0.25}$		0.50	0.54
$V_c = 145\ \alpha\ f'_{m90}$	kips	156	130
Mode 4: Diagonal Tension Failure			
σ_t	ksi	0.120	0.085
$V_{cr} = 685\ \sigma_t$	kips	82	58
Mode 5: Sliding Shear Failure			
ξ_o	ksi	0.115	0.090
ϕ	(deg)	41	44.4
V_s	kips	60	57
V_{expt}		37.8	34.9
$\frac{V_{expt}}{V_{theory}}$		0.63	0.61

Empirical Strength Assessment:

The empirical code-based design principles used for determining the shear strength of concrete/masonry beams/walls can also be applied to the assessment of infill panels, such that the ultimate shear strength is given by

$$V_u = V_m + V_c + V_s$$

in which $V_m = v_m t_m b$ is the contribution of the brick masonry to the shear strength where v_m = nominal masonry shear capacity (quantified below), t_m = brick wall thickness (3.5"), and b = width of the masonry infill panel; $V_c = v_c t_c b$ is the shear carried by the ferrocement overlay where v_c = nominal concrete shear capacity, and t_c = thickness of ferrocement, $V_s = \rho f_y b t_c$ = shear carried by the mesh in the ferrocement; where ρ = volumetric ratio of the mesh (0.004) and f_y = yield strength of the mesh (listed in Table 2.1). Based on the recommendations of Paulay and Priestley, the contribution of shear carried by the masonry can be considered to have initial and final capacities respectively based on monotonic and cyclic loading effects as follows:

$$v_{mi} = 2\sqrt{f'_m}$$
$$v_{mf} = 0.6\sqrt{f'_m} = 0.3\, v_{mi} \qquad (5\text{-}19)$$

Similarly, for the ferrocement mortar.

$$v_{ci} = 2\sqrt{f'_c}$$
$$v_{cf} = 0.6\sqrt{f'_m} = 0.3\, v_{ci} \qquad (5\text{-}20)$$

These strength capacities are summarized for each of the stages of loading for the infills in Table 5.2. The upper and lower bounds of shear capacity based on the aforementioned initial and final quantities are shown for all tests in Fig. 5.17. From these graphs it is evident that a reasonably reliable prediction of the bounds of strength can be obtained by using this modified ACI code

approach to the assessment of shear strength. It should be noted that in the strength assessment strength of the ferrocement coated infills that after about the second reversed cycle of loading, the shear carried by the bricks tends to vanish with only the steel carrying the shear.

Table 5.2 Summary of Strength Properties

				Specimen:	1		2	3		
				Phase:	O[a]	R[b]	R[c]	I	II	III
Material parameters:	Masonry thickness	t_m	in		3.5	3.5	3.5	3.5	3.5	3.5
	Ferrocement thickness	t_c	in			0.5	0.5			0.5
	Masonry strength	f'_m	psi		3400	3400	2200	2900	2900	2900
	Concrete strength	f'_c	psi			4080	4150			3700
	Mesh yield strength	f_y	ksi			60.7	60.7			60.04
Shear Capacities:										
Initial shear capacity of masonry		$V_{mi} = 2\sqrt{f'_m}\, b t_m$	kips		37.6	11.3	30.3	34.8	10.4	10.4
Final shear capacity of masonry		$V_{mf} = 0.3\, V_{mi}$	kips		11.3	0	9.1	10.4	0	0
Shear capacity of ferrocement mortar		$V_c = 2\sqrt{f'_c}\, b t_c$	kips			5.9	5.9			11.2
Shear carried by steel mesh and rebars		$V_s = \rho f_y b t_c + (V_{sd})$	kips			12.5	12.5	(6.9)[d]	(6.9)	31.7
Initial ultimate shear capacity		$V_{ui} = V_{mi} + V_{ci} + V_s$	**kips**		**37.6**	**29.7**	**48.8**	**41.7**	**17.3**	**53.4**
Final ultimate shear capacity		$V_{uf} = V_{mf} + V_{cf} + V_s$	**kips**		**11.3**	**14.3**	**23.5**	**17.3**	**6.9**	**35.1**
Observed strengths:	reversed direction	V^-_{exp}	kips		-37.8	-26.5	-31.8	-34.9	-25.4	-46.0
	forward direction	V^+_{exp}	kips		33.1	18.5	26.7	19.0	17.5	41.6
Strength ratios		V^-_{exp} / V_{ui}			1.00	0.89	0.65	0.84	1.47	0.86
		V^+_{exp} / V_{uf}			2.93	1.31	1.14	1.10	2.54	1.18

[a]Ordinary infill, [b]Repaired infill, [c]Retrofitted infill, [d]Diagonal rebar engaged on negative levels only.

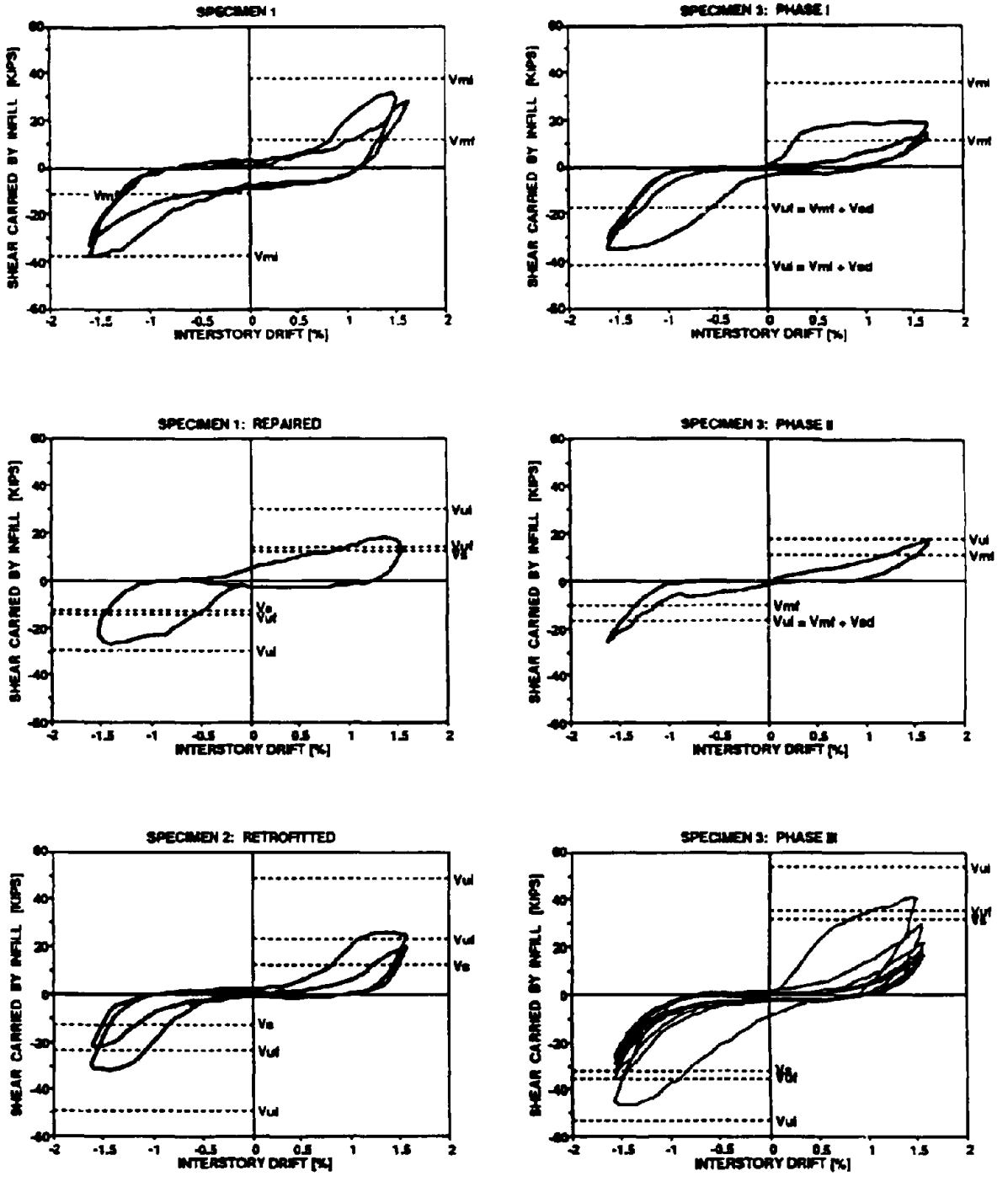

Fig. 5.17 Experimental Shear Carried by Infill Compared with Code-based Shear Strength Predictions

SECTION 6
SUMMARY AND CONCLUSIONS

The following conclusions can be made from this study:

1. Unreinforced clay brick masonry infills, within steel frames, behave in a ductile fashion under in-plane lateral loadings. However, bricks are loosened within the frame during load cycling such that this may leave the infill vulnerable to fall-out from out-of-plane loads. Nevertheless, if fallout of the infill is not a problem, unreinforced clay brick masonry infills can act as a ductile lateral load resisting elements in multi-story frames.

2. Although the experiments on ordinary brick infills demonstrated a reasonable ductility capability, by the end of testing the panels were quite loose within their frames. It is likely that the out-of-plane integrity of infills with ferrocement overlays is improved due to tensile membrane action. However, it is considered that some testing should be carried out to assess the out-of-plane integrity of ordinary and repaired/retrofitted brick infills.

3. Using an enhanced ferrocement overlay on the infill panel, which also contains diagonal rebars as reinforcement, provides an improved ductility capacity for the infill panel. An enhanced overlay should improve the general seismic performance of such an infilled wall system. The diagonal reinforcement adds strength and energy dissipation capability through a confinement action. Tension cracks are dispersed along each diagonal with this class of ferrocement overlay. The diagonal rebars also help to prevent out-of-plane buckling of the ferrocement at the center of the panel. Such rehabilitated infills could be used in the lower story of a multi-story frame where plastic hinging would normally be expected to occur in structural walls under earthquake loading.

4. Shear strength assessments of the infill panels based on first principles to determine failure modes due to the most critical of (i) diagonal compression, (ii) diagonal tension, and (iii) sliding shear overpredicted that lateral load capacities by some **60%** . However, improved predictions were made by using the classical code-based empirical approach using $V_u = V_c + V_s$. To allow for cyclic loadings effects, shear strengths can be bounded by initial and final shear

SECTION 7

REFERENCES

1. Dawe, J.L., Schriver, A.B., and Sofocleous, C. "Masonry Infilled Steel Frames Subjected to Dynamic Load", Canadian Journal of Civil Engineering, 1989, Vol 16, pp. 877-885.

2. DiCorso, P.J., "Response of Frames With Bolted Semi-Rigid Connections Subjected to Seismic Loading", Masters Thesis, Department of Civil Engineering, State Univeristy of New York at Buffalo, January, 1989.

3. Lee, H.H., Prawel, S.P., 1991. "The Seismic Renovation and Repair Potential of Ferrocement Coatings Applied to Old Brick Masonry Walls." Proceedings of the Sixth World Conference on Earthquake Engineering, State University of New York at Buffalo, Buffalo, NY, June 1991, 663-670.

4. Ma, J., "Experiments on Upgraded Brick-Infilled Steel Frames Under Reversed Cyclic Lateral Load", Masters Project, Department of Civil Engineering, State University of New York at Buffalo, August, 1990.

5. Moghaddam, H.A., Dowling, P.J. "The State of Art in Infilled Frames", Civil Engineering Department, Imperial College, ESEE Research Report No. 87-2, London, August 1987.

6. Paulay and Priestley, (1992) "Seismic Design of Reinforced Concrete and Masonry Buildings", J. Wiley and Sons, NY, 1992, 744 pp.

7. Riddington, J.R., Ghazali, M.Z., "Hypothesis for Shear Failure in Masonry Joints", Proceedings of the Institution of Civil Engineers, Part 2-Research and Theory, Vol. 89, March 1990, pp. 89-102.

8. Sheppard, P. and Terceli, "The Effect of Repair and Strengthening Method for Masonry Walls", Proceedings, 7th WCEE, Istanbul, 1980, Vol 6, pp. 255.

9. Wood, R.H. "Plasticity, Composite Action and Collapse Design of Unreinforced Shear Wall Panels in Frames", Proceedings, Institution of Civil Engineers, Part 2, 1978, Vol 65, June, pp. 381-411.

10. Wotjkowski, K.M., "Experiments on brick-infilled steel frames under reversed cyclic lateral load", Masters Project, Department of Civil Engineering, State University of New York at Buffalo, January, 1990.

APPENDIX A RESULTS FROM BARE FRAME TESTS

Following each infilled frame test the masonry was removed and the frame tested; firstly with the diagonal braces present, and finally without the braces. These post-infill tests are presented here in Appendix A. For these post-infill tests, the drift amplitude was kept the same as the final subtest used for the infill, i.e. 1.5%. Sub-tests which included two complete reversed cycles of at drift amplitudes of ±0.25%, ±1.0%, ±2.0% and ±3.0% were run. Between each sub-test, the specimen was inspected for visible damage. Careful attention was paid to the behavior of the semi-rigid connections in order to ascertain the yield line pattern.

A.1 Results of Bare Frame Test on Specimen 1 after the Repaired Infill Test

The force-drift response of the bare frame test after the brick infill was tested and removed is shown in Fig. A.1. The difference in area between the repaired infill test and the bare frame test clearly indicate that the coated brick infill is the primary energy dissipating mechanism. However, it is evident that the energy dissipation capacity diminishes rapidly with cycling.

The joint rotation response of the bare frame test is shown in Fig. A.2 (a) and (b). Significant hysteresis can be seen and it indicates that the angle connections had yielded.

The bending moment of the right column and bottom beam for the first cycle of positive and negative loading are shown in Fig. A.3 (a) and (b). As expected, the moments show straight lines with the point of contraflexure at midspan of the beams. From Fig. A.3 (a) it is interesting to note that the column moments are not symmetrical about the mid-height of the column. This indicates that different loads are being provided by the upper and lower bracing, respectively. Also note that the column moments are slightly curved in a "S" shape over their height. The departure from a straight line distribution is due to secondary moments arising from P-delta effects in the column.

A.2 Results of the Bare Frame Test on Specimen 2

Fig. A.4 (a) shows the force-drift response of the bare frame with bracing. From these hysteresis loops, it can be clearly seen that the semi-rigid bolted connections of the bare frame absorb a

minimal amount of energy in contrast to the complete infill frame.

Fig. A.4 (b) shows the force-drift response of the bare frame without bracing to the ±1.5% drift amplitudes. The results from both bare frame tests show insignificant degradation in strength with cyclic loading.

For comparison with the Bare Frame Specimen two additional cycles were performed at a ±2.0% drift amplitude with the result plotted in Fig. A.4 (c). This can be compared with the relevant two cycles at the 2% amplitude taken from Fig. 3.2 (Fig. A.4 (d)) for the Bare Frame Specimen.

The load vs. joint rotation response of the bare frame with bracing test is shown in Figs. A.5 (a) and (b). Differences in joint rotation for a given load level appears to be due to the previous asymmetric yielding when the infill panel was present. The difference in joint rotation and drift is due to elastic deformations of the frame.

The load vs. joint rotation response of the bare frame without bracing test is shown in Figs. A.6 (a) and (b).

Figs. A.7 to A.10 respectively show the implied bending moments measured from the strain gages for: the top and bottom beam when the bracing was present; a column with bracing; and the column when the frame was retested without bracing.

A.3 Results of the Bare Frame Test on Specimen 3

Figs. A.11 to A.13 show: the force-drift response of the bare frame with and without bracing; the lateral load-joint rotation response for an upper and lower semi-rigid bolted connection and the bending moments for the upper and lower beams.

A.4 Discussion of Results

This section has presented the lateral load-drift response of bare frames with and without the diagonal bracing in the end half-bays.

The results from this section are used to obtain the response of the steel frame which can be subtracted from the gross infilled frame response to obtain the net effect of the infill on the overall performance. This is discussed previously in Section 5.

The distributions of moments in all cases agree well with theoretical expectations. This gives confidence to the results obtained when the bricks are present where distribution of moments are significantly altered due to the presence of local contact stresses.

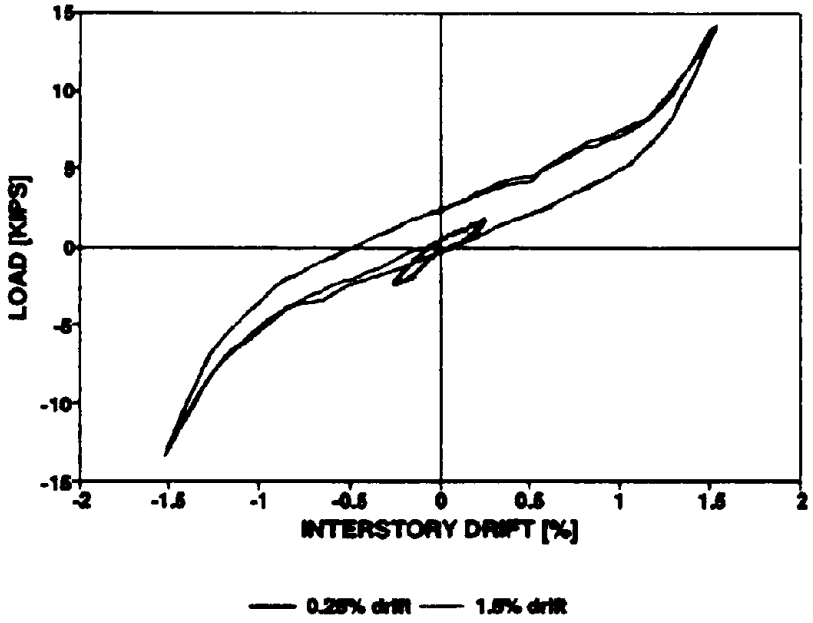

Fig. A.1 Lateral load-drift response of bare frame (Repaired Specimen 1)

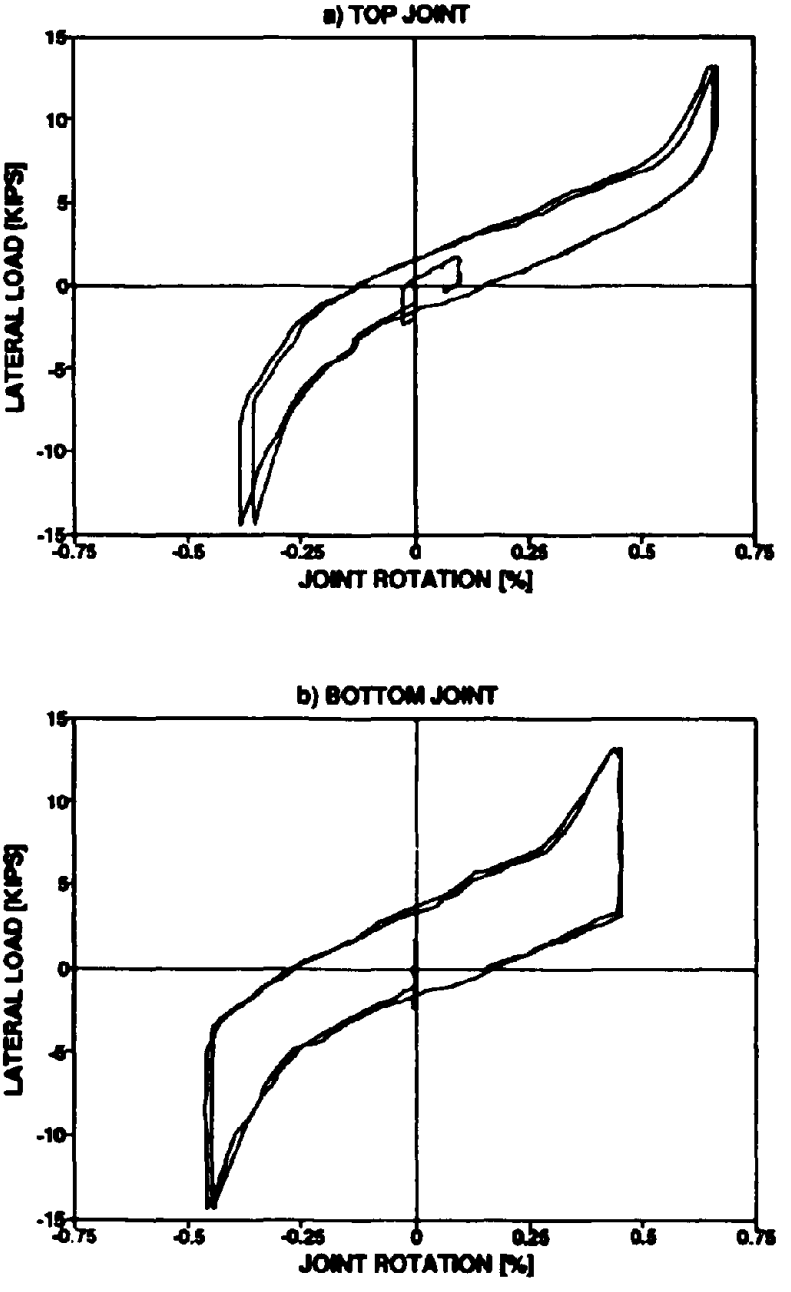

Fig. A.2 Joint rotation response of bare frame (Repaired Specimen 1)

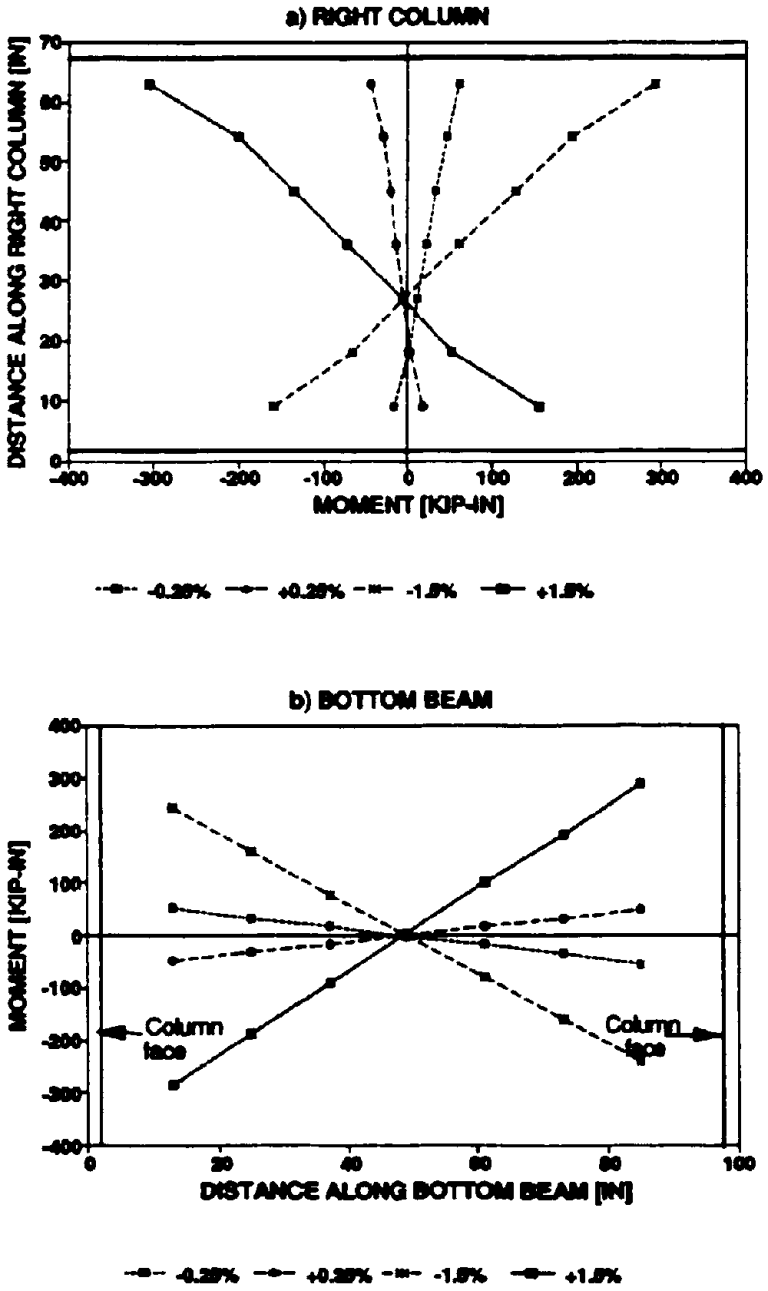

Fig. A.3 Implied bending moments along the beam of bare frame (Repaired Specimen 1)

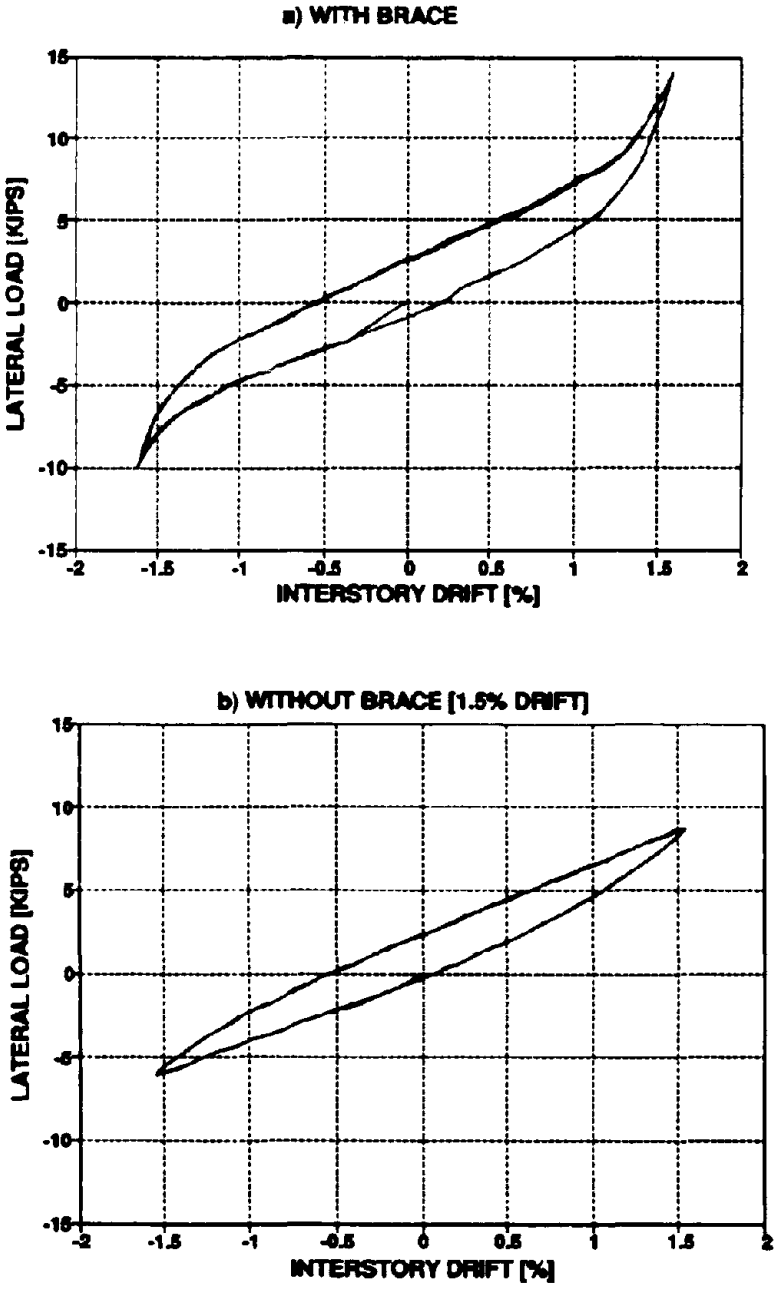

Fig. A.4 Lateral load-drift response of bare frame (Retrofitted Specimen 2)

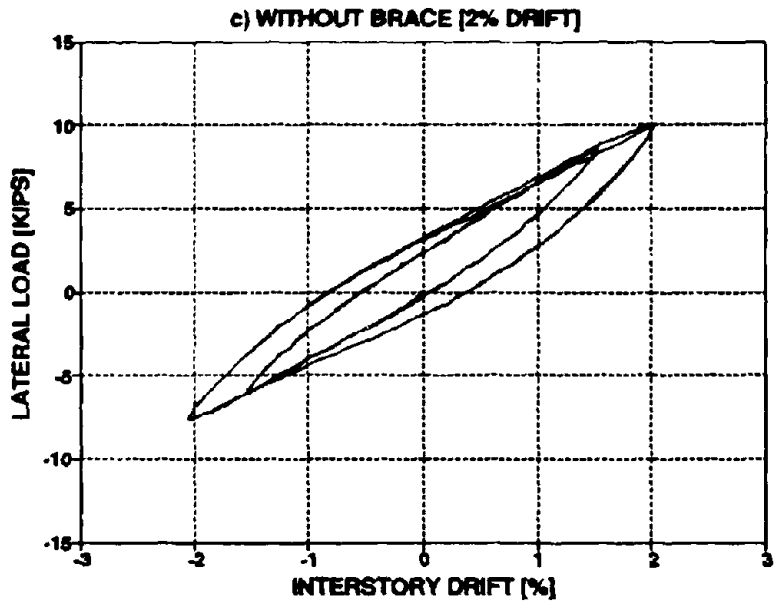
c) WITHOUT BRACE [2% DRIFT]
LATERAL LOAD [KIPS]
INTERSTORY DRIFT [%]

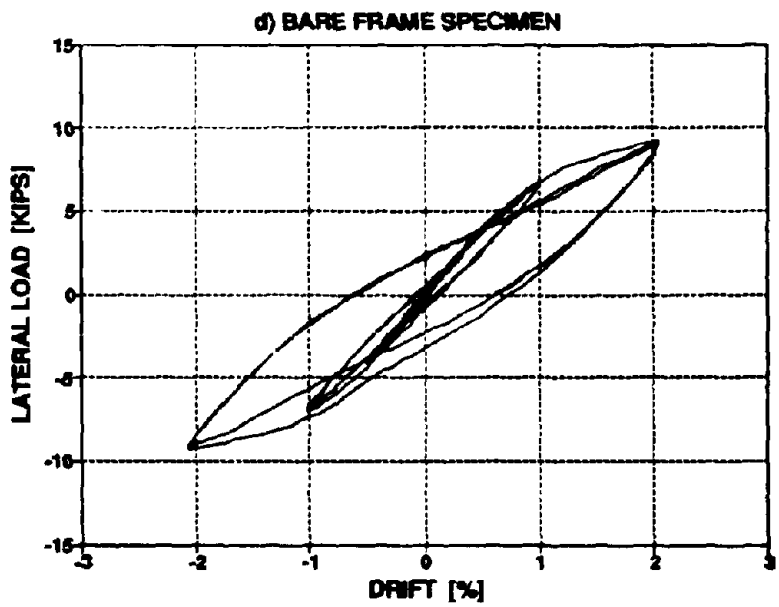
d) BARE FRAME SPECIMEN
LATERAL LOAD [KIPS]
DRIFT [%]

Fig. A.4 (c) and (d)

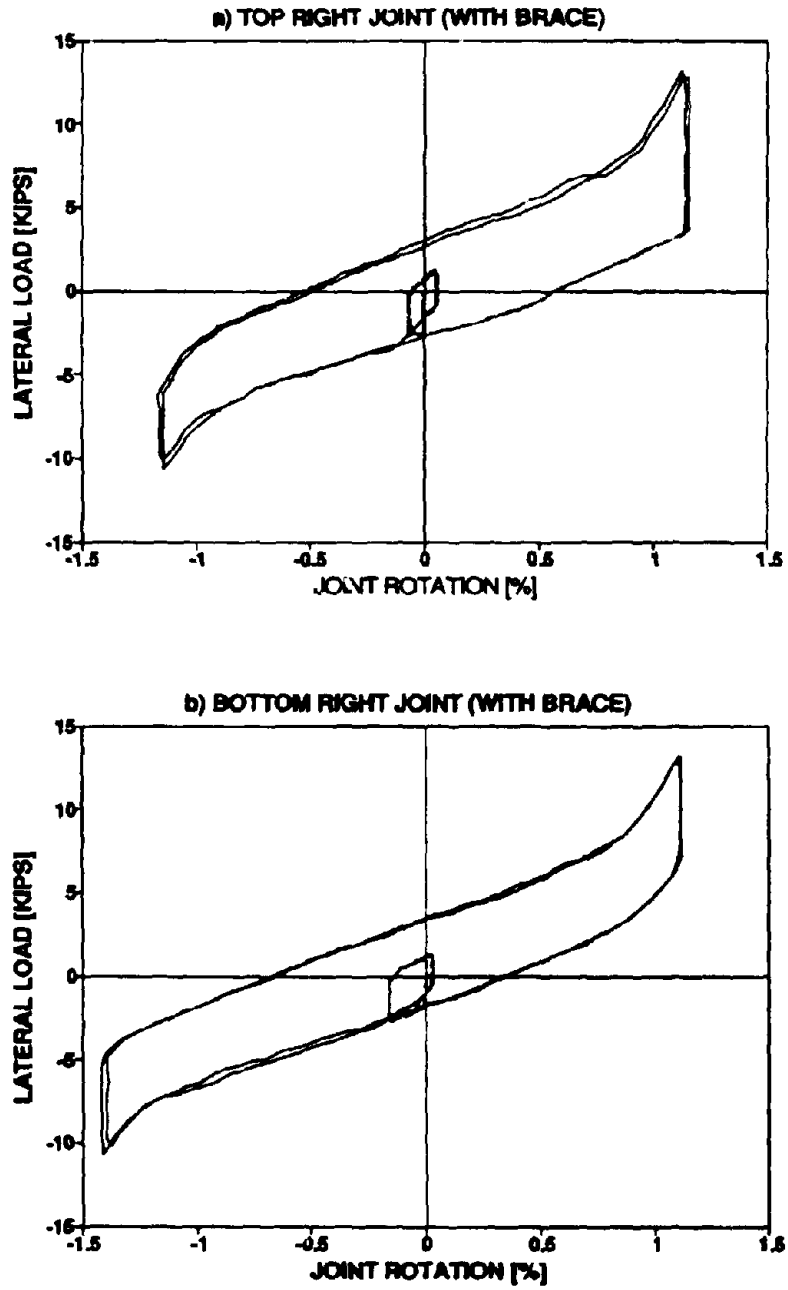

Fig. A.5 Joint rotation response of bare frame with braces (Retrofitted Specimen 2)

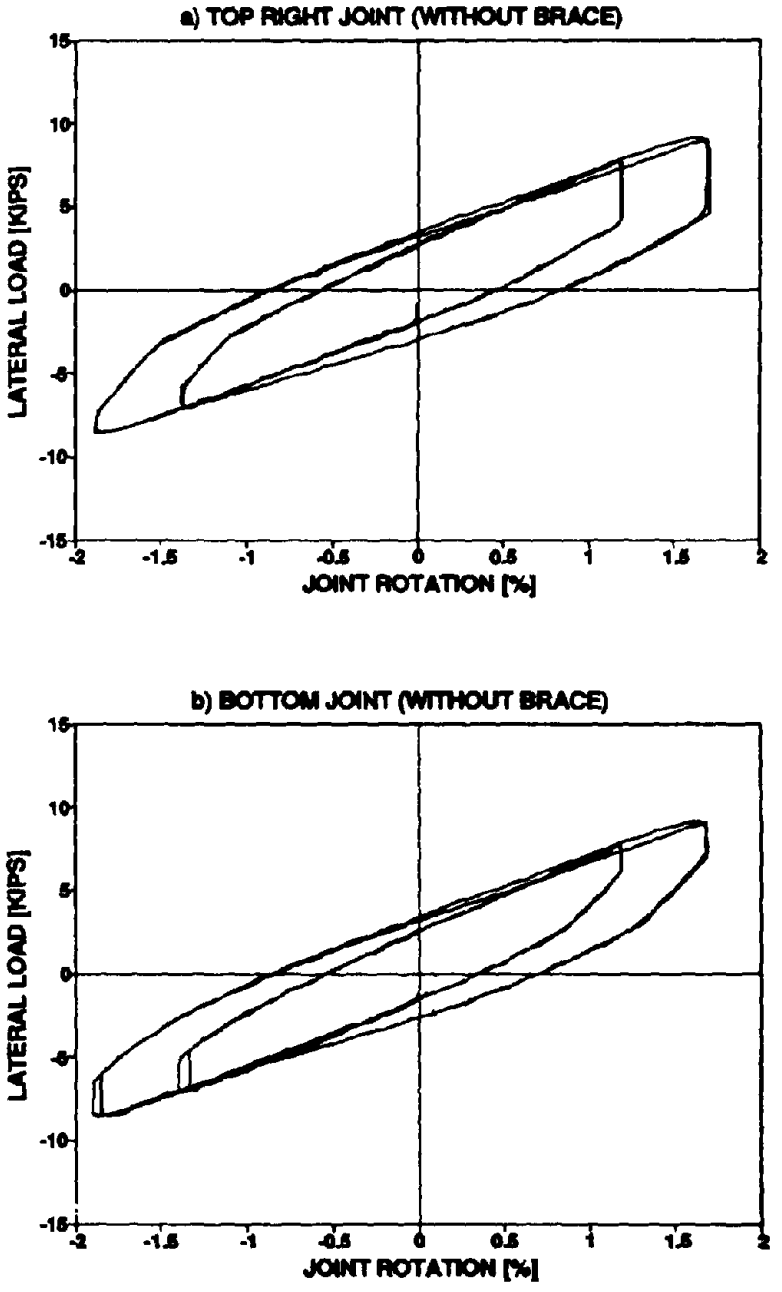

Fig. A.6 Joint rotation response of bare frame without braces (Retrofitted Specimen 2)

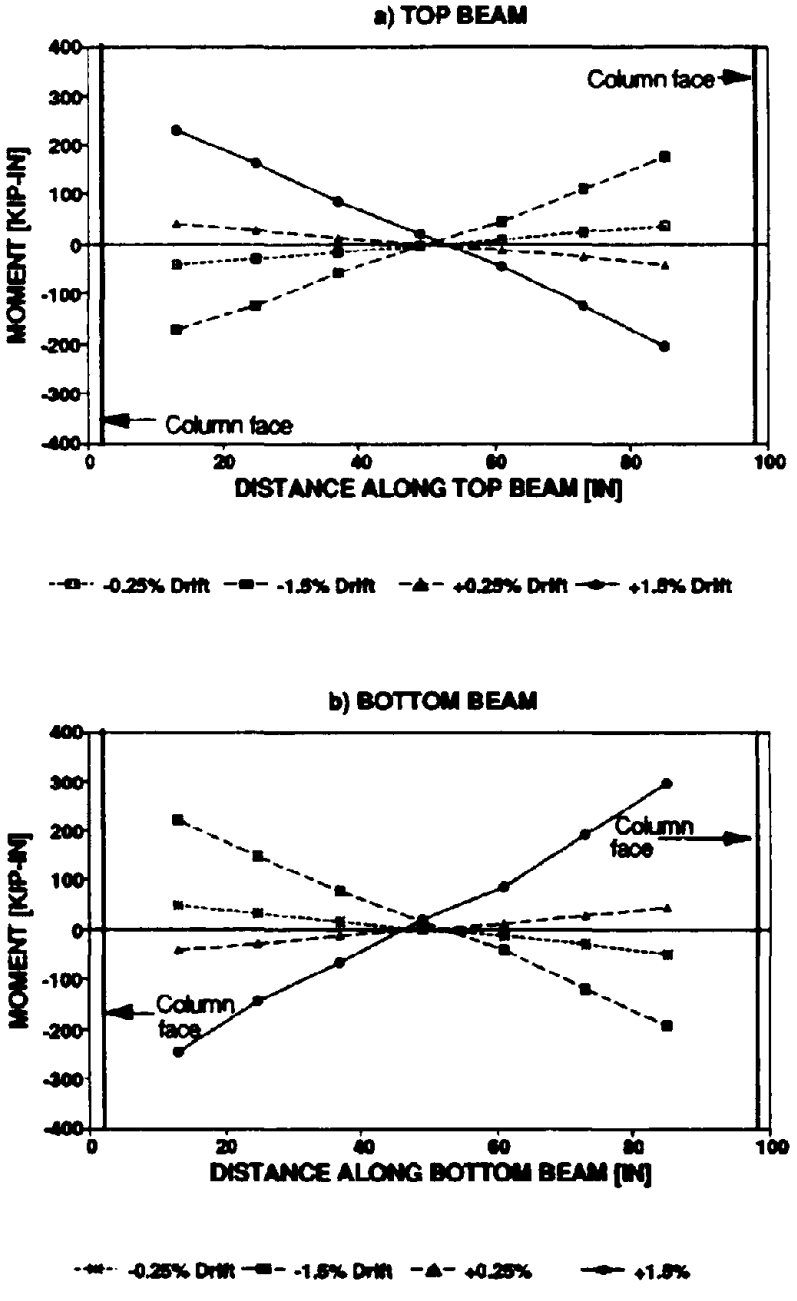

Fig. A.7 Implied moments along beam of the bare frame (Retrofitted Specimen 2)

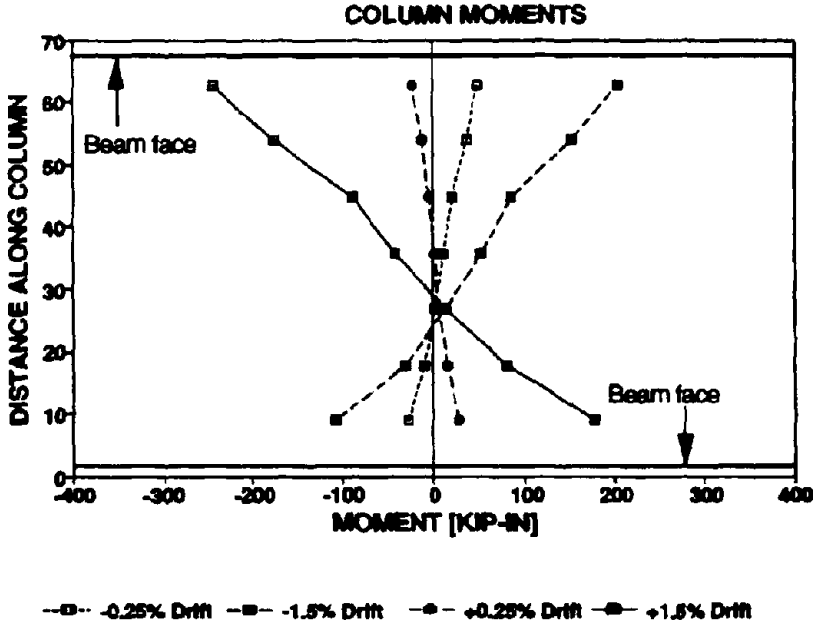

Fig. A.8 Implied bending moments on the right column of bare frame (Retrofitted Specimen 2)

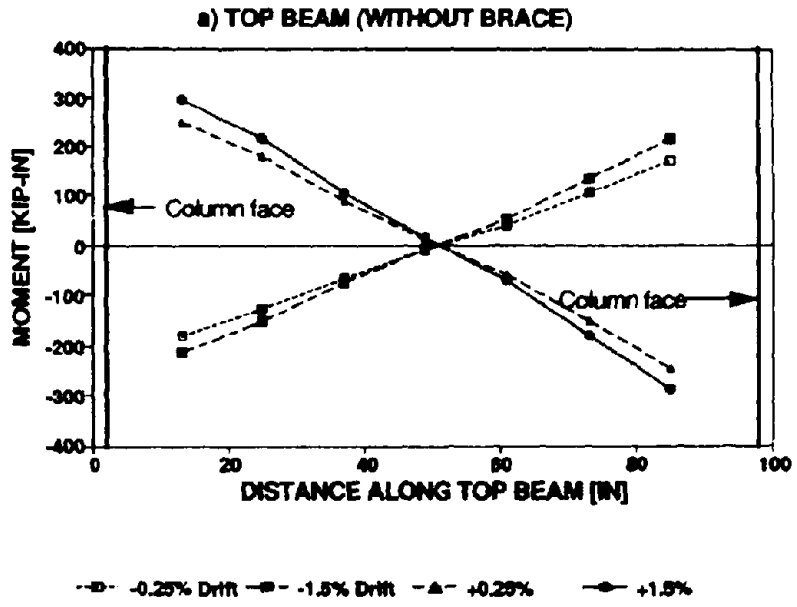

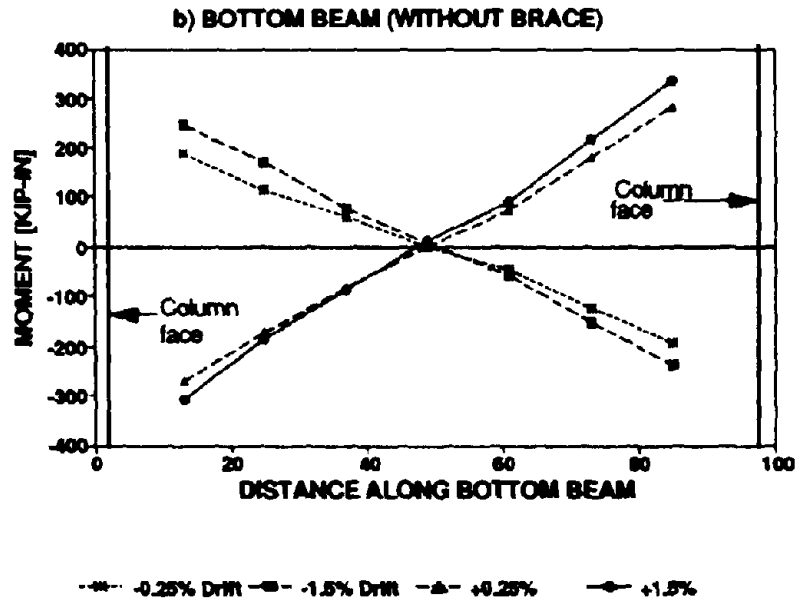

Fig. A.9 Implied beam moments of bare frame without braces (Retrofitted Specimen 2)

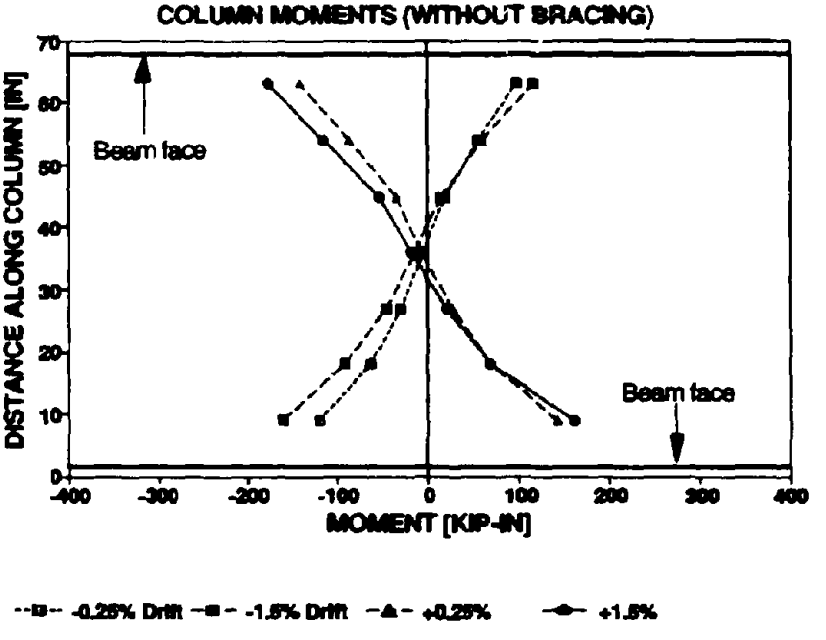

Fig. A.10 Implied moments along right column of the bare frame without braces (Retrofitted Specimen 2)

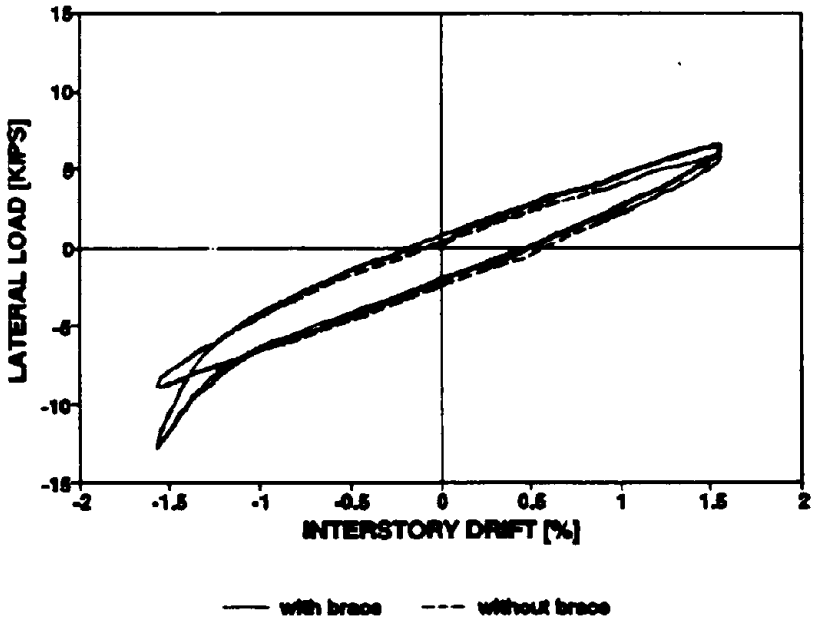

Fig. A.11 Lateral load-drift response of bare frame of Specimen 3

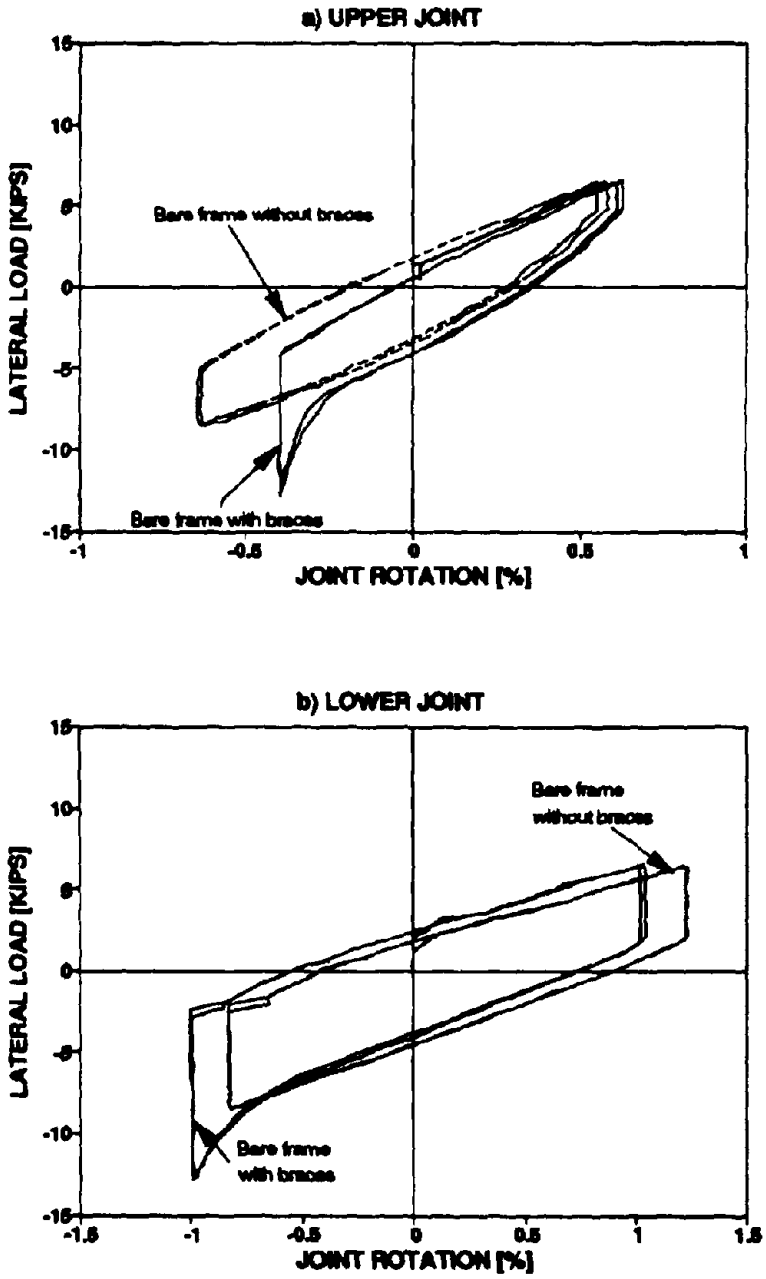

Fig. A.12 Joint rotation response of bare frame of Specimen 3

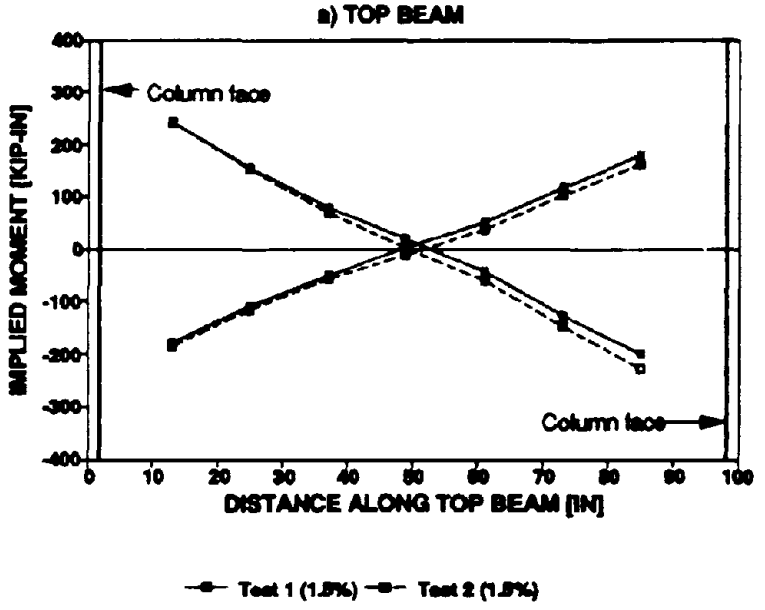

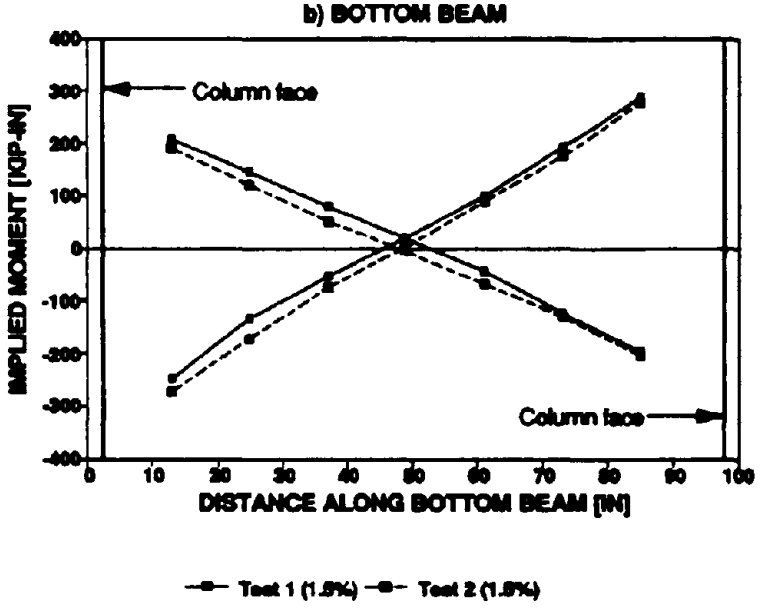

Fig. A.13 Implied bending moments along the beam of Specimen 3

NATIONAL CENTER FOR EARTHQUAKE ENGINEERING RESEARCH
LIST OF TECHNICAL REPORTS

The National Center for Earthquake Engineering Research (NCEER) publishes technical reports on a variety of subjects related to earthquake engineering written by authors funded through NCEER. These reports are available from both NCEER's Publications Department and the National Technical Information Service (NTIS). Requests for reports should be directed to the Publications Department, National Center for Earthquake Engineering Research, State University of New York at Buffalo, Red Jacket Quadrangle, Buffalo, New York 14261. Reports can also be requested through NTIS, 5285 Port Royal Road, Springfield, Virginia 22161. NTIS accession numbers are shown in parenthesis, if available.

NCEER-87-0001 "First Year Program in Research, Education and Technology Transfer," 3/5/87, (PB88-134275/AS).

NCEER-87-0002 "Experimental Evaluation of Instantaneous Optimal Algorithms for Structural Control," by R.C. Lin, T.T. Soong and A.M. Reinhorn, 4/20/87, (PB88-134341/AS).

NCEER-87-0003 "Experimentation Using the Earthquake Simulation Facilities at University at Buffalo," by A.M. Reinhorn and R.L. Ketter, to be published.

NCEER-87-0004 "The System Characteristics and Performance of a Shaking Table," by J.S. Hwang, K.C. Chang and G.C. Lee, 6/1/87, (PB88-134259/AS). This report is available only through NTIS (see address given above).

NCEER-87-0005 "A Finite Element Formulation for Nonlinear Viscoplastic Material Using a Q Model," by O. Gyebi and G. Dasgupta, 11/2/87, (PB88-213764/AS).

NCEER-87-0006 "Symbolic Manipulation Program (SMP) - Algebraic Codes for Two and Three Dimensional Finite Element Formulations," by X. Lee and G. Dasgupta, 11/9/87, (PB88-219522/AS).

NCEER-87-0007 "Instantaneous Optimal Control Laws for Tall Buildings Under Seismic Excitations," by J.N. Yang, A. Akbarpour and P. Ghaemmaghami, 6/10/87, (PB88-134333/AS).

NCEER-87-0008 "IDARC: Inelastic Damage Analysis of Reinforced Concrete Frame - Shear-Wall Structures," by Y.J. Park, A.M. Reinhorn and S.K. Kunnath, 7/20/87, (PB88-134325/AS).

NCEER-87-0009 "Liquefaction Potential for New York State: A Preliminary Report on Sites in Manhattan and Buffalo," by M. Budhu, V. Vijayakumar, R.F. Giese and L. Baumgras, 8/31/87, (PB88-163704/AS). This report is available only through NTIS (see address given above).

NCEER-87-0010 "Vertical and Torsional Vibration of Foundations in Inhomogeneous Media," by A.S. Veletsos and K.W. Dotson, 6/1/87, (PB88-134291/AS).

NCEER-87-0011 "Seismic Probabilistic Risk Assessment and Seismic Margins Studies for Nuclear Power Plants," by Howard H.M. Hwang, 6/15/87, (PB88-134267/AS).

NCEER-87-0012 "Parametric Studies of Frequency Response of Secondary Systems Under Ground-Acceleration Excitations," by Y. Yong and Y.K. Lin, 6/10/87, (PB88-134309/AS).

NCEER-87-0013 "Frequency Response of Secondary Systems Under Seismic Excitation," by J.A. HoLung, J. Cai and Y.K. Lin, 7/31/87, (PB88-134317/AS).

NCEER-87-0014 "Modelling Earthquake Ground Motions in Seismically Active Regions Using Parametric Time Series Methods," by G.W. Ellis and A.S. Cakmak, 8/25/87, (PB88-134283/AS).

NCEER-87-0015 "Detection and Assessment of Seismic Structural Damage," by E. DiPasquale and A.S. Cakmak, 8/25/87, (PB88-163712/AS).

NCEER-88-0006 "Combining Structural Optimization and Structural Control," by F.Y. Cheng and C.P. Pantelides, 1/10/88, (PB88-213814/AS).

NCEER-88-0007 "Seismic Performance Assessment of Code-Designed Structures," by H.H-M. Hwang, J-W. Jaw and H-J. Shau, 3/20/88, (PB88-219423/AS).

NCEER-88-0008 "Reliability Analysis of Code-Designed Structures Under Natural Hazards," by H.H-M. Hwang, H. Ushiba and M. Shinozuka, 2/29/88, (PB88-229471/AS).

NCEER-88-0009 "Seismic Fragility Analysis of Shear Wall Structures," by J-W Jaw and H.H-M. Hwang, 4/30/88, (PB89-102867/AS).

NCEER-88-0010 "Base Isolation of a Multi-Story Building Under a Harmonic Ground Motion - A Comparison of Performances of Various Systems," by F-G Fan, G. Ahmadi and I.G. Tadjbakhsh, 5/18/88, (PB89-122238/AS).

NCEER-88-0011 "Seismic Floor Response Spectra for a Combined System by Green's Functions," by F.M. Lavelle, L.A. Bergman and P.D. Spanos, 5/1/88, (PB89-102875/AS).

NCEER-88-0012 "A New Solution Technique for Randomly Excited Hysteretic Structures," by G.Q. Cai and Y.K. Lin, 5/16/88, (PB89-102883/AS).

NCEER-88-0013 "A Study of Radiation Damping and Soil-Structure Interaction Effects in the Centrifuge," by K. Weissman, supervised by J.H. Prevost, 5/24/88, (PB89-144703/AS).

NCEER-88-0014 "Parameter Identification and Implementation of a Kinematic Plasticity Model for Frictional Soils," by J.H. Prevost and D.V. Griffiths, to be published.

NCEER-88-0015 "Two- and Three- Dimensional Dynamic Finite Element Analyses of the Long Valley Dam," by D.V. Griffiths and J.H. Prevost, 6/17/88, (PB89-144711/AS).

NCEER-88-0016 "Damage Assessment of Reinforced Concrete Structures in Eastern United States," by A.M. Reinhorn, M.J. Seidel, S.K. Kunnath and Y.J. Park, 6/15/88, (PB89-122220/AS).

NCEER-88-0017 "Dynamic Compliance of Vertically Loaded Strip Foundations in Multilayered Viscoelastic Soils," by S. Ahmad and A.S.M. Israil, 6/17/88, (PB89-102891/AS).

NCEER-88-0018 "An Experimental Study of Seismic Structural Response With Added Viscoelastic Dampers," by R.C. Lin, Z. Liang, T.T. Soong and R.H. Zhang, 6/30/88, (PB89-122212/AS). This report is available only through NTIS (see address given above).

NCEER-88-0019 "Experimental Investigation of Primary - Secondary System Interaction," by G.D. Manolis, G. Juhn and A.M. Reinhorn, 5/27/88, (PB89-122204/AS).

NCEER-88-0020 "A Response Spectrum Approach For Analysis of Nonclassically Damped Structures," by J.N. Yang, S. Sarkani and F.X. Long, 4/22/88, (PB89-102909/AS).

NCEER-88-0021 "Seismic Interaction of Structures and Soils: Stochastic Approach," by A.S. Veletsos and A.M. Prasad, 7/21/88, (PB89-122196/AS).

NCEER-88-0022 "Identification of the Serviceability Limit State and Detection of Seismic Structural Damage," by E. DiPasquale and A.S. Cakmak, 6/15/88, (PB89-122188/AS). This report is available only through NTIS (see address given above).

NCEER-88-0023 "Multi-Hazard Risk Analysis: Case of a Simple Offshore Structure," by B.K. Bhartia and E.H. Vanmarcke, 7/21/88, (PB89-145213/AS).

NCEER-88-0024 "Automated Seismic Design of Reinforced Concrete Buildings," by Y.S. Chung, C. Meyer and M. Shinozuka, 7/5/88, (PB89-122170/AS). This report is available only through NTIS (see address given above).

NCEER-88-0025 "Experimental Study of Active Control of MDOF Structures Under Seismic Excitations," by L.L. Chung, R.C. Lin, T.T. Soong and A.M. Reinhorn, 7/10/88, (PB89-122600/AS).

NCEER-88-0026 "Earthquake Simulation Tests of a Low-Rise Metal Structure," by J.S. Hwang, K.C. Chang, G.C. Lee and R.L. Ketter, 8/1/88, (PB89-102917/AS).

NCEER-88-0027 "Systems Study of Urban Response and Reconstruction Due to Catastrophic Earthquakes," by F. Kozin and H.K. Zhou, 9/22/88, (PB90-162348/AS).

NCEER-88-0028 "Seismic Fragility Analysis of Plane Frame Structures," by H.H-M. Hwang and Y.K. Low, 7/31/88, (PB89-131445/AS).

NCEER-88-0029 "Response Analysis of Stochastic Structures," by A. Kardara, C. Bucher and M. Shinozuka, 9/22/88, (PB89-174429/AS).

NCEER-88-0030 "Nonnormal Accelerations Due to Yielding in a Primary Structure," by D.C.K. Chen and L.D. Lutes, 9/19/88, (PB89-131437/AS).

NCEER-88-0031 "Design Approaches for Soil-Structure Interaction," by A.S. Veletsos, A.M. Prasad and Y. Tang, 12/30/88, (PB89-174437/AS). This report is available only through NTIS (see address given above).

NCEER-88-0032 "A Re-evaluation of Design Spectra for Seismic Damage Control," by C.J. Turkstra and A.G. Tallin, 11/7/88, (PB89-145221/AS).

NCEER-88-0033 "The Behavior and Design of Noncontact Lap Splices Subjected to Repeated Inelastic Tensile Loading," by V.E. Sagan, P. Gergely and R.N. White, 12/8/88, (PB89-163737/AS).

NCEER-88-0034 "Seismic Response of Pile Foundations," by S.M. Mamoon, P.K. Banerjee and S. Ahmad, 11/1/88, (PB89-145239/AS).

NCEER-88-0035 "Modeling of R/C Building Structures With Flexible Floor Diaphragms (IDARC2)," by A.M. Reinhorn, S.K. Kunnath and N. Panahshahi, 9/7/88, (PB89-207153/AS).

NCEER-88-0036 "Solution of the Dam-Reservoir Interaction Problem Using a Combination of FEM, BEM with Particular Integrals, Modal Analysis, and Substructuring," by C-S. Tsai, G.C. Lee and R.L. Ketter, 12/31/88, (PB89-207146/AS).

NCEER-88-0037 "Optimal Placement of Actuators for Structural Control," by F.Y. Cheng and C.P. Pantelides, 8/15/88, (PB89-162846/AS).

NCEER-88-0038 "Teflon Bearings in Aseismic Base Isolation: Experimental Studies and Mathematical Modeling," by A. Mokha, M.C. Constantinou and A.M. Reinhorn, 12/5/88, (PB89-218457/AS). This report is available only through NTIS (see address given above).

NCEER-88-0039 "Seismic Behavior of Flat Slab High-Rise Buildings in the New York City Area," by P. Weidlinger and M. Ettouney, 10/15/88, (PB90-145681/AS).

NCEER-88-0040 "Evaluation of the Earthquake Resistance of Existing Buildings in New York City," by P. Weidlinger and M. Ettouney, 10/15/88, to be published.

NCEER-88-0041 "Small-Scale Modeling Techniques for Reinforced Concrete Structures Subjected to Seismic Loads," by W. Kim, A. El-Attar and R.N. White, 11/22/88, (PB89-189625/AS).

NCEER-88-0042 "Modeling Strong Ground Motion from Multiple Event Earthquakes," by G.W. Ellis and A.S. Cakmak, 10/15/88, (PB89-174445/AS).

NCEER-88-0043 "Nonstationary Models of Seismic Ground Acceleration," by M. Grigoriu, S.E. Ruiz and E. Rosenblueth, 7/15/88, (PB89-189617/AS).

NCEER-88-0044 "SARCF User's Guide: Seismic Analysis of Reinforced Concrete Frames," by Y.S. Chung, C. Meyer and M. Shinozuka, 11/9/88, (PB89-174452/AS).

NCEER-88-0045 "First Expert Panel Meeting on Disaster Research and Planning," edited by J. Pantelic and J. Stoyle, 9/15/88, (PB89-174460/AS).

NCEER-88-0046 "Preliminary Studies of the Effect of Degrading Infill Walls on the Nonlinear Seismic Response of Steel Frames," by C.Z. Chrysostomou, P. Gergely and J.F. Abel, 12/19/88, (PB89-208383/AS).

NCEER-88-0047 "Reinforced Concrete Frame Component Testing Facility - Design, Construction, Instrumentation and Operation," by S.P. Pessiki, C. Conley, T. Bond, P. Gergely and R.N. White, 12/16/88, (PB89-174478/AS).

NCEER-89-0001 "Effects of Protective Cushion and Soil Compliancy on the Response of Equipment Within a Seismically Excited Building," by J.A. HoLung, 2/16/89, (PB89-207179/AS).

NCEER-89-0002 "Statistical Evaluation of Response Modification Factors for Reinforced Concrete Structures," by H.H-M. Hwang and J-W. Jaw, 2/17/89, (PB89-207187/AS).

NCEER-89-0003 "Hysteretic Columns Under Random Excitation," by G-Q. Cai and Y.K. Lin, 1/9/89, (PB89-196513/AS).

NCEER-89-0004 "Experimental Study of 'Elephant Foot Bulge' Instability of Thin-Walled Metal Tanks," by Z-H. Jia and R.L. Ketter, 2/22/89, (PB89-207195/AS).

NCEER-89-0005 "Experiment on Performance of Buried Pipelines Across San Andreas Fault," by J. Isenberg, E. Richardson and T.D. O'Rourke, 3/10/89, (PB89-218440/AS).

NCEER-89-0006 "A Knowledge-Based Approach to Structural Design of Earthquake-Resistant Buildings," by M. Subramani, P. Gergely, C.H. Conley, J.F. Abel and A.H. Zaghw, 1/15/89, (PB89-218465/AS).

NCEER-89-0007 "Liquefaction Hazards and Their Effects on Buried Pipelines," by T.D. O'Rourke and P.A. Lane, 2/1/89, (PB89-218481).

NCEER-89-0008 "Fundamentals of System Identification in Structural Dynamics," by H. Imai, C-B. Yun, O. Maruyama and M. Shinozuka, 1/26/89, (PB89-207211/AS).

NCEER-89-0009 "Effects of the 1985 Michoacan Earthquake on Water Systems and Other Buried Lifelines in Mexico," by A.G. Ayala and M.J. O'Rourke, 3/8/89, (PB89-207229/AS).

NCEER-89-R010 "NCEER Bibliography of Earthquake Education Materials," by K.E.K. Ross, Second Revision, 9/1/89, (PB90-125352/AS).

NCEER-89-0011 "Inelastic Three-Dimensional Response Analysis of Reinforced Concrete Building Structures (IDARC-3D), Part I - Modeling," by S.K. Kunnath and A.M. Reinhorn, 4/17/89, (PB90-114612/AS).

NCEER-89-0012 "Recommended Modifications to ATC-14," by C.D. Poland and J.O. Malley, 4/12/89, (PB90-108648/AS).

NCEER-89-0013 "Repair and Strengthening of Beam-to-Column Connections Subjected to Earthquake Loading," by M. Corazao and A.J. Durrani, 2/28/89, (PB90-109885/AS).

NCEER-89-0014 "Program EXKAL2 for Identification of Structural Dynamic Systems," by O. Maruyama, C-B. Yun, M. Hoshiya and M. Shinozuka, 5/19/89, (PB90-109877/AS).

NCEER-89-0015 "Response of Frames With Bolted Semi-Rigid Connections, Part I - Experimental Study and Analytical Predictions," by P.J. DiCorso, A.M. Reinhorn, J.R. Dickerson, J.B. Radziminski and W.L. Harper, 6/1/89, to be published.

NCEER-89-0016 "ARMA Monte Carlo Simulation in Probabilistic Structural Analysis," by P.D. Spanos and M.P. Mignolet, 7/10/89, (PB90-109893/AS).

NCEER-89-P017 "Preliminary Proceedings from the Conference on Disaster Preparedness - The Place of Earthquake Education in Our Schools," Edited by K.E.K. Ross, 6/23/89.

NCEER-89-0017 "Proceedings from the Conference on Disaster Preparedness - The Place of Earthquake Education in Our Schools," Edited by K.E.K. Ross, 12/31/89, (PB90-207895). This report is available only through NTIS (see address given above).

NCEER-89-0018 "Multidimensional Models of Hysteretic Material Behavior for Vibration Analysis of Shape Memory Energy Absorbing Devices, by E.J. Graesser and F.A. Cozzarelli, 6/7/89, (PB90-164146/AS).

NCEER-89-0019 "Nonlinear Dynamic Analysis of Three-Dimensional Base Isolated Structures (3D-BASIS)," by S. Nagarajaiah, A.M. Reinhorn and M.C. Constantinou, 8/3/89, (PB90-161936/AS). This report is available only through NTIS (see address given above).

NCEER-89-0020 "Structural Control Considering Time-Rate of Control Forces and Control Rate Constraints," by F.Y. Cheng and C.P. Pantelides, 8/3/89, (PB90-120445/AS).

NCEER-89-0021 "Subsurface Conditions of Memphis and Shelby County," by K.W. Ng, T-S. Chang and H-H.M. Hwang, 7/26/89, (PB90-120437/AS).

NCEER-89-0022 "Seismic Wave Propagation Effects on Straight Jointed Buried Pipelines," by K. Elhmadi and M.J. O'Rourke, 8/24/89, (PB90-162322/AS).

NCEER-89-0023 "Workshop on Serviceability Analysis of Water Delivery Systems," edited by M. Grigoriu, 3/6/89, (PB90-127424/AS).

NCEER-89-0024 "Shaking Table Study of a 1/5 Scale Steel Frame Composed of Tapered Members," by K.C. Chang, J.S. Hwang and G.C. Lee, 9/18/89, (PB90-160169/AS).

NCEER-89-0025 "DYNA1D: A Computer Program for Nonlinear Seismic Site Response Analysis - Technical Documentation," by Jean H. Prevost, 9/14/89, (PB90-161944/AS). This report is available only through NTIS (see address given above).

NCEER-89-0026 "1:4 Scale Model Studies of Active Tendon Systems and Active Mass Dampers for Aseismic Protection," by A.M. Reinhorn, T.T. Soong, R.C. Lin, Y.P. Yang, Y. Fukao, H. Abe and M. Nakai, 9/15/89, (PB90-173246/AS).

NCEER-89-0027 "Scattering of Waves by Inclusions in a Nonhomogeneous Elastic Half Space Solved by Boundary Element Methods," by P.K. Hadley, A. Askar and A.S. Cakmak, 6/15/89, (PB90-145699/AS).

NCEER-89-0028 "Statistical Evaluation of Deflection Amplification Factors for Reinforced Concrete Structures," by H.H.M. Hwang, J-W. Jaw and A.L. Ch'ng, 8/31/89, (PB90-164633/AS).

NCEER-89-0029 "Bedrock Accelerations in Memphis Area Due to Large New Madrid Earthquakes," by H.H.M. Hwang, C.H.S. Chen and G. Yu, 11/7/89, (PB90-162330/AS).

NCEER-89-0030 "Seismic Behavior and Response Sensitivity of Secondary Structural Systems," by Y.Q. Chen and T.T. Soong, 10/23/89, (PB90-164658/AS).

NCEER-89-0031 "Random Vibration and Reliability Analysis of Primary-Secondary Structural Systems," by Y. Ibrahim, M. Grigoriu and T.T. Soong, 11/10/89, (PB90-161951/AS).

NCEER-89-0032 "Proceedings from the Second U.S. - Japan Workshop on Liquefaction, Large Ground Deformation and Their Effects on Lifelines, September 26-29, 1989," Edited by T.D. O'Rourke and M. Hamada, 12/1/89, (PB90-209388/AS).

NCEER-89-0033 "Deterministic Model for Seismic Damage Evaluation of Reinforced Concrete Structures," by J.M. Bracci, A.M. Reinhorn, J.B. Mander and S.K. Kunnath, 9/27/89.

NCEER-89-0034 "On the Relation Between Local and Global Damage Indices," by E. DiPasquale and A.S. Cakmak, 8/15/89, (PB90-173865).

NCEER-89-0035 "Cyclic Undrained Behavior of Nonplastic and Low Plasticity Silts," by A.J. Walker and H.E. Stewart, 7/26/89, (PB90-183518/AS).

NCEER-89-0036 "Liquefaction Potential of Surficial Deposits in the City of Buffalo, New York," by M. Budhu, R. Giese and L. Baumgrass, 1/17/89, (PB90-208455/AS).

NCEER-89-0037 "A Deterministic Assessment of Effects of Ground Motion Incoherence," by A.S. Veletsos and Y. Tang, 7/15/89, (PB90-164294/AS).

NCEER-89-0038 "Workshop on Ground Motion Parameters for Seismic Hazard Mapping," July 17-18, 1989, edited by R.V. Whitman, 12/1/89, (PB90-173923/AS).

NCEER-89-0039 "Seismic Effects on Elevated Transit Lines of the New York City Transit Authority," by C.J. Costantino, C.A. Miller and E. Heymsfield, 12/26/89, (PB90-207887/AS).

NCEER-89-0040 "Centrifugal Modeling of Dynamic Soil-Structure Interaction," by K. Weissman, Supervised by J.H. Prevost, 5/10/89, (PB90-207879/AS).

NCEER-89-0041 "Linearized Identification of Buildings With Cores for Seismic Vulnerability Assessment," by I-K. Ho and A.E. Aktan, 11/1/89, (PB90-251943/AS).

NCEER-90-0001 "Geotechnical and Lifeline Aspects of the October 17, 1989 Loma Prieta Earthquake in San Francisco," by T.D. O'Rourke, H.E. Stewart, F.T. Blackburn and T.S. Dickerman, 1/90, (PB90-208596/AS).

NCEER-90-0002 "Nonnormal Secondary Response Due to Yielding in a Primary Structure," by D.C.K. Chen and L.D. Lutes, 2/28/90, (PB90-251976/AS).

NCEER-90-0003 "Earthquake Education Materials for Grades K-12," by K.E.K. Ross, 4/16/90, (PB91-113415/AS).

NCEER-90-0004 "Catalog of Strong Motion Stations in Eastern North America," by R.W. Busby, 4/3/90, (PB90-251984)/AS.

NCEER-90-0005 "NCEER Strong-Motion Data Base: A User Manual for the GeoBase Release (Version 1.0 for the Sun3)," by P. Friberg and K. Jacob, 3/31/90 (PB90-258062/AS).

NCEER-90-0006 "Seismic Hazard Along a Crude Oil Pipeline in the Event of an 1811-1812 Type New Madrid Earthquake," by H.H.M. Hwang and C-H.S. Chen, 4/16/90(PB90-258054).

NCEER-90-0007 "Site-Specific Response Spectra for Memphis Sheahan Pumping Station," by H.H.M. Hwang and C.S. Lee, 5/15/90, (PB91-108811/AS).

NCEER-90-0008 "Pilot Study on Seismic Vulnerability of Crude Oil Transmission Systems," by T. Ariman, R. Dobry, M. Grigoriu, F. Kozin, M. O'Rourke, T. O'Rourke and M. Shinozuka, 5/25/90, (PB91-108837/AS).

NCEER-90-0009 "A Program to Generate Site Dependent Time Histories: EQGEN," by G.W. Ellis, M. Srinivasan and A.S. Cakmak, 1/30/90, (PB91-108829/AS).

NCEER-90-0010 "Active Isolation for Seismic Protection of Operating Rooms," by M.E. Talbott, Supervised by M. Shinozuka, 6/8/9, (PB91-110205/AS).

NCEER-90-0011 "Program LINEARID for Identification of Linear Structural Dynamic Systems," by C-B. Yun and M. Shinozuka, 6/25/90, (PB91-110312/AS).

NCEER-90-0012 "Two-Dimensional Two-Phase Elasto-Plastic Seismic Response of Earth Dams," by A.N. Yiagos, Supervised by J.H. Prevost, 6/20/90, (PB91-110197/AS).

NCEER-90-0013 "Secondary Systems in Base-Isolated Structures: Experimental Investigation, Stochastic Response and Stochastic Sensitivity," by G.D. Manolis, G. Juhn, M.C. Constantinou and A.M. Reinhorn, 7/1/90, (PB91-110320/AS).

NCEER-90-0014 "Seismic Behavior of Lightly-Reinforced Concrete Column and Beam-Column Joint Details," by S.P. Pessiki, C.H. Conley, P. Gergely and R.N. White, 8/22/90, (PB91-108795/AS).

NCEER-90-0015 "Two Hybrid Control Systems for Building Structures Under Strong Earthquakes," by J.N. Yang and A. Danielians, 6/29/90, (PB91-125393/AS).

NCEER-90-0016 "Instantaneous Optimal Control with Acceleration and Velocity Feedback," by J.N. Yang and Z. Li, 6/29/90, (PB91-125401/AS).

NCEER-90-0017 "Reconnaissance Report on the Northern Iran Earthquake of June 21, 1990," by M. Mehrain, 10/4/90, (PB91-125377/AS).

NCEER-90-0018 "Evaluation of Liquefaction Potential in Memphis and Shelby County," by T.S. Chang, P.S. Tang, C.S. Lee and H. Hwang, 8/10/90, (PB91-125427/AS).

NCEER-90-0019 "Experimental and Analytical Study of a Combined Sliding Disc Bearing and Helical Steel Spring Isolation System," by M.C. Constantinou, A.S. Mokha and A.M. Reinhorn, 10/4/90, (PB91-125385/AS).

NCEER-90-0020 "Experimental Study and Analytical Prediction of Earthquake Response of a Sliding Isolation System with a Spherical Surface," by A.S. Mokha, M.C. Constantinou and A.M. Reinhorn, 10/11/90, (PB91-125419/AS).

NCEER 90-0021 "Dynamic Interaction Factors for Floating Pile Groups," by G. Gazetas, K. Fan, A. Kaynia and E. Kausel, 9/10/90, (PB91-170381/AS).

NCEER-90-0022 "Evaluation of Seismic Damage Indices for Reinforced Concrete Structures," by S. Rodriguez-Gomez and A.S. Cakmak, 9/30/90, PB91-171322/AS).

NCEER-90-0023 "Study of Site Response at a Selected Memphis Site," by H. Desai, S. Ahmad, E.S. Gazetas and M.R. Oh, 10/11/90, (PB91-196857/AS).

NCEER-90-0024 "A User's Guide to Strongmo: Version 1.0 of NCEER's Strong-Motion Data Access Tool for PCs and Terminals," by P.A. Friberg and C.A.T. Susch, 11/15/90, (PB91-171272/AS).

NCEER-90-0025 "A Three-Dimensional Analytical Study of Spatial Variability of Seismic Ground Motions," by L-L. Hong and A.H.-S. Ang, 10/30/90, (PB91-170399/AS).

NCEER-90-0026 "MUMOID User's Guide - A Program for the Identification of Modal Parameters," by S. Rodriguez-Gomez and E. DiPasquale, 9/30/90, (PB91-171298/AS).

NCEER-90-0027 "SARCF-II User's Guide - Seismic Analysis of Reinforced Concrete Frames," by S. Rodriguez-Gomez, Y.S. Chung and C. Meyer, 9/30/90, (PB91-171280/AS).

NCEER-90-0028 "Viscous Dampers: Testing, Modeling and Application in Vibration and Seismic Isolation," by N. Makris and M.C. Constantinou, 12/20/90 (PB91-190561/AS).

NCEER-90-0029 "Soil Effects on Earthquake Ground Motions in the Memphis Area," by H. Hwang, C.S. Lee, K.W. Ng and T.S. Chang, 8/2/90, (PB91-190751/AS).

NCEER-91-0001 "Proceedings from the Third Japan-U.S. Workshop on Earthquake Resistant Design of Lifeline Facilities and Countermeasures for Soil Liquefaction, December 17-19, 1990," edited by T.D. O'Rourke and M. Hamada, 2/1/91, (PB91-179259/AS).

NCEER-91-0002 "Physical Space Solutions of Non-Proportionally Damped Systems," by M. Tong, Z. Liang and G.C. Lee, 1/15/91, (PB91-179242/AS).

NCEER-91-0003 "Seismic Response of Single Piles and Pile Groups," by K. Fan and G. Gazetas, 1/10/91, (PB92-174994/AS).

NCEER-91-0004 "Damping of Structures: Part 1 - Theory of Complex Damping," by Z. Liang and G. Lee, 10/10/91, (PB92-197235/AS).

NCEER-91-0005 "3D-BASIS - Nonlinear Dynamic Analysis of Three Dimensional Base Isolated Structures: Part II," by S. Nagarajaiah, A.M. Reinhorn and M.C. Constantinou, 2/28/91, (PB91-190553/AS).

NCEER-91-0006 "A Multidimensional Hysteretic Model for Plasticity Deforming Metals in Energy Absorbing Devices," by E.J. Graesser and F.A. Cozzarelli, 4/9/91, (PB92-108364/AS).

NCEER-91-0007 "A Framework for Customizable Knowledge-Based Expert Systems with an Application to a KBES for Evaluating the Seismic Resistance of Existing Buildings," by E.G. Ibarra-Anaya and S.J. Fenves, 4/9/91, (PB91-210930/AS).

NCEER-91-0008 "Nonlinear Analysis of Steel Frames with Semi-Rigid Connections Using the Capacity Spectrum Method," by G.G. Deierlein, S-H. Hsieh, Y-J. Shen and J.F. Abel, 7/2/91, (PB92-113828/AS).

NCEER-91-0009 "Earthquake Education Materials for Grades K-12," by K.E.K. Ross, 4/30/91, (PB91-212142/AS).

NCEER-91-0010 "Phase Wave Velocities and Displacement Phase Differences in a Harmonically Oscillating Pile," by N. Makris and G. Gazetas, 7/8/91, (PB92-108356/AS).

NCEER-91-0011 "Dynamic Characteristics of a Full-Size Five-Story Steel Structure and a 2/5 Scale Model," by K.C. Chang, G.C. Yao, G.C. Lee, D.S. Hao and Y.C. Yeh," 7/2/91.

NCEER-91-0012 "Seismic Response of a 2/5 Scale Steel Structure with Added Viscoelastic Dampers," by K.C. Chang, T.T. Soong, S-T. Oh and M.L. Lai, 5/17/91 (PB92-110816/AS).

NCEER-91-0013 "Earthquake Response of Retaining Walls; Full-Scale Testing and Computational Modeling," by S. Alampalli and A-W.M. Elgamal, 6/20/91, to be published.

NCEER-91-0014 "3D-BASIS-M: Nonlinear Dynamic Analysis of Multiple Building Base Isolated Structures," by P.C. Tsopelas, S. Nagarajaiah, M.C. Constantinou and A.M. Reinhorn, 5/28/91, (PB92-113885/AS).

NCEER-91-0015 "Evaluation of SEAOC Design Requirements for Sliding Isolated Structures," by D. Theodossiou and M.C. Constantinou, 6/10/91, (PB92-114602/AS).

NCEER-91-0016 "Closed-Loop Modal Testing of a 27-Story Reinforced Concrete Flat Plate-Core Building," by H.R. Somaprasad, T. Toksoy, H. Yoshiyuki and A.E. Aktan, 7/15/91, (PB92-129980/AS).

NCEER-91-0017 "Shake Table Test of a 1/6 Scale Two-Story Lightly Reinforced Concrete Building," by A.G. El-Attar, R.N. White and P. Gergely, 2/28/91, (PB92-222447/AS).

NCEER-91-0018 "Shake Table Test of a 1/8 Scale Three-Story Lightly Reinforced Concrete Building," by A.G. El-Attar, R.N. White and P. Gergely, 2/28/91.

NCEER-91-0019 "Transfer Functions for Rigid Rectangular Foundations," by A.S. Veletsos, A.M. Prasad and W.H. Wu, 7/31/91.

NCEER-91-0020 "Hybrid Control of Seismic-Excited Nonlinear and Inelastic Structural Systems," by J.N. Yang, Z. Li and A. Danielians, 8/1/91, (PB92-143171/AS).

NCEER-91-0021 "The NCEER-91 Earthquake Catalog: Improved Intensity-Based Magnitudes and Recurrence Relations for U.S. Earthquakes East of New Madrid," by L. Seeber and J.G. Armbruster, 8/28/91, (PB92-176742/AS).

NCEER-91-0022 "Proceedings from the Implementation of Earthquake Planning and Education in Schools: The Need for Change - The Roles of the Changemakers," by K.E.K. Ross and F. Winslow, 7/23/91, (PB92-129998/AS).

NCEER-91-0023 "A Study of Reliability Based Criteria for Seismic Design of Reinforced Concrete Frame Buildings," by H.H.M. Hwang and H.-M. Hsu, 8/10/91, (PB92-140235/AS).

NCEER-91-0024 "Experimental Verification of a Number of Structural System Identification Algorithms," by R.G. Ghanem, H. Gavin and M. Shinozuka, 9/18/91, (PB92-176577/AS).

NCEER-91-0025 "Probabilistic Evaluation of Liquefaction Potential," by H.H.M. Hwang and C.S. Lee," 11/25/91, (PB92-143429/AS).

NCEER-91-0026 "Instantaneous Optimal Control for Linear, Nonlinear and Hysteretic Structures - Stable Controllers," by J.N. Yang and Z. Li, 11/15/91, (PB92-163807/AS).

NCEER-91-0027 "Experimental and Theoretical Study of a Sliding Isolation System for Bridges," by M.C. Constantinou, A. Kartoum, A.M. Reinhorn and P. Bradford, 11/15/91, (PB92-176973/AS).

NCEER-92-0001 "Case Studies of Liquefaction and Lifeline Performance During Past Earthquakes, Volume 1: Japanese Case Studies," Edited by M. Hamada and T. O'Rourke, 2/17/92, (PB92-197243/AS).

NCEER-92-0002 "Case Studies of Liquefaction and Lifeline Performance During Past Earthquakes, Volume 2: United States Case Studies," Edited by T. O'Rourke and M. Hamada, 2/17/92, (PB92-197250/AS).

NCEER-92-0003 "Issues in Earthquake Education," Edited by K. Ross, 2/3/92, (PB92-222389/AS).

NCEER-92-0004 "Proceedings from the First U.S. - Japan Workshop on Earthquake Protective Systems for Bridges," 2/4/92, to be published.

NCEER-92-0005 "Seismic Ground Motion from a Haskell-Type Source in a Multiple-Layered Half-Space," A.P. Theoharis, G. Deodatis and M. Shinozuka, 1/2/92, to be published.

NCEER-92-0006 "Proceedings from the Site Effects Workshop," Edited by R. Whitman, 2/29/92, (PB92-197201/AS).

NCEER-92-0007 "Engineering Evaluation of Permanent Ground Deformations Due to Seismically-Induced Liquefaction," by M.H. Baziar, R. Dobry and A-W.M. Elgamal, 3/24/92, (PB92-222421/AS).

NCEER-92-0008 "A Procedure for the Seismic Evaluation of Buildings in the Central and Eastern United States," by C.D. Poland and J.O. Malley, 4/2/92, (PB92-222439/AS).

NCEER-92-0009 "Experimental and Analytical Study of a Hybrid Isolation System Using Friction Controllable Sliding Bearings," by M.Q. Feng, S. Fuji and M. Shinozuka, 5/15/92, (PB93-150282/AS).

NCEER-92-0010 "Seismic Resistance of Slab-Column Connections in Existing Non-Ductile Flat-Plate Buildings," by A.J. Durrani and Y. Du, 5/18/92.

NCEER-92-0011 "The Hysteretic and Dynamic Behavior of Brick Masonry Walls Upgraded by Ferrocement Coatings Under Cyclic Loading and Strong Simulated Ground Motion," by H. Lee and S.P. Prawel, 5/11/92, to be published.

NCEER-92-0012 "Study of Wire Rope Systems for Seismic Protection of Equipment in Buildings," by G.F. Demetriades, M.C. Constantinou and A.M. Reinhorn, 5/20/92.

NCEER-92-0013 "Shape Memory Structural Dampers: Material Properties, Design and Seismic Testing," by P.R. Witting and F.A. Cozzarelli, 5/26/92.

NCEER-92-0014 "Longitudinal Permanent Ground Deformation Effects on Buried Continuous Pipelines," by M.J. O'Rourke, and C. Nordberg, 6/15/92.

NCEER-92-0015 "A Simulation Method for Stationary Gaussian Random Functions Based on the Sampling Theorem," by M. Grigoriu and S. Balopoulou, 6/11/92, (PB93-127496/AS).

NCEER-92-0016 "Gravity-Load-Designed Reinforced Concrete Buildings: Seismic Evaluation of Existing Construction and Detailing Strategies for Improved Seismic Resistance," by G.W. Hoffmann, S.K. Kunnath, J.B. Mander and A.M. Reinhorn, 7/15/92, to be published.

NCEER-92-0017 "Observations on Water System and Pipeline Performance in the Limón Area of Costa Rica Due to the April 22, 1991 Earthquake," by M. O'Rourke and D. Ballantyne, 6/30/92, (PB93-126811/AS).

NCEER-92-0018 "Fourth Edition of Earthquake Education Materials for Grades K-12," Edited by K.E.K. Ross, 8/10/92.

NCEER-92-0019 "Proceedings from the Fourth Japan-U.S. Workshop on Earthquake Resistant Design of Lifeline Facilities and Countermeasures for Soil Liquefaction," Edited by M. Hamada and T.D. O'Rourke, 8/12/92, (PB93-163939/AS).

NCEER-92-0020 "Active Bracing System: A Full Scale Implementation of Active Control," by A.M. Reinhorn, T.T. Soong, R.C. Lin, M.A. Riley, Y.P. Wang, S. Aizawa and M. Higashino, 8/14/92, (PB93-127512/AS).

NCEER-92-0021 "Empirical Analysis of Horizontal Ground Displacement Generated by Liquefaction-Induced Lateral Spreads," by S.F. Bartlett and T.L. Youd, 8/17/92.

NCEER-92-0022 "IDARC Version 3.0: Inelastic Damage Analysis of Reinforced Concrete Structures," by S.K. Kunnath, A.M. Reinhorn and R.F. Lobo, 8/31/92, to be published.

NCEER-92-0023 "A Semi-Empirical Analysis of Strong-Motion Peaks in Terms of Seismic Source, Propagation Path and Local Site Conditions, by M. Kamiyama, M.J. O'Rourke and R. Flores-Berrones, 9/9/92, (PB93-150266/AS).

NCEER-92-0024 "Seismic Behavior of Reinforced Concrete Frame Structures with Nonductile Details, Part I: Summary of Experimental Findings of Full Scale Beam-Column Joint Tests," by A. Beres, R.N. White and P. Gergely, 9/30/92, to be published.

NCEER-92-0025 "Experimental Results of Repaired and Retrofitted Beam-Column Joint Tests in Lightly Reinforced Concrete Frame Buildings," by A. Beres, S. El-Borgi, R.N. White and P. Gergely, 10/29/92, to be published.

NCEER-92-0026 "A Generalization of Optimal Control Theory: Linear and Nonlinear Structures," by J.N. Yang, Z. Li and S Vongchavalitkul, 11/2/92.

NCEER-92-0027 "Seismic Resistance of Reinforced Concrete Frame Structures Designed Only for Gravity Loads: Part I - Design and Properties of a One-Third Scale Model Structure," by J.M. Bracci, A.M. Reinhorn and J.B. Mander, 12/1/92.

NCEER-92-0028 "Seismic Resistance of Reinforced Concrete Frame Structures Designed Only for Gravity Loads: Part II - Experimental Performance of Subassemblages," by L.E. Aycardi, J.B. Mander and A.M. Reinhorn, 12/1/92.

NCEER-92-0029 "Seismic Resistance of Reinforced Concrete Frame Structures Designed Only for Gravity Loads: Part III - Experimental Performance and Analytical Study of a Structural Model," by J.M. Bracci, A.M. Reinhorn and J.B. Mander, 12/1/92, to be published.

NCEER-92-0030 "Evaluation of Seismic Retrofit of Reinforced Concrete Frame Structures: Part I - Experimental Performance of Retrofitted Subassemblages," by D. Choudhuri, J.B. Mander and A.M. Reinhorn, 12/8/92.

NCEER-92-0031 "Evaluation of Seismic Retrofit of Reinforced Concrete Frame Structures: Part II - Experimental Performance and Analytical Study of a Retrofitted Structural Model," by J.M. Bracci, A.M. Reinhorn and J.B. Mander, 12/8/92.

NCEER-92-0032 "Experimental and Analytical Investigation of Seismic Response of Structures with Supplemental Fluid Viscous Dampers," by M.C. Constantinou and M.D. Symans, 12/21/92.

NCEER-92-0033 "Reconnaissance Report on the Cairo, Egypt Earthquake of October 12, 1992," by M. Khater, 12/23/92.

NCEER-92-0034 "Low-Level Dynamic Characteristics of Four Tall Flat-Plate Buildings in New York City," by H. Gavin, S. Yuan, J. Grossman, E. Pekelis and K. Jacob, 12/28/92.

NCEER-93-0001 "An Experimental Study on the Seismic Performance of Brick-Infilled Steel Frames With and Without Retrofit," by J.B. Mander, B. Nair, K. Wojtkowski and J. Ma, 1/29/93.